TURUN YLIOPISTON JULKAISUJA
ANNALES UNIVERSITATIS TURKUENSIS

SARJA - SER. A I OSA - TOM. 427

ASTRONOMICA - CHEMICA - PHYSICA - MATHEMATICA

UPCONVERTING PHOSPHOR TECHNOLOGY:

Exceptional Photoluminescent Properties Light Up Homogeneous Bioanalytical Assays

by

Terhi Riuttamäki
(née Rantanen)

TURUN YLIOPISTO
UNIVERSITY OF TURKU
Turku 2011

From the Department of Biochemistry and Food Chemistry / Biotechnology
University of Turku
Turku, Finland

Supervised by

Professor Tero Soukka, Ph.D.
Department of Biochemistry and Food Chemistry / Biotechnology
University of Turku
Turku, Finland

and

Professor Emeritus Timo Lövgren, Ph.D.
Department of Biochemistry and Food Chemistry / Biotechnology
University of Turku
Turku, Finland

Reviewed by

Professor Sakari Kulmala, Ph.D.
Analytical Chemistry
Aalto University
School of Chemical Technology
Espoo, Finland

and

Professor Emeritus Ulf-Håkan Stenman, M.D., Ph.D.
Department of Clinical Chemistry
Helsinki University and Helsinki University Central Hospital
Helsinki, Finland

Opponent

Professor Stefan Andersson-Engels, Ph.D.
Department of Physics
Lund University
Lund, Sweden

ISBN 978-951-29-4742-3 (PRINT)
ISBN 978-951-29-4743-0 (PDF)
ISSN 0082-7002
Painosalama Oy – Turku, Finland 2011

Knowing is not enough, we must apply.
Willing is not enough, we must do.

– Goethe

CONTENTS

LIST OF ORIGINAL PUBLICATIONS

This thesis is based on the following original publications, referred to in the text by their Roman numerals (**I-IV**)

I **Terhi Rantanen**, Henna Päkkilä, Laura Jämsen, Katri Kuningas, Telle Ukonaho, Timo Lövgren & Tero Soukka (2007). Tandem dye acceptor used to enhance upconversion fluorescence resonance energy transfer in homogeneous assays. *Anal Chem* **79**(16):6312–6318.

II **Terhi Rantanen**, Marja-Leena Järvenpää, Johanna Vuojola, Katri Kuningas & Tero Soukka (2008) Fluorescence-quenching-based enzyme-activity assay by using photon upconversion. *Angew Chem Int Ed* **47**:3811–3813.

III **Terhi Rantanen**, Marja-Leena Järvenpää, Johanna Vuojola, Riikka Arppe, Katri Kuningas & Tero Soukka (2009) Upconverting phosphors in a dual-parameter LRET-based hybridization assay. *Analyst* **134**:1713–1716.

IV **Terhi Riuttamäki,** Iko Hyppänen, Jouko Kankare & Tero Soukka (2011) Decrease in luminescence lifetime indicating nonradiative energy transfer from upconverting phosphors to fluorescent acceptors in aqueous suspensions. *J Phys Chem C* **115**:17736–17742.

In addition, some unpublished data is presented.

ABBREVIATIONS

1D	one-dimensional
2D	two-dimensional
AF…	Alexa Fluor fluorophore
APTE	addition of photons by transfer of energy (upconversion mechanism)
APTS	3-aminopropyltriethoxysilane (organosilane)
BBQ650	BlackBerry Quencher 650
BPE	B-phycoerythrin (fluorescent protein)
BSA	bovine serum albumin
CCD	charge-coupled device (light detector)
CR	cross-relaxation
CTAB	cetyltrimethylammonium bromide (cationic surfactant)
EDC	1-ethyl-3-(3-dimethylaminopropyl) carbodiimide
EDTA	ethylenediaminetetraacetic acid (chelating agent)
ELISA	enzyme-linked immunosorbent assay
Er	erbium (rare earth element)
ESA	excited-state absorption (upconversion mechanism)
ETU	energy transfer upconversion (upconversion mechanism)
FD	frequency-domain
f-PSA	free prostate-specific antigen (prostate cancer marker)
GSA	ground-state absorption
hCG	human chorionic gonadotropin (pregnancy hormone)
HLA-B27	human leukocyte antigen B27 (genetic marker for certain autoimmune disorders)
Ho	holmium (rare earth element)
LbL	layer-by-layer (coating method)
LD	laser diode (excitation source)
LED	light emitting diode (excitation source)
LF	lateral flow (assay format)
LOD	limit of detection
LOQ	limit of quantification
LRET	lanthanide resonance energy transfer
NHS	*N*-hydroxysuccinimide
NIR	near-infrared radiation (wavelength 750–1400 nm)
PA	photon avalanche (upconversion mechanism)
PAA	poly(acrylic acid)
PAH	poly(allylamine hydrochloride)
PCR	polymerase chain reaction
PEG	polyethylene glycol
PEI	polyethyleneimine
PMT	photomultiplier tube (light detector)
POCT	point-of-care testing
PSS	poly(styrene sulfonate)
PVP	polyvinylpyrrolidone
R_0	Förster radius (the distance at which energy transfer efficiency is 50%)
RET	resonance energy transfer (nonradiative energy transfer mechanism)
SEB	Staphylococcal enterotoxin B
SET	surface energy transfer
sulfo-NHS	*N*-hydroxysulfo-succinimide
TEM	transmission electron microscopy
TEOS	tetraethyl orthosilicate
Tm	thulium (rare earth element)
UCP	upconverting phosphor (photoluminescent inorganic compound)
UC-RET	upconversion resonance energy transfer
UV	ultraviolet radiation (wavelength <380 nm)
Yb	ytterbium (rare earth element)

ABSTRACT

The aim of the present study was to demonstrate the wide applicability of the novel photoluminescent labels called upconverting phosphors (UCPs) in proximity-based bioanalytical assays. The exceptional features of the lanthanide-doped inorganic UCP compounds stem from their capability for photon upconversion resulting in anti-Stokes photoluminescence at visible wavelengths under near-infrared (NIR) excitation. Major limitations related to conventional photoluminescent labels are avoided, rendering the UCPs a competitive next-generation label technology. First, the background luminescence is minimized due to total elimination of autofluorescence. Consequently, improvements in detectability are expected. Second, at the long wavelengths (>600 nm) used for exciting and detecting the UCPs, the transmittance of sample matrixes is significantly greater in comparison with shorter wavelengths. Colored samples are no longer an obstacle to the luminescence measurement, and more flexibility is allowed even in homogeneous assay concepts, where the sample matrix remains present during the entire analysis procedure, including label detection.

To transform a UCP particle into a biocompatible label suitable for bioanalytical assays, it must be colloidal in an aqueous environment and covered with biomolecules capable of recognizing the analyte molecule. At the beginning of this study, only UCP bulk material was available, and it was necessary to process the material to submicrometer-sized particles prior to use. Later, the ground UCPs, with irregular shape, wide size-distribution and heterogeneous luminescence properties, were substituted by a smaller-sized spherical UCP material. The surface functionalization of the UCPs was realized by producing a thin hydrophilic coating. Polymer adsorption on the UCP surface is a simple way to introduce functional groups for bioconjugation purposes, but possible stability issues encouraged us to optimize an optional silica-encapsulation method which produces a coating that is not detached in storage or assay conditions. An extremely thin monolayer around the UCPs was pursued due to their intended use as short-distance energy donors, and much attention was paid to controlling the thickness of the coating.

The performance of the UCP technology was evaluated in three different homogeneous resonance energy transfer-based bioanalytical assays: a competitive ligand binding assay, a hybridization assay for nucleic acid detection and an enzyme activity assay. To complete the list, a competitive immunoassay has been published previously. Our systematic investigation showed that a nonradiative energy transfer mechanism is indeed involved, when a UCP and an acceptor fluorophore are brought into close proximity in aqueous suspension. This process is the basis for the above-mentioned homogeneous assays, in which the distance between the fluorescent species depends on a specific biomolecular binding event. According to the studies, the submicrometer-sized UCP labels allow versatile proximity-based bioanalysis with low detection limits (a low-nanomolar concentration for biotin, 0.01 U for benzonase enzyme, 0.35 nM for target DNA sequence).

1 INTRODUCTION

Bioanalytical assays are used in medical diagnostics as well as in food safety assurance and environmental monitoring to determine the concentration of analytes, such as proteins, nucleic acids, carbohydrates, hormones, toxins, drugs and whole cells. The specific recognition capabilities of biomolecules are exploited to capture the analytes from complex sample matrixes and the analyte concentration is translated into a detectable signal by utilizing a selected label technology. In addition to the binder molecule quality and the label properties, the assay design is also a key element in a bioaffinity assay. The recent trend in assay development has been towards point-of-care testing (POCT) (Junker *et al.*, 2010), which aims at fast-performing and ready-to-use solutions with low equipment demand. Nonetheless, the testing should be precise, accurate, cost-effective and highly sensitive. POCT does not replace the huge capacities of centralized laboratory testing but will reshape the conventions of the sample analysis. In the future, an increasing number of tests will be available near the patient or on the site of the food and environmental sampling locations.

The bioanalytical assays are classified as heterogeneous or homogeneous assays based on whether they use a washing step or not (Davies, 2005). Heterogeneous assays provide the most sensitive results, but the washing step separating the unbound fraction of the labeled component before signal measurement requires extra time and additional instrumentation. Even though the detection limit is usually compromised in separation-free homogeneous assays, where the binding event itself modulates the signal, the format is superior for faster and simpler solutions, such as POCT.

To keep the detection limits of homogeneous assays at a satisfactory level, the label technology used for quantification plays an important role. The first labels, introduced back in 1960, were radioisotopes (Yalow and Berson, 1960; Ekins, 1960), but the disadvantages (e.g., limited shelf-life, low specific activity and health risks) motivated scientists to seek non-isotopic options. Presently, photoluminescent labels have accelerated the performance time, and the sensitivities achieved with the radiolabels have been exceeded (Ekins, 1998). However, other problems related to photoluminescence measurements need to be overcome to further improve the performance of bioanalytical assays. First, autofluorescence originating mainly from biological material increases the background fluorescence, limiting the assay sensitivity. Second, absorption properties of the non-transparent and colored sample matrixes severely interfere at ultraviolet (UV) and visible wavelengths, and only heterogeneous assays are normally feasible if absorption coincides with either the excitation or the measurement wavelength. Time-resolved fluorometry, exploiting the long emission lifetime of lanthanide labels, has provided a partial solution since the late 1970s by eliminating the short-lived autofluorescence with time-gated measurement (Soini and Hemmilä, 1979; Soini *et al.*, 1987). However, excitation at the UV region restricts the use of optically non-transparent samples. A comprehensive solution can be realized with label technologies based on near-infrared-to-visible photon upconversion. Simultaneous or sequential absorption of multiple low-energy near-infrared (NIR) photons results in anti-Stokes emission detectable at visible wavelengths, and autofluorescence is totally avoided (He *et al.*, 2008; Hänninen *et al.*, 2008; Auzel, 2004). Inorganic upconverting phosphor compounds show the most efficient upconversion capabilities (Auzel, 2004), rendering them highly promising luminescent labels for ultrasensitive homogeneous assays (Haase and Schäfer, 2011).

2 REVIEW OF THE LITERATURE

2.1 Photon upconversion mechanisms

Photon upconversion is a process generating higher-energy emission from low-energy radiation. The increase in energy is achieved by absorbing multiple (usually two or three) photons per single emitted photon. The transition from the excited electronic state back to the ground state, or to another lower-lying energy level, produces luminescence at wavelengths shorter than the original excitation wavelength. This nonlinear optical process, also called anti-Stokes photoluminescence, involves intermediate excited states, which can be either virtual or real electronic states. Utilization of non-existing virtual intermediate states requires an extremely high excitation power density (10^6–10^9 W/cm^2) because multiple photons need to be absorbed simultaneously (Auzel, 2004). To avoid thermal decomposition of the sample under intense radiation, expensive ultrafast pulse lasers are employed as excitation sources, for example in multi-photon microscopy (Denk *et al.*, 1990). An affordable continuous wave laser diode with ~10^6 times lower output power is sufficient to promote the photon upconversion in certain inorganic compounds having real metastable intermediate states because the photons can be absorbed one after the other instead of simultaneously. This thesis concentrates only on those exceptional inorganic materials, while mechanisms based on, for example, multiphoton absorption (Kaiser and Garrett, 1961) and second-harmonic generation (i.e., frequency doubling) (Franken *et al.*, 1961; Armstrong *et al.*, 1962), both of which lack the intermediate energy state, are excluded.

Several upconversion mechanisms have been recognized (Figure 1), and they may appear alone or in combinations. The most efficient mechanism usually dominates in the case of low excitation power density, but an increase in the pumping power enables emergence of the less-efficient mechanisms, too (Mita, 2007). Some upconversion mechanisms involve only one type of ion and are relatively insensitive to ion concentration, while the other mechanisms stipulate the contribution of separate energy transfer sensitizer and activator ions (Gamelin and Güdel, 2001). In the latter case, the concentration and distribution of the operational ions has an influence on the upconversion mechanism due to the dependence of energy transfer rate constant on the ionic distance (Zhang *et al.*, 2001).

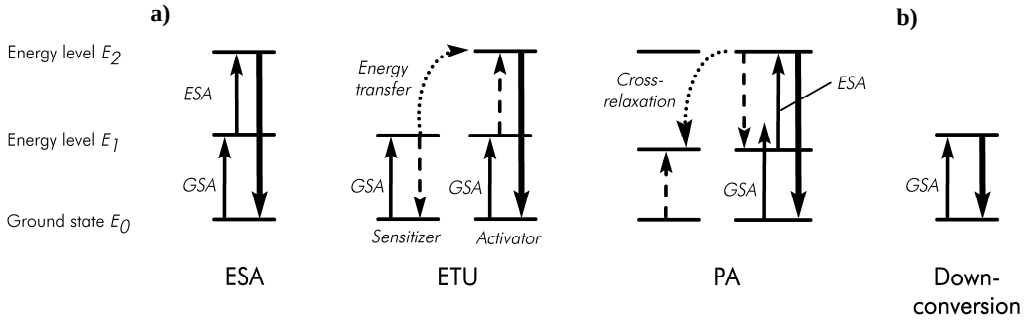

Figure 1. Simplified energy diagrams of (**a**) the most significant upconversion mechanisms and (**b**) a downconversion mechanism for comparison. Upward and downward solid arrows represent absorption and emission processes, respectively, while dashed arrows symbolize transitions related to energy transfer between the sensitizer and the activator or cross-relaxation between neighboring ions. *GSA, ground-state absorption; ESA, excited state absorption; ETU, energy transfer upconversion; PA, photon avalanche*. Based on a figure by Wang and Liu (2009).

The simplest upconversion process involving only a single ion is *excited-state absorption (ESA)*, which was the mechanism responsible for the near-infrared-to-visible photon upconversion discovered first by Bloembergen (1959). The first pump photon populates the intermediate excited state E_1 (ground-state absorption, GSA), followed by a second absorption (ESA) triggering the upconversion emission from the higher E_2 state. An upconversion mechanism featuring two different neighboring ions (a sensitizer and an activator) is referred to as an *energy transfer upconversion (ETU)* or alternatively as addition of photons by transfer of energy (APTE) (Auzel, 1966b; Auzel, 1966a). In this mechanism, the GSA is followed by a nonradiative resonant energy transfer from the sensitizer ion to the activator ion, which leads to population of the higher excited state E_2 of the latter. A good sensitizer ion has no resonant energy states above state E_1 of its own, which makes the energy transfer process more efficient due to the lack of competing processes. This mechanism is about 100 times more efficient than the ESA mechanism. *Photon avalanche (PA)*, involving cross-relaxation energy transfer between neighboring ions, is a more complex mechanism observed when the pump flux exceeds a certain critical threshold (Chivian *et al.*, 1979; Joubert *et al.*, 1993). The cross-relaxation step assists in population of the intermediate excited state E_1 because the excitation energy is not resonant with the GSA transition directly but only with the following ESA transition. The GSA step in the beginning is eminently inefficient, but subsequently the ESA step populates the higher excited state E_2 very effectively. The cross-relaxation step results in population of the intermediate state E_1 of both neighboring ions, and the avalanche process is boosted. Even though PA is eventually a highly efficient upconversion mechanism, it is poorly exploitable due to the slow response to the excitation (up to seconds). *Cooperative mechanisms* with lower upconversion efficiencies were omitted from Figure 1 in order to focus attention on the more significant upconversion mechanisms. These mechanisms sum up the photon energy of multiple sensitizer ions by sensitization or by emission (Snitzer and Woodcock, 1965; Ovsyankin and Feofilov, 1966; Nakazawa and Shionoya, 1970).

The likelihood of populating the higher luminescent energy level E_2 by re-excitation depends on the lifetime of the lower intermediate state E_1 acting as "an energy store" (Gamelin and Güdel, 2001). Excited molecules can relax to the ground state (or another lower-lying electronic state) either through a *radiative* or a *nonradiative* path. The former involves the emission of a photon with energy determined by the energy difference of the two states. Nonradiative relaxations comprise all alternative relaxations but those leading to luminescence. In like manner to the quantum of light called a photon, the quantum of lattice vibrational energy in solid state is termed a phonon. If the energy gap to the next lower energy level is small, the number of phonons required to match the gap is low, resulting in an elevated probability for a multiphonon decay, which represents one prevalent form of nonradiative relaxation. A third relaxation option is to *transfer the energy* in a nonradiative manner to a suitable energy acceptor in close proximity. All the three above-mentioned depopulation paths of the intermediate state E_1 should be minimized in order to increase the excited state lifetime and, consequently, the upconversion efficiency. The lifetime defines the power density needed for generation of photon upconversion (Morgan *et al.*, 2008). The upconversion processes are not limited to two absorbed photons (as illustrated in Figure 1), but three or even more photons can be involved to reach even higher energy levels.

From the 1960s when research began in this area, it was known that the upconversion luminescence intensity I is proportional to the nth power of the absorbed pump power P

($I \propto P^n$), where n denotes the number of pump photons absorbed per upconversion photon emitted. In other words, when I versus P is plotted in a double-logarithmic representation, the slope is n. As more powerful NIR excitation sources became available, saturation of the upconversion-induced luminescence was observed, and it was realized that the power-dependence of upconversion emission bands changes with excitation power (Suyver *et al.*, 2005b; Pollnau *et al.*, 2000). In reality, the dependence decreases from P^n down to P^1 with increasing excitation power and, accordingly, the above-mentioned slope will approach 1 (regardless of the number of photons involved). However, it is crucial to note that the excitation power has a higher impact on the luminescence intensity in the case of photon upconversion (n >1) than in the case of common photon downconversion (n = 1).

2.2 Upconverting phosphors

2.2.1 Composition

Photon upconversion can be exploited in bioanalytical assays in the form of labels called upconverting phosphors (UCPs). They are inorganic crystals composed of a transparent host lattice doped with certain trivalent lanthanide ions or transition metals. In order to tune the photophysical properties (emission wavelength and intensity) of upconverting materials, the role of each element needs to be understood.

Host material

The host material forms a crystalline lattice that maintains the correct arrangement of the hybrid material. Suitable inorganic compounds comprise trivalent rare earth ions (Y^{3+}, La^{3+}, Gd^{3+}, Sc^{3+}), alkaline earth ions (Ca^{2+}, Sr^{2+}, Ba^{2+}) or certain transition metals (Zr^{4+}, Ti^{4+}) (Wang and Liu, 2009). A low phonon energy lattice is essential in order to reduce the multiphonon relaxation (minimized energy losses) and to increase the lifetime of the intermediate states involved in upconversion (maximized radiative emission) (Riedener *et al.*, 1995; Suyver *et al.*, 2005a). The most practical hosts are halides (e.g., $NaYF_4$, YF_3, LaF_3), oxides (e.g., Y_2O_3, ZrO_2) and oxysulfides (e.g., Y_2O_2S, La_2O_2S) (Suyver *et al.*, 2005a; Zarling *et al.*, 1994; Güdel, 1998). The lowest phonon energies are typical for the halide-based lattices (<400 cm^{-1}), but only the lightest halide, fluoride, is practical in actual use due to the hygroscopic nature of the heavier ones (Ong *et al.*, 2010). Oxide-based lattices have better chemical stability, but they suffer from relatively high phonon energies (>500 cm^{-1}) (Wang and Liu, 2009; Ong *et al.*, 2010).

Dopant ions

The dopant ions play a central role by actually absorbing and emitting the photons. They determine, for example, the color of the emitted light. Many trivalent lanthanide ions have metastable intermediate electronic states (“energy stores”) that are suitable for generation of the upconversion emission. The favorable photoluminescent properties of lanthanides are predominated by the 4*f* electrons, which are well shielded by the lower-energy 5*s* and 5*p* electrons spatially locating outside of the 4*f* orbital (Cotton, 2006; Bünzli and Piguet, 2005). Electron–phonon coupling to *f–f* transitions is reduced, making the multiphonon relaxation processes less competitive, and forbidden *f–f* transitions result in long-lived excited states (up to 100 ms). Energy levels having sufficiently large gaps to the next lowest level are more likely relaxed radiatively (triggering photon emission) than through multiphonon relaxation. Appropriately spaced ladder-like energy levels of Er^{3+}, Tm^{3+},

Ho^{3+}, and less frequently also Pr^{3+}, Nd^{3+} and Dy^{3+}, render these ions suitable dopants in upconverting materials. The dopant ion occupies part of the cation sites in the host lattice and the similar size of the dopants and host lattice cations can be regarded as an advantage.

To further enhance the upconversion efficiency, UCPs are commonly co-doped with a Yb^{3+} sensitizer ion (Suyver *et al.*, 2005a), which has a relatively large absorption cross-section describing the probability of an absorption process (approximately ten-fold compared to Er^{3+} ion at 980 nm (Zhang *et al.*, 2001; Wybourne, 1965)). In addition, the Yb^{3+} ions have a lesser tendency for concentration-dependent quenching compared to the other lanthanide ions and, therefore, quite high Yb^{3+} concentrations can be used to boost the excitation probability of the activator ions (Suyver *et al.*, 2006). The $^2F_{5/2}$ energy level of the Yb^{3+} coincides with the 980-nm radiation (Figure 2), and it is possible to transfer energy to the above-mentioned lanthanide ions by the ETU mechanism under NIR excitation. The energy levels of Yb^{3+} ($^2F_{5/2}$) and Er^{3+} ($^4I_{11/2}$) are almost perfectly resonant (only a few cm^{-1} energy mismatch), thus enabling highly efficient energy transfer to the Er^{3+} ion without a phonon-mediated step (Suyver *et al.*, 2005c). Therefore, it is not surprising that Yb^{3+}–Er^{3+} pair produces the brightest anti-Stokes photoluminescence and a major part of this emission is Yb^{3+}-sensitized (i.e., the ETU mechanism dominates the ESA mechanism).

As each dopant ion (excluding the Yb^{3+}) has several emissive energy states, each relaxation path produces a different colored emission (Figure 2). The phonon energies of the host lattice partly define which pathway dominates (Mita, 2007). For example, the green emission of Er^{3+} (at 520 and 540 nm) predominates in the low phonon energy fluoride hosts because the multiphonon relaxation processes required for populating the red-emitting level ($^4F_{9/2}$) are rather unlikely due to the relatively large energy gaps ($^4S_{3/2} \rightarrow {}^4F_{9/2}$ ~3200 cm^{-1}, $^4I_{11/2} \rightarrow {}^4I_{13/2}$ ~3600 cm^{-1}). In contrast, the hosts with higher phonon energy may promote the dominating red emission. Similarly, external factors (e.g., surface defects and contaminants) may provide extra vibrational quanta, leading to a reduced green-to-red ratio (Vetrone *et al.*, 2003). Also, the doping level and the excitation power density discussed in the next section and in chapter 2.2.5, respectively, affect the ratio of the emission colors.

In addition to the lanthanides, some transition metals (including Ti^{2+}, Ni^{2+}, Mo^{3+}, Re^{4+} and Os^{4+}) are capable of photon upconversion (for review see Gamelin and Güdel (2001)), but the degree of nonradiative relaxation of the excited *d*-electrons is higher than that of the lanthanide *f*-electrons. Due to the lower upconversion efficiency of the transition metal dopants, the applications in the bioanalytical field are non-existent.

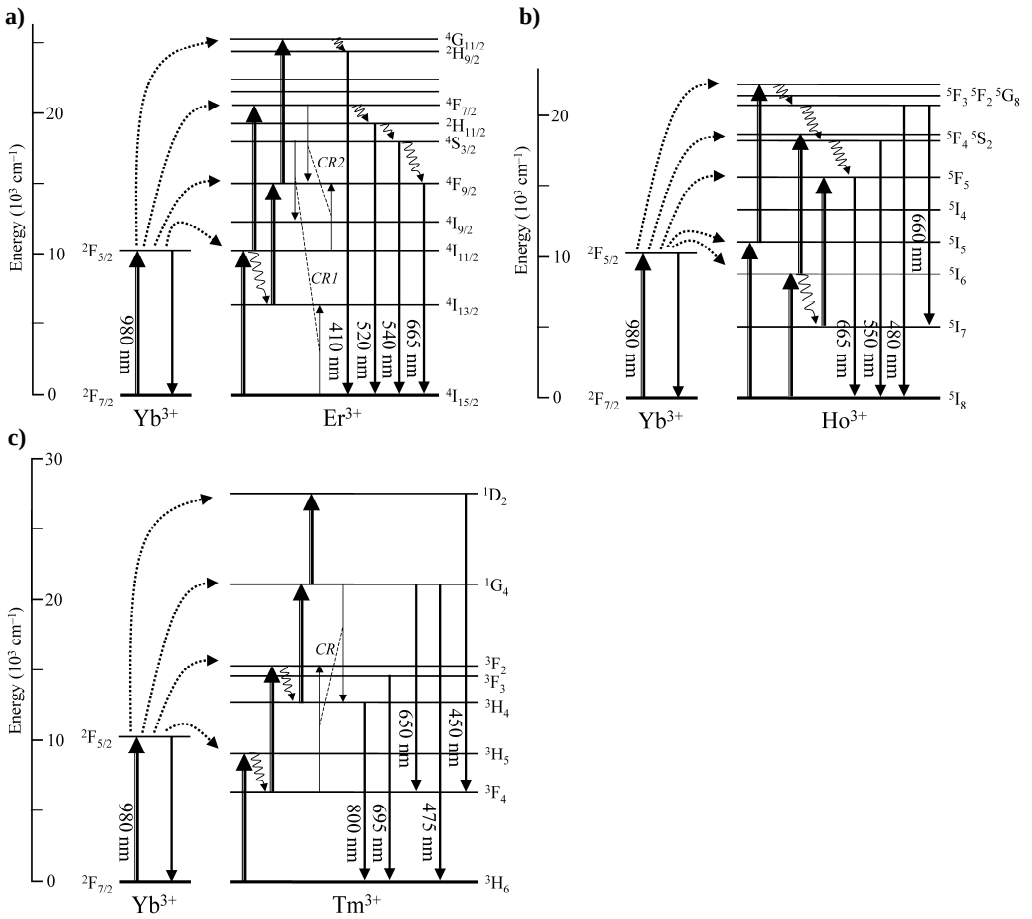

Figure 2. Energy diagrams of the dopant ions used in the most applicable upconverting phosphor materials. Highly efficient photon upconversion is achieved with the ETU mechanism involving Yb^{3+} as a sensitizer ion and (**a**) Er^{3+}, (**b**) Ho^{3+} or (**c**) Tm^{3+} as an emitting activator ion. The bold arrows indicate absorbed pump photons, the dotted arrows symbolize nonradiative energy transfer, curled arrows represent nonradiative multiphonon decay and the downward arrows emission. Cross-relaxation (CR) is illustrated with a pair of reversed arrows. Only those transitions producing emission at the visible region or ≤800 nm are expressed. Modified from Suyver *et al.* (2005a), Wang and Liu (2009) and Wei *et al.* (2007).

Doping level

To maximize the upconversion efficiency, the amount of sensitizer and activator ions must be optimal in the host lattice. Logically, the emission intensity increases along with the growing activator ion (e.g., Er^{3+} or Tm^{3+}) concentration, but a too-dense population of the activators leads to concentration quenching caused by cross-relaxation processes between the neighboring activator ions (Mita, 2007; Zeng *et al.*, 2005; Zhang *et al.*, 2011). The ratio of different emission colors may even be fine-tuned by changing the distance between the activator ions (i.e., the doping level) (Krämer *et al.*, 2004; Mai *et al.*, 2007; Wang and Liu, 2008). For example, the green-to-red ratio decreases along with increasing Er^{3+} concentration because the energy state normally producing the green emission becomes depopulated through a cross-relaxation step (CR1 in Figure 2a) (Suyver *et al.*, 2006) and the red-emitting energy state, in turn, may be populated through another cross-relaxation step (CR2 in Figure 2a) (Wang *et al.*, 2009b). The Yb^{3+} sensitizer is not sensitive to the

concentration quenching as mentioned earlier; therefore, the concentration may be multifold compared to the activator ion. In the optimal case, the activator ions should be surrounded by as many Yb^{3+} neighbors as possible to enable an efficient ETU process (Zhang *et al.*, 2001; Lu *et al.*, 2010; Chen *et al.*, 2010b). However, the dopant ions must be diluted with a sufficient number of "inactive" ions (such as Y^{3+} or La^{3+} in the host material) to limit the energy migration from the activator ions to killer traps, which cause quenching of the desired luminescence (Zeng *et al.*, 2005; Krämer *et al.*, 2004). In addition, extremely high Yb^{3+} concentrations promote energy back-transfer from the activator ions to the Yb^{3+}. The back-transfer results in a suppressed population of certain emitting energy levels of the activator and may, therefore, also be utilized in fine-tuning the emission color of a UCP (Wang and Liu, 2008; Liang *et al.*, 2004).

To summarize, the molar percentages of rare earth dopants are in the range of 5–30% (generally 18% or 25%) for Yb^{3+} in combination with either 1–3% (generally 2%) Er^{3+} or 0.1–0.6% (generally 0.3%) Tm^{3+} or Ho^{3+} (Zarling *et al.*, 1994; Liang *et al.*, 2004).

2.2.2 Recent development trends in upconverting materials

Phase-purity of $NaYF_4$-based UCPs

The most efficient upconverting materials known today are hexagonal (β-phase) $NaYF_4$:Yb^{3+},Er^{3+} and $NaYF_4$:Yb^{3+},Tm^{3+} (Suyver *et al.*, 2006; Krämer *et al.*, 2004; Liang *et al.*, 2004; Aebischer *et al.*, 2006). The crystallographic phase is absolutely essential as the cubic (α-phase) structure produces approximately an order of magnitude less anti-Stokes photoluminescence than the hexagonal one (Krämer *et al.*, 2004; Yi and Chow, 2007; Hyppänen *et al.*, 2009; Schäfer *et al.*, 2009). Harju *et al.* (2011) anticipated that there are at least two reasons causing the differences between the α- and β-phases. The more densely packed β-phase allows more efficient energy transfer between the lanthanide ions, and the close-to-stoichiometric structure of the β-phase contains fewer defects than the α-phase, which needs additional F^- ions to balance the charge of the enriched rare earth ions. Much research has lately been carried out to identify controlled ways to produce phase-pure hexagonal $NaYF_4$:Yb^{3+},Er^{3+}/Tm^{3+}, and constantly diminishing attention has been addressed to the other UCP materials intended for bioanalytical applications. Despite expanded knowledge of UCPs, it remains unclear why this particular fluoride host material is so superior compared to others. The extraordinary low phonon energies naturally play an important role (Suyver *et al.*, 2006), but further research is required to clarify the phenomenon in detail.

Factors affecting the upconversion efficiency and phase-purity of the fluorides include the dopant concentrations, the ratio of sodium to rare earth ions, the impurities, the crystal growth temperature and time (Suyver *et al.*, 2005a; Krämer *et al.*, 2004; Liang *et al.*, 2011; Li and Lin, 2010). Phase transitions follow the temperature, so at low synthesis temperatures the α-phase is formed while higher temperatures favor β-phase formation until certain point where the α-phase begins to predominate again (Krämer *et al.*, 2004; Hyppänen *et al.*, 2009; Yi *et al.*, 2004; Mathews *et al.*, 2004). The exact transition temperatures depend on the UCP synthesis method.

Upconverting $NaYF_4$:Yb^{3+},Er^{3+} bulk material was first introduced in the 1970s (Menyuk *et al.*, 1972; Kano *et al.*, 1972; Sommerdijk, 1973; Bril *et al.*, 1975). The hexagonal phase usually dominates in bulk materials (Yi and Chow, 2006), but it must be taken into account

while examining the literature that some studies of the $NaYF_4$-based materials may have suffered from impure structure in terms of the crystallographic phase. UCP bulk material is applicable to areas such as NIR sensors, lasers and displays, but is unsuitable for applications in the bioanalytical field due to its large size, which impedes colloidal dispersions. Krämer *et al*. (2004) succeeded in optimizing the reproducible solid-state synthesis of micrometer-sized β-phase $NaYF_4$ powders. However, in order to reduce the light scattering in UCP suspensions, the trend has more recently been towards nano-sized UCPs with a uniform size and shape. As a consequence, other parameters in addition to the crystallographic phase need to be simultaneously controlled.

Down to nano-sized UCP particles

Variables affecting the crystal size during the synthesis step comprise the concentration of the metal precursors, the nature of the solvent, the reaction time and the temperature (Wang *et al.*, 2010). When the physical dimensions of the UCP particle are reduced to the nano-scale (<50 nm), different kinds of problems causing decreased upconversion efficiency are encountered (Wang and Liu, 2009). First, as the surface area-to-volume ratio increases, a relatively larger proportion of the emitting ions are situated close to the surface, exposed to quenchers and surface defects. Second, high surface tension triggers the phase transformation from hexagonal to less efficient cubic form (Wang *et al.*, 2010).

Several shielding options have been proposed to protect the near-surface dopant ions from nonradiative relaxation processes induced by the surrounding high-energy vibrational oscillators such as the OH- and CH-groups of organic ligands and solvents (Suyver *et al.*, 2005a; Heer *et al.*, 2004). The quantum yield of nanocrystalline UCPs has been increased multifold by growing an inert, undoped $NaYF_4$ shell (with a thickness of a few nanometers) around an Yb^{3+}–Er^{3+}-doped $NaYF_4$ core (Yi and Chow, 2007; Boyer and van Veggel, 2010). The addition of an inorganic shell also lengthens the decay time constant and affects the green-to-red emission intensity ratio (Wang *et al.*, 2009b). Dominating red emission from $NaYF_4$:Yb^{3+},Er^{3+} nanocrystals is a clear indication of nearby oscillators as the red-emitting energy level ($^4F_{9/2}$) is not efficiently populated without assistance of high-energy phonons (Bogdan *et al.*, 2011). An inorganic shell provides better protection for the near-surface dopants than organic shells as possible interactions between UCPs and organic molecules may still cause quenching (Yi and Chow, 2007). However, an organic coating has other advantages related to direct biofunctionalization discussed in chapter 2.3.1.

To promote the hexagonal phase in nano-sized UCPs, different synthesis methods have been developed (see next section), and also doping with Gd^{3+} ions has been suggested to favor the desired phase. Wang *et al.* (2010) studied systematically how the addition of light lanthanides with a large ionic radii affects the physical and photophysical properties of $NaYF_4$:Yb^{3+},Er^{3+}/Tm^{3+}. Partial substitution of Y^{3+} ions with larger Gd^{3+} (molar percentage 30%) leads to expansion in unit-cell volume, and no traces of α-phase were observed even though a lower synthesis temperature (200°C instead of 300°C) was used. Based on the calculations, it was stated that $NaGdF_4$ is energetically more stable than $NaYF_4$ in β-phase. The particle size of Gd^{3+}-doped UCPs was decreased (from 25 nm to 10 nm) due to a slowed crystal growth rate, which was explained by an increased electron charge density. Phase transition to the β-phase increased the upconversion efficiency, but the reduction in particle size had the opposite effect. Gd^{3+} itself is not involved in the upconversion process as the lowest excited state lies in the UV region and is therefore out of reach. In brief, the

Gd^{3+} doping solved one problem but another complication led to an outcome similar to the initial state with reduced luminescence intensity.

The nano-sized UCPs have not generally been available, but research groups have mainly been synthesizing the nanocrystals themselves or have acquired them through collaboration. Commercial activities have started lately, and, for example, Intelligent Material Solutions Inc. (Princeton, NJ, USA) provides custom-made nano-sized UCPs. The size category smaller than nanoparticles is unlikely. There seems to be a minimum particle size capable of supporting efficient upconversion luminescence. Boyer and van Veggel (2010) observed a 95% decrease in quantum yield when the particle size was reduced from 30 nm to 10 nm. Apparently, it is impossible to produce upconverting lanthanide-comprising organic ligand complexes that generate anti-Stokes photoluminescence with the same efficient mechanisms as the inorganic UCPs. It is likely that the high-energy C–H and C–C vibrational oscillations of the organic ligands would effectively quench the luminescence of nearby lanthanide ions (Reinhard and Güdel, 2002). Xiao *et al.* (2005) prepared lanthanide chelates producing anti-Stokes photoluminescence in aqueous solution, but the power densities required for excitation were enormous compared to those used with inorganic UCPs.

From solid-state synthesis to solution-phase methods

The UCP synthesis (for bioanalytical applications) aims at the following characteristics: monodisperse, well-shaped, water-dispersible and phase-pure nanocrystals with a uniform size (preferably ∅ <50 nm) and high luminescence yield. The nano-sized UCPs have been synthesized using several methods, from which the most commonly used processes are co-precipitation, thermal decomposition, crystallization in high-boiling-point organic solvent, hydro- and solvothermal methods (for review see Wang and Liu (2009) or Li and Lin (2010)).

The co-precipitation method involves a particle growth step in aqueous environment (at room temperature) followed by precipitation of the precursor material and finally an annealing step in which the lattice structure of the dried UCP material is rearranged under high temperature (typically ~400°C) to reduce the number of lattice defects (Wei *et al.*, 2007; Yi *et al.*, 2004). Unfortunately, the resulting particles sinter together in the final step, which is crucial for activating the optical properties of the UCP material (Wei *et al.*, 2007). Smaller-sized material was pursued by milling and crushing (Zarling *et al.*, 1994), but fractured crystalline lattice structure results in decreased emission intensity. Kuningas *et al.* (2005c) reported that the ground UCP material (∅ 200–400 nm) produced a considerably lower luminescence intensity (only 15%) than an equal mass of the original micrometer-sized bulk material, although there were several issues of uncertainty (e.g., sedimentation of large particles during the measurement and contaminating non-fluorescent material from the grinding balls). A synthesis procedure directly leading to non-sintered UCPs was developed and patented by Sanjuro *et al.* (2000). The fluidized-bed process maintained the particle size and the monodispersity of the precursor material as the particles were kept in constant movement relative to one another by utilizing either inert or reactive gases (Li *et al.*, 2002).

The following synthetic routes do not include a post-annealing step at all as the growth of the crystals already takes place at elevated temperature. Metal trifluoroacetates thermally

decompose to give the corresponding metal fluorides at relatively low temperatures (~300°C). The thermal decomposition method in ambient pressure utilizes high-boiling organic solvents (e.g., 1-octadecene, oleylamine) in combination with organic additives containing polar capping groups and long hydrocarbon chains (e.g., oleic acid, oleylamine) (Yi and Chow, 2006; Mai *et al.*, 2006; Boyer *et al.*, 2006; Boyer *et al.*, 2007; Ye *et al.*, 2010; Cheng *et al.*, 2011). The precursors are toxic, and the experimental conditions are very rigorous as they demand a water- and oxygen-free environment protected with an inert gas. However, the quality of the resulting UCP crystals is excellent. Similar reaction conditions have also been exploited to crystallize other precursors than trifluoroacetates (e.g., rare earth chlorides) in high-boiling organic solvents (Liang *et al.*, 2011; Wang *et al.*, 2010; Heer *et al.*, 2004; Rufaihah and Zhang, 2008), but no generic name for this route has been established.

Even lower reaction temperatures (<250°C) are used in hydro- and solvothermal synthesis. Elevated pressure combined with the heat is exploited to alleviate the crystallization of precursor components (typically containing rare earth chlorides or nitrates) either in aqueous environment (hydrothermal route (Zhang *et al.*, 2009b; Ma *et al.*, 2009; Kumar and Zhang, 2009) or in organic solvent (e.g., alcohol; solvothermal route (Wang and Liu, 2008; Vetrone *et al.*, 2010a)) supplemented with organic additives (e.g., oleic acid, ethylenediaminetetraacetic acid (EDTA), cetyltrimethylammonium bromide (CTAB) or sodium citrate). The reaction conditions are easily controllable, the yields are high, and the costs are lower than those of thermal decomposition method. However, the reaction times are long (up to days) and due to the high pressure, a specialized Teflon-lined reaction vessel (i.e., an autoclave) is required.

Additives in the synthesis reactions are essential to control the morphology and especially the size of the UCPs. A chelating agent, EDTA, is known to reduce the particle size. It is anticipated that the controlled release of rare earth cations from the EDTA complex helps to separate the nucleation and the growth stages (Zeng *et al.*, 2005), which is the primary requisite for the formation of uniform particles according to the LaMer model (LaMer and Dinegar, 1950). In addition, the prepared nanoparticles are capped with EDTA on the surface, which prevents further aggregation (Zeng *et al.*, 2005). However, EDTA seems to suppress the phase transition of $NaYF_4$ material from α- to β-phase, and a higher reaction temperature is required in presence of EDTA (Wei *et al.*, 2007; Yi *et al.*, 2004). As a consequence, it may be difficult to produce phase-pure β-$NaYF_4$ materials in presence of EDTA. Similarly, oleic acid has been used to stabilize the nanoparticles, but the resulting UCPs are dispersible only to non-polar solvents and manipulation of the surface chemistry is required to realize a transformation to a hydrophilic form (Li and Lin, 2010). Other capping ligands include, for example, polyethyleneimine (PEI) (Wang and Liu, 2008), which directly functionalizes the surface with amine groups, and a water-soluble polyvinylpyrrolidone (PVP) (Li and Zhang, 2006). The addition of a cationic surfactant, CTAB, promotes formation of rod-shaped UCPs (Zeng *et al.*, 2005), but this morphology has less use in bioanalytical applications than spherical monodispersed crystals.

The first nano-sized UCPs (phosphate host lattice) prepared by the solvothermal method (Haase *et al.*, 2002) were published in 2003 (Lehmann *et al.*, 2003; Heer *et al.*, 2003), and two years later $NaYF_4$ nanocrystals with purely hexagonal crystallographic phase were reported (Zeng *et al.*, 2005; Wang *et al.*, 2005). In future, the development of UCP synthesis may be directed towards low-cost and low-temperature pathways, and methods

avoiding toxic organic solvents (Li and Lin, 2010). Safety concerns are also related to excessive fluoride reagents having low decomposition temperatures, thus possibly resulting in the production of HF gas and fluorinated species at elevated temperatures (Li *et al.*, 2008). The reproducibility and scale-up of UCP nanocrystal synthesis are limited by sensitive kinetics related to solution-phase synthesis methods (Chan *et al.*, 2010). Variation in synthesis may be caused due to alteration in heating and cooling rates, side reactions and the presence of impurities. Operations difficult to control (such as the rapid injection of precursors) hinder the scale-up attempts and automated systems with precisely controlled reaction parameters might be an attractive choice in future. Chan *et al*. (2010) have already taken the first step by introducing an automated platform for inorganic nanoparticle synthesis.

2.2.3 Upconversion efficiency

Controversial upconversion efficiencies have been reported for micrometer-sized bulk materials, and it is impossible to estimate if the discrepancy is caused by the differences in excitation power density, crystallographic phase or some other reason. These parameters are not always reported at all, and the present study conditions differ from those available in the 1970s. The modern powerful laser diodes enable excitation power densities leading to the saturation of the anti-Stokes photoluminescence, and the progress in the UCP synthesis methods has probably increased the phase-purity of the studied samples. Some sources claim that the upconversion efficiency value for Yb^{3+}–Er^{3+} doped $NaYF_4$ is maximally 3–6% (Bril *et al.*, 1975; Boyer and van Veggel, 2010; Page *et al.*, 1998), while Suyver *et al.* (2005a) reported values up to 50% for a phase-pure hexagonal material. For another dopant ion pair, Yb^{3+}–Tm^{3+}, the studies have been more congruent, stating that 1–2% of the absorbed NIR photons were upconverted and emitted at visible wavelengths no matter whether phase-purity was confirmed or not (Suyver *et al.*, 2005a; Page *et al.*, 1998). The Tm^{3+}-doped material involves a higher order process (3 or 4 absorbed photons) compared to the 2-photon system characteristic to the Er^{3+}-doped material, which explains the lower efficiency. However, the infrared emission of Tm^{3+} at 800 nm (2 absorbed photons) has an efficiency of 35% in purely hexagonal material according to Suyver *et al.* (2005a). This NIR-to-NIR upconversion might open up additional applications for the Tm^{3+}-doped UCPs in future (e.g., high contrast imaging or deep tissue imaging (Nyk *et al.*, 2008) and diffuse optical tomography (Xu *et al.*, 2009)). The upconversion efficiency of other activator ions has not been extensively studied.

2.2.4 Advantages as bioanalytical labels

Excitation with near-infrared radiation

NIR excitation provides a basis for several advantageous features that make the UCPs such interesting labels for bioanalytical applications. The main merit of the UCP-based assay technology is the absence of autofluorescence at visible wavelengths, which commonly deteriorates the detection limits of assays involving biological components. The autofluorescence originates from endogenous fluorophores of biological material and is observed at wavelengths longer than the excitation radiation, just like the fluorescence of downconverting labels utilized in the bioanalytical tests. However, under NIR excitation the possible autofluorescence is observed at the NIR region several hundred nanometers away from the visible wavelengths where the emission of UCPs is collected (anti-Stokes' shift up to 500 nm). This advantage enables, at least in theory, more sensitive bioanalytical

assays as the background fluorescence can be minimized. Another way to eliminate the autofluorescence is to use a pulsed excitation source and time-gated measurement in combination with labels having a long emission lifetime (Siitari *et al.*, 1983; Siitari *et al.*, 1983; Hemmilä *et al.*, 1984). However, time-resolution requires more sophisticated instrumentation than the technology based on photon upconversion, which relies on spectral separation of the autofluorescence.

UV radiation is recognized as harmful for several different reasons in bioanalytical assays, but is commonly used for exciting the conventional downconverting labels, while the lower-energy NIR excitation would be a convenient substitute. The absorption band of Yb^{3+} at 980 nm lies on the wavelength region of 600–1200 nm, where tissues have the lowest absorption (originating mainly from water, blood and pigments) (Waynant *et al.*, 2001; Simpson *et al.*, 1998). The penetration depth of NIR excitation in biological tissue is much greater compared to the highly absorptive UV region. In addition, NIR radiation does not cause damage to the biological specimen. This issue is more prominent in applications involving long illumination times (e.g., imaging). Straightforward reading of the luminescence intensity (e.g., from a reaction vessel) is usually a quite rapid one-time event, and the damage is negligible. Not only the specimen but also the label itself may be harmed by the high-energy UV radiation causing photodegradation, especially to organic fluorophores (Gaigalas *et al.*, 2007; Eggeling *et al.*, 1998). The NIR-excitable inorganic UCPs show extremely high photochemical stability in repeated excitation cycles (Krämer *et al.*, 2004; Ukonaho *et al.*, 2007), although some diverging data has also been published. An inexplicable photobleaching that takes place during the first minute of continuous excitation was reported by Morgan and Mitchell (2007), but an external cause such as a temperature change (Vetrone *et al.*, 2010b) might be more probable than actual photobleaching of the UCP emission. As high excitation intensities may be utilized without photodegradation of the UCPs, high signal levels are expected even from a relatively small number of UCPs. Weak emission can be collected and integrated over a longer time period under continuous excitation (Zarling *et al.*, 1994).

If energy transfer from one fluorophore to another is exploited (e.g., in proximity-based bioanalytical assays), the excitation should be perfectly selective to avoid direct excitation of the acceptor fluorophores. Exceptionally, NIR radiation allows exclusive excitation of the UCP donor, and background fluorescence originating from the acceptor is eliminated.

Photophysical properties of lanthanides

Highly structured emission is characteristic to lanthanides (Cotton, 2006), which in practice means that between the sharp emission bands (bandwidths ~20–50 nm) there is no detectable emission at all. Those wavelengths can be exploited to accurately measure the emission of other fluorescent labels without spectral contamination, which is important in applications concerning energy transfer to another fluorophore or in multiplexed assays with several fluorophores involved. Conventional organic fluorophores have much wider excitation and emission bands, which results in unwanted spectral overlap and unselective detection in systems comprising more than one such fluorophore.

UCPs with different compositions each produce different emissions (blue, green, red or NIR), and this enables detection of at least two targets or analytes simultaneously based on discriminating emission colors (Corstjens *et al.*, 2005). One excitation source is compatible

with all these materials as the Yb^{3+} ion acts as a sensitizer in all UCP materials favored presently. Similarly, quantum dots producing multiple emission colors depending on their diameter are well-known for their wide excitation band at the UV region, which suits perfectly multiplexed assays requiring only one excitation source (Hu *et al.*, 2010; Peng *et al.*, 2009). However, the UV excitation has certain drawbacks, discussed above.

Lanthanide chelates and cryptates have been utilized in the time-resolved fluorometry exploiting the long excited state lifetimes of lanthanides (Soini and Kojola, 1983; Bazin *et al.*, 2002; Selvin, 2002; Eliseeva and Bünzli, 2010). The UCPs based on lanthanide dopants share this feature (Sun *et al.*, 2009a; Bednarkiewicz *et al.*, 2010), but no applications based on the time-gated measurement has been published. There is no practical motivation to complicate the collection of the emission by waiting until the short-lived endogenous fluorescence has faded because all autofluorescence is already eliminated due to the photon upconversion.

Several emitting centers are incorporated into each UCP particle leading to high specific activity. In combination with all above-mentioned advantageous characteristics reducing the background fluorescence, this feature results in the high signal-to-background ratios appreciated in ultrasensitive bioanalytical assays.

2.2.5 Challenges in bioanalytical applications

The UCPs are inorganic hydrophobic crystals originally bearing no functional groups at all. Surface modification is used to transform the particles into a more hydrophilic form and to introduce useful functional groups on the surface. Production of a stable, reproducible coating with a desired thickness is quite challenging as such, but also the agglomeration of UCP particles during (or due to) the modification procedure must be avoided. Various solutions for surface modification are discussed in the next chapter.

The findings presented in the literature are not directly comparable because the spectral properties of the UCPs (e.g., the ratio between the emission colors (Suyver *et al.*, 2005c; Wang *et al.*, 2009b)) depend on the excitation power density. The green emission of $NaYF_4:Yb^{3+},Er^{3+}$ predominates at low power density occasions, while the intensity of the red emission increases more rapidly along with the power density followed by the emergence of a violet emission (Suyver *et al.*, 2005c; Morgan and Mitchell, 2007; Morgan and Mitchell, 2006). Suyver *et al.* (2005c) showed that population of the $^4I_{13/2}$ energy state becomes a two-photon process (possibly through a cross-relaxation CR1 in Figure 2) at high excitation power, while it otherwise is populated through a multiphonon relaxation from the state $^4I_{11/2}$ (one-photon process). Increased population of $^4I_{13/2}$ further enhances the population of the red-emitting state. The power density used is seldom reported in research papers. The power of the excitation source is easily available, but no straightforward standard method for determining the cross-section of the laser beam reaching the UCPs has been presented, and the situation remains unsolved. In addition, the results from the same set-up are not completely comparable in all cases. An increase in the sample turbidity may lead to an increased scattering of the excitation radiation. A broadened excitation area results in a lower power density and, thus, may bias the result. For example, the volume of blood cells (i.e., hematocrit) in a sample varies between patients (Zeng *et al.*, 2001), resulting in dissimilar scattering properties and unequal power densities. However, significant problems are not expected due to the scattering as the effects are mostly marginal.

Heterogeneous composition of the UCPs resulting in non-uniform spectroscopic properties may produce anomalous results in bioanalytical tests. Morgan and Mitchell (2008) found that one particular commercial UCP bulk material contained differing UCP particles, from which part produced a dominantly red emission while the others were mainly emitting at green wavelengths.

2.3 Bioconjugates of UCPs

2.3.1 Surface functionalization

After the surface modification step, UCPs are conjugated with vulnerable biomolecules, which tend to lose their functionality and three-dimensional structure at extreme conditions. Therefore, UCPs must be compatible with a water-based environment having a pH close to the physiological value (pH 7.4). A hydrophilic coating with uniform functional groups is preferred.

The modification step itself or the final result must not induce agglomeration of the individual UCP particles. Repulsion between the UCPs may be evoked by introducing either negatively or positively charged groups favoring the even distribution of the separate particles. The coating should be sufficiently transparent at excitation and emission wavelengths and stable in storage and assay conditions. The thickness of the coating layer becomes extremely relevant in the applications based on resonance energy transfer from the UCP donors to acceptor molecules, and a very thin monolayer is preferred in this case.

A universal route to functionalize an inorganic particle is to grow an amorphous *silica shell* around the particles (Figure 3a) (Graf *et al.*, 2003; Yi *et al.*, 2005; Selvan *et al.*, 2005; Darbandi *et al.*, 2005). The chemistry of silica is well known, and the properties of silica are very advantageous. It is nontoxic, chemically inert and optically transparent at visible wavelengths. In addition, a silica layer increases the negative charge of the surface and therefore enhances the dispersibility of particles in polar solvents. Hydrolysis reaction of monomeric tetraethyl orthosilicate (TEOS) followed by a condensation step generates a hydrophilic polymer that encloses UCPs while growing 3-dimensionally. The type of functionalization (e.g., amino, thiol or carboxyl group) is easily tuned by adding an appropriate organosilane (e.g., 3-aminopropyltriethoxysilane (APTS), 3-mercaptopropyl-triethoxysilane or 11-dimethylchlorosilyl undecanoyl chloride) to copolymerize with TEOS. The polymerization reaction may be carried out in alcohol (modified Stöber method (Li *et al.*, 2002; Stöber *et al.*, 1968; Ohmori and Matijevic, 1992)) in the case of UCPs already dispersible to polar solvents (Li and Zhang, 2006; Lu *et al.*, 2004; Sivakumar *et al.*, 2006; Kumar *et al.*, 2009). Hydrophobic UCPs must be coated in reverse microemulsion (Rufaihah and Zhang, 2008; Li *et al.*, 2008; Jiang and Zhang, 2010; Ylihärsilä *et al.*, 2011). Either an acid or a base catalyst (usually ammonium hydroxide) can be chosen to accelerate the reaction. The thickness of the silica shell can be adjusted from only few nanometers to tens of nanometers (Ohmori and Matijevic, 1992). In the microemulsion route, the amount of surfactant plays an important role in determining the morphology of the formed silica shell. Other critical parameters are the reaction time, temperature, concentration of reagents and the speed of stirring (Darbandi *et al.*, 2005).

Hydrophilic UCPs may be coated with a multilayer film by consecutive adsorption of polyanions (e.g., poly(styrene sulfonate); PSS) and polycations (e.g., poly(allylamine hydrochloride); PAH) (Wang *et al.*, 2005; Decher, 1997). The *layer-by-layer* (LbL)

assembly (Figure 3b) based on electrostatic attraction between the oppositely charged polymers is highly universal, allowing the use of large variety of polyelectrolytes. The thickness of the coating is controlled by limiting the number of deposited layers (one layer ~1.5 nm thick (Caruso *et al.*, 1999)). Repeated washing steps in between the deposition cycles complicate the process, but technical solutions may alleviate this inconvenience. Alternatively, adsorption of poly(acrylic acid) (PAA) without any addition of polycations has been exploited to introduce carboxylic acid groups on the UCP surface (Ukonaho *et al.*, 2007; Kuningas *et al.*, 2005a). In general, polymeric molecules build a more stable coating compared to small molecular weight monomers in adsorption-based methods as several bonds are formed simultaneously.

If a capping additive was used during the UCP synthesis, these coordinated ligands may be transformed into a functionalized coating trough oxidation, ligand attraction or ligand exchange (Figure 3c–e). Oleic acid contains a double bond in the middle of the carbon chain that can be *oxidized* into two azelaic acid molecules with the Lemieux–von Rudloff reagent containing periodate and permanganate (Lemieux and von Rudloff, 1955). The resulting particles are water dispersible and functionalized with carboxylic acid groups (Chen *et al.*, 2008). In the case of some other hydrophobic ligand not bearing a suitable double bond to oxidize, the UCP may be converted into a hydrophilic form by adding an amphiphilic copolymer (e.g., modified PAA (Yi and Chow, 2007) or modified polyethylene glycol (PEG) (Cheng *et al.*, 2011)). The original capping ligand binds the polymer by *attracting* their hydrophobic alkyl chains, and consequently the ligand is masked while hydrophilic segments of the copolymer bearing the selected functional groups cover the outer surface. Alternatively, the capping ligand may be *exchanged* to another one (e.g., to PEG diacid (Yi and Chow, 2006), dendrimer (Bogdan *et al.*, 2010), hexanedioic acid (Zhang *et al.*, 2009a) or PEG-phosphonate (Boyer *et al.*, 2010)) that coordinates more tightly on the UCP surface and provides the desired properties.

The protective inorganic shells described in the context of the nanocrystalline UCPs (see chapter 2.2.2) are not suitable for the surface functionalization, because they do not contain any functional groups. Even though several practical methods are used for surface functionalization of inorganic crystals (including quantum dots, downconverting phosphors, metallic and magnetic particles), controlled coating of colloids still remains a true technical challenge. The monomer polymerization may encapsulate several particles in a single shell and reproducible control over the thickness is challenging. The coating methods relying on the adsorption of polymers or on the coordination of ligands may suffer from stability problems during storage or in variable environments as no irreversible bond is formed between the inorganic particle and the coating. For example, Bogdan *et al.* (2011) discovered that oleate ligand protonates around pH 4 resulting in the release of oleic acid from the surface.

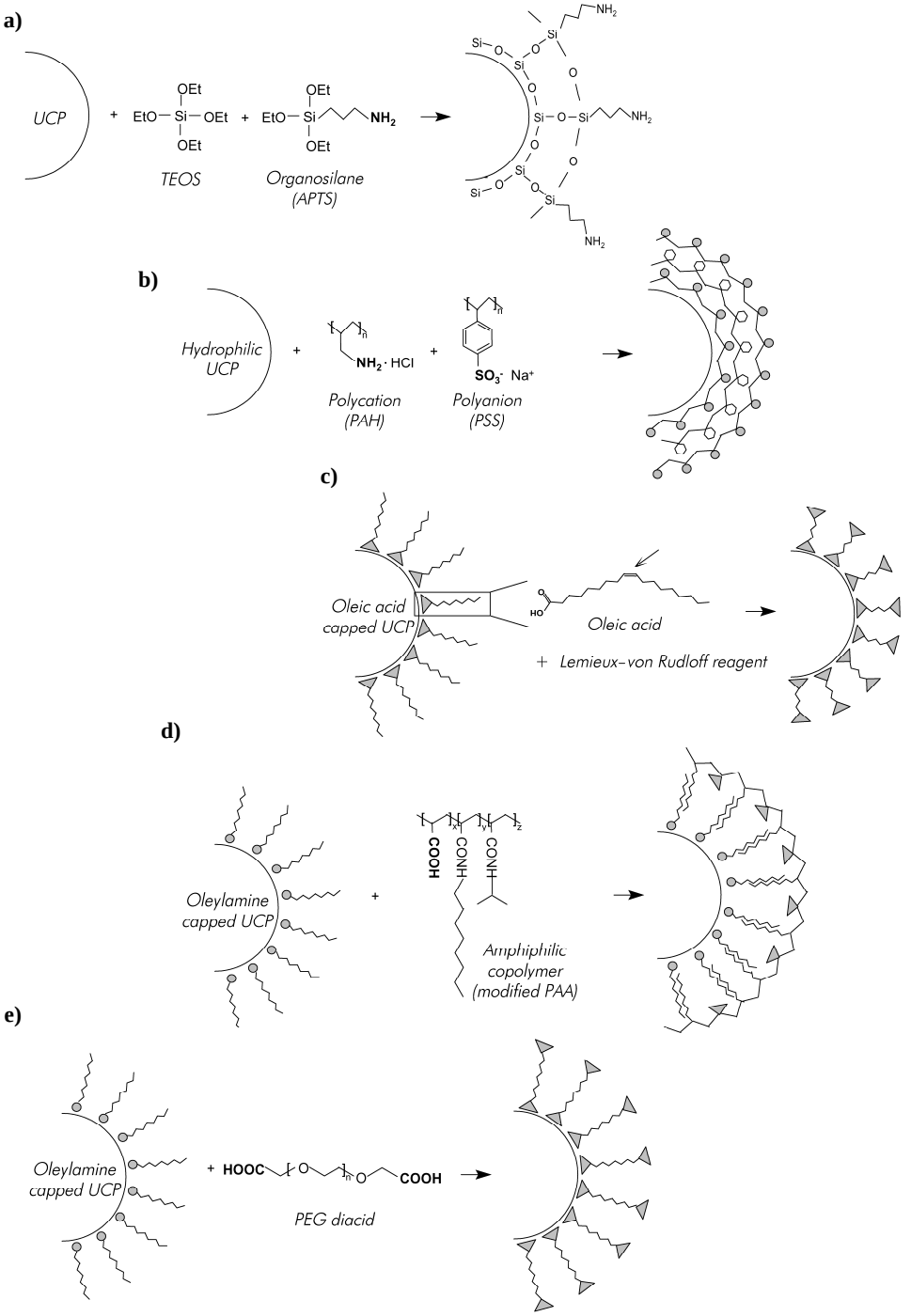

Figure 3. Selection of methods and representative reagents used for the UCP surface functionalization. (**a**) Silica-encapsulation. (**b**) Layer-by-layer assembly. (**c**) Oxidation of oleic acid ligand. (**d**) Ligand attraction. (**e**) Ligand exchange. The *gray circles* represent amino groups and the *gray triangles* carboxylic acid groups, which are both convenient groups for bioconjugation. *TEOS, tetraethyl orthosilicate; APTS, 3-aminopropyltriethoxysilane; PAH, poly(allylamine hydrochloride); PSS, poly(styrene sulfonate); PAA, poly(acrylic acid); PEG, poly(ethylene glycol).* Modified from Wang and Liu (2009).

No dramatic changes in luminescence intensity have been reported due to the UCP functionalization. The absorption properties of coating molecules are assumed to be negligible as no conjugated systems are involved. The possible effects are more likely related to the multiphonon decays of the near-surface emitting ions promoted by vibrational oscillators (e.g., OH and CH groups). A slight decrease (around 20%) in the luminescence intensity after silica-encapsulation has been discovered by a few groups (Yi *et al.*, 2004; Li and Zhang, 2006; Li *et al.*, 2008). Most of the studies involving ligand-capped UCPs have not paid any attention to the effects of functionalization, and some papers (Yi and Chow, 2006; Chen *et al.*, 2008) have stated that there are no noticeable differences in the luminescence intensity.

2.3.2 Bioconjugation

The combination of an easily-detectable UCP and a biomolecule with highly specific binding properties forms an excellent pair to be utilized in bioanalytical applications. Both parties, the biomolecule and the UCP, must bear suitable functional groups that react with each other, forming a covalent bond. Physical adsorption of biomolecules on the surface of UCP may also be exploited, but the stability of the conjugate in assay and storage conditions cannot be assured, which renders the covalent bioconjugation a more favorable method. Commonly used chemistries involve carboxylic acid, amino and thiol groups (Hermanson, 2008), which can be found in natural biomolecules composed of amino acids. Abundance of these functional groups in biomolecules is considered as an advantage, but it becomes a disadvantage if selective conjugation is targeted. Modifications including *N*-hydroxysuccinimide (NHS), maleimide and isothiocyanate groups can also be exploited especially as part of the non-biological party (e.g., UCPs or fluorophores). Another selective conjugation method known as click-chemistry involves Cu^{+}-catalyzed cycloaddition of an azido group to a terminal alkyne group (Rostovtsev *et al.*, 2002; Tornoe *et al.*, 2002). Mader *et al.* (2010) recently introduced a simple one-step click-chemistry protocol suitable for bioconjugation of the UCPs in an aqueous solution at room temperature.

The challenge in bioconjugation is to maintain the functionality of the biomolecule. In addition, the orientation of the attached molecule is critical to ensure the access to the analyte recognition site. Favorable binding orientation affects the assay performance significantly (Zhang and Meyerhoff, 2006). After the conjugation step, the excess biomolecules should be removed thoroughly without losing the UCP conjugates, and the success of the bioconjugation needs to be confirmed.

2.4 Bioanalytical applications

The various bioanalytical applications utilizing UCP labels are here divided based on the type of assay concept. The number of publications in this field has grown enormously during the last five years, expressing the ample interest among the scientists. The critical features of bioanalytical assays include limit of detection (LOD) and limit of quantification (LOQ), selectivity (effects of interferents, such as structurally similar molecules), dynamic range (the range from lowest to highest reliably measurable concentration), precision (reproducibility, repeatability) and accuracy (trueness of the measured concentration) (Davies, 2005; www.clinchem.org). Sometimes also other completely different properties, such as the time required for the final result, overall costs, portability of the analyzer or ease of use, play an important role. Depending on the analyte, its clinically relevant levels

and the intended application, some characteristics of the test are more important than others, influencing the choice of the assay type.

Photodynamic therapy exploiting the UCPs is part of the biological sciences but is excluded from this thesis, which is concentrating solely on the diagnostic applications. More borderline cases are the microscopy applications based on the UCP labels, because imaging may be regarded as a tool for pathology, drug delivery follow-up and so forth but is also used for diagnostic purposes. Although the UCPs are an extremely hot topic in the *in vivo* imaging field, it lies outside of the scope of this thesis.

2.4.1 Heterogeneous bioaffinity assays

The bound and unbound label molecules are physically separated in heterogeneous bioaffinity assays before the final measurement step. The analytes and the labels are collected onto a solid support (e.g., walls of reaction vessel, surface of particles) (Figure 4) to enable the washing procedure, usually resulting in more sensitive assays compared to the separation-free homogeneous assays. A few examples of UCP-based heterogeneous bioaffinity assays are listed in Table 1. As the luminescent label in this case is a particle, kinetics and steric hindrance play important roles, and the size of the particle also affects the assay performance. Generally, the smaller particles resembling molecular labels are more practical, but the thermodynamic instability of the nanoparticles increases with decreasing size, leading to particle aggregation. According to Näreoja *et al.* (2009), the particle size (25–100 nm) does not influence the non-specific binding, but the LOD of the assay may be improved by limiting the number of label particles in the bioaffinity reaction.

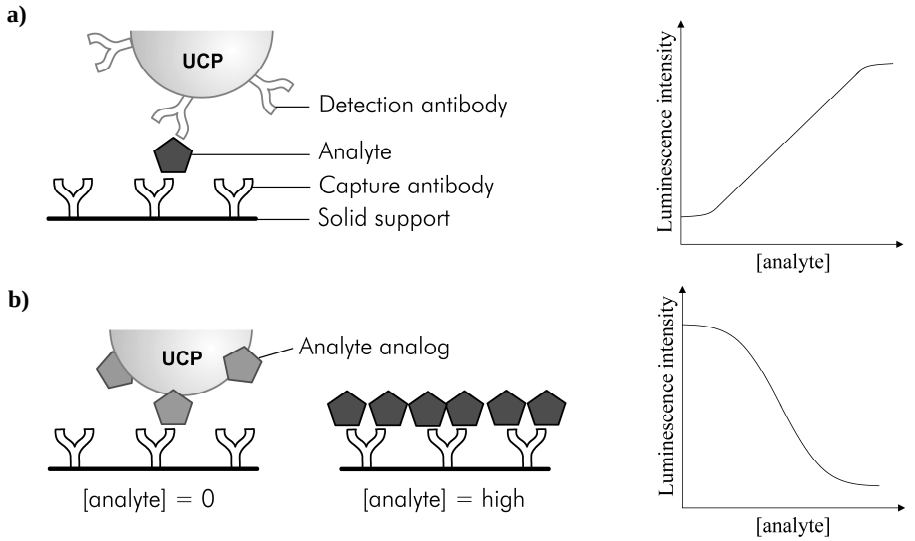

Figure 4. Principles of the basic immunoassay types. (**a**) A sandwich assay also called an immunometric assay or a two-site bioaffinity assay. The UCP conjugate is bound to the solid support through the analyte and a sandwich complex is formed. The number of bound UCPs increases with the analyte concentration. (**b**) A competitive assay. The analyte analog conjugated to the UCP and the actual analyte compete for the binding sites on the solid support, resulting in a decreasing UCP emission intensity with the growing analyte concentration.

The very first papers introducing the UCPs in bioanalytical application were published by the researchers working for SRI International (California, USA) in the late 1990s. Wright *et al.* (1997) carried out a sandwich immunoassay for a food poisoning Staphylococcal

enterotoxin B (SEB) both in a glass capillary providing miniature binding regions and on magnetic glass beads. The washing steps in capillary were realized with a peristaltic pump creating a liquid flow. Magnetic beads, in turn, are easy to control with a magnetic field, which enabled repeated replacement of the surrounding liquid to remove the unbound components. It was documented that the LOD of the SEB assay (35 fmol in capillary or 180 fmol on beads) was limited only by the non-specific binding of the UCPs. A sandwich immunoassay in a microtiter plate format has been reported for free prostate-specific antigen (f-PSA) (Ukonaho *et al.*, 2007), which is widely used as a prostate cancer marker. The dynamic range of this relatively sensitive assay (LOD 20 fM for f-PSA) extended over three orders of magnitude, after which there were no more UCP conjugates left to form the sandwich complexes. An increased number of UCPs in the reaction vessel would enable detection of even greater concentrations of f-PSA, but the LOD would consequently be compromised due to increased non-specific binding of the label. A similar sandwich assay in dual-parametric format was constructed to recognize both IgM and IgG antibodies against cytomegalovirus in order to differentiate the early and the secondary immune response (Corstjens *et al.*, 2005). Green-emitting Yb^{3+}–Er^{3+} doped UCPs and blue-emitting Yb^{3+}–Tm^{3+} doped UCPs were utilized to discriminate between the two analytes in the same reaction. In addition to the protein analytes, single-stranded DNA has also been detected in the femtomole range. Wollenberg *et al.* (1997) and Wang and Li (2006) have reported sandwich hybridization assays utilizing magnetic beads as a solid support.

The features of the ground UCP bulk material ($NaYF_4$:Yb^{3+},Er^{3+}, ∅ 280 nm) in heterogeneous model assays carried out in standard microtiter wells were studied by Kuningas *et al.* (2005a). The lowest detectable amount of these UCPs bound to a microtiter well through a strong biotin–streptavidin interaction was determined to be 0.75 ng. Actually, the focused laser beam excited only less than 1% of the surface area of the well and probably only few picograms of UCPs were bound to that area, corresponding roughly to tens of individual particles. According to this result, the UCPs should enable highly sensitive assays if non-specific binding is minimal. The luminescence intensity of the UCPs increased linearly over 4 orders of magnitude, demonstrating the high specific activity of the UCP labels, which allows a wide dynamic range in heterogeneous assays. A reflective solid surface (white-colored microtiter well) appears to enhance the anti-Stokes photoluminescence by about 100 times, from which only a 5-fold increase can be explained by the reflections, while the basis of the phenomenon leading to the remaining 20-fold increase remains unclear (Kuningas *et al.*, 2005b). The effect was discovered both in fluoride and oxysulfide hosts doped with Yb^{3+}–Er^{3+} pair and was even more pronounced at the red emission wavelengths compared to the green ones. Unfortunately, the LOD (1.5 fmol) of the model sandwich assay for biotinylated protein was not improved in white wells compared to the transparent ones as the luminescence arising from the non-specifically bound UCPs was enhanced equally.

The major obstacle limiting the LOD of the heterogeneous assays is the non-specific binding of the UCPs, which is a problem shared by particle labels collectively. The fact that the UCP technology avoids all the other sources of background luminescence especially highlights the importance of minimizing this problem.

Table 1. Examples of heterogeneous bioaffinity assays based on the UCP labels.

Analyte	Type of assay	Limit of detection	Sample volume	UCP material (coating, diameter)	Reference
In glass capillary					
Staphylococcal enterotoxin B (SEB)	Sandwich immunoassay	35 fmol	- (spiked buffer)	Y_2O_2S:Yb,Er (silica, ∅ 400 nm)	Wright *et al.* (1997)
On magnetic beads					
Staphylococcal enterotoxin B (SEB)	Sandwich immunoassay	180 fmol (1.8 nM)	100 µL (spiked buffer)	Y_2O_2S:Yb,Er (silica, ∅ 400 nm)	Wright *et al.* (1997)
Target DNA (model assay)	Sandwich hybridization	- (7.8 nM)	- (spiked buffer)	$NaYF_4$:Yb,Er (LbL, ∅ 50 nm)	Wang L. & Li (2006)
Streptococcus pneumoniae lytA gene (pathogen)	Sandwich hybridization	low amol range (<1 ng genomic DNA)	- (isolated genomic DNA)	Y_2O_2S:Yb,Er (silica, ∅ 400 nm)	Corstjens *et al.* (2005)
In microtiter wells					
Biotinylated small molecule (model assay)	Competitive bioaffinity assay	~50 fmol (1 nM)	50 µL (spiked buffer)	$NaYF_4$:Yb,Er [a)] (PAA, ∅ 280 nm)	Kuningas *et al.* (2005a)
Biotinylated large molecule (model assay)	Sandwich bioaffinity assay	~0.75 fmol (15×10^{-3} nM)	50 µL (spiked buffer)	$NaYF_4$:Yb,Er [a)] (PAA, ∅ 280 nm)	Kuningas *et al.* (2005a)
		1.5 fmol (30×10^{-3} nM)	50 µL (spiked buffer)	$NaYF_4$:Yb,Er [a)] (PAA, ∅ 240 nm)	Kuningas *et al.* (2005b)
Anti-cytomegalo-virus IgM & IgG (immune response)	Dual-parameter sandwich immunoassay	10 000-fold dilution of positive serum	- (serum)	Y_2O_2S:Yb,Er & Y_2O_2S:Yb,Tm (silica, ∅ 400 nm)	Corstjens *et al.* (2005)
Free prostate specific antigen (f-PSA) (cancer marker)	Sandwich immunoassay	0.2×10^{-3} fmol (20×10^{-6} nM)	10 µL (spiked buffer)	Y_2O_2S:Yb,Er [a)] (PAA, ∅ 260 nm)	Ukonaho *et al.* (2007)

Abbreviations: LbL, layer-by-layer coating; PAA, poly(acrylic acid) coating.
[a)] Ground UCP bulk material

2.4.2 Array-type multiplexed assays

If several analytes are connected somehow to the condition under investigation, it may be cost-effective to use multiplexed assays capable of analyzing them all simultaneously from one reaction mixture. If the detection of analytes is based on different-colored fluorophores, maximally 4 to 5 analytes may be simultaneously distinguished due to the limitations set by the overlapping fluorescence spectra. Usually computer algorithms are required to solve the relative proportions of slightly overlapping fluorophores. The analytes must be separated by location instead of fluorescence color to open up the opportunities for infinite multiplexing. If the analytes are identified based on the location of the binding

region at the array, all bound analytes can be visualized with the same fluorescent label molecule (e.g., UCP).

Both oligonucleotides and proteins have been spotted on glass slides and detected with UCP conjugates. The simplest test involved spotting of biotinylated immunoglobulins on the slides and direct visualization of the spots (diameter 900 µm) with streptavidin-conjugated UCPs ($NaYF_4$:Yb^{3+},Er^{3+} with magnetic core, ∅ 68 nm) (Lu *et al.*, 2004). A more practical nucleic acid microarray (spot diameter 150 µm) was constructed to measure the expression levels of 24 housekeeping genes of bladder carcinoma cells (van de Rijke *et al.*, 2001). UCPs were detected with a modified fluorescence microscope, which had a Xenon lamp as an excitation source instead of more optimal laser diode. Nonetheless, the bright emission of UCPs (Y_2O_2S:Yb^{3+},Er^{3+}, ∅ ~400 nm) allowed 4 times better LOD than an organic cyanine dye Cy5, which is in common use in microarray applications.

The high-content capacity of microarrays has been transferred from glass slides to microtiter wells, which are widely used reaction vessels in high-throughput concepts. Ylihärsilä *et al.* (2011) demonstrated genotyping of ten common adenovirus genotypes with an array-in-well platform and validated the assay successfully with clinical samples. Eleven selective probe spots (diameter 375 µm) in three replicas and positive control oligonucleotide spots were printed on the bottom of standard 96-well plates. Extracted DNA was amplified using generic biotinylated primers, which allowed the detection of all adenovirus genotypes with streptavidin-conjugated UCPs ($NaYF_4$:Yb^{3+},Er^{3+}, ∅ 55 nm). Cross-hybridization of similar sequences creates a challenge when a large number of probes is combined in one array. Therefore, the identification of the genotype was based on a hybridization pattern rather than hybridization with only one type of probe. The UCPs were detected with a special imaging device, which is simpler and the acquisition costs lower compared to a confocal microscope scanner.

The repetitive scanning and long-lasting imaging of microarrays expose the fluorescent labels to the excitation radiation for an extended period of time and the stability of the label becomes relevant. The organic fluorophores tend to lose their fluorescent properties gradually under intense excitation. As the emitting ions of the UCPs are located in a protective inorganic crystal lattice, no photodegradation is expected. In addition to the outstanding photostability of the UCPs, the high emission intensity renders the UCPs an attractive label option for microarray applications. Now that nano-sized UCPs are available, the dynamic range in the compact binding region is less limited by the size of UCPs and the diameter of the spots may be reduced to allow larger amounts of information per certain area of solid support.

2.4.3 Lateral flow tests

Lateral flow (LF) tests, also known as immunochromatographic tests, are typically carried out on nitrocellulose-based strips or other polymeric materials allowing capillary flow of the solution containing the sample and labels (Figure 5). The LF platform is attractive due to its suitability for low-resource situations such as point-of-care and on-site testing. The simple home pregnancy test is a well-known example of a qualitative LF test providing a visual result evaluated with the naked eye. Colored particle labels (e.g., colloidal gold, latex beads) are used for applications utilizing visual readout. More sensitive and also quantitative results are obtained if an optical reader is used for detecting the label in question.

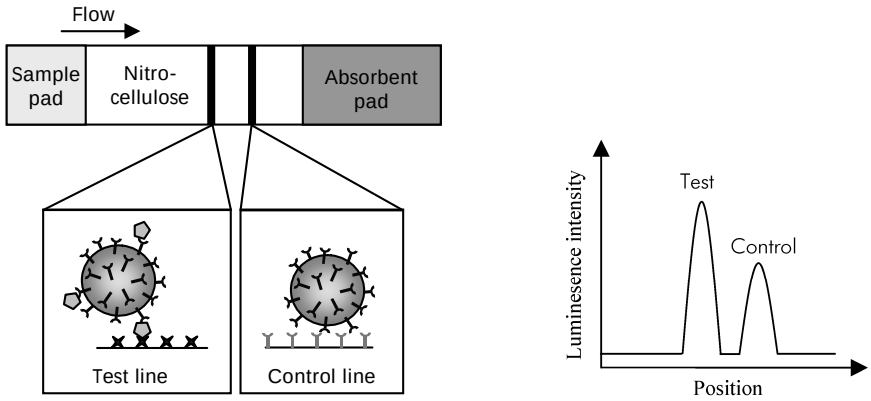

Figure 5. Principle of the sandwich-type lateral flow test based on the UCP labels. Sample together with the UCP conjugates flow through the nitrocellulose membrane towards the absorbent pad. UCP labels are captured on the test line via the analyte (*gray pentagon*), while binding to the control line occurs irrespective of the analyte and verifies the successful flow. The strip is optically scanned to record the UCP emission at capture lines.

OraSure Technologies, Inc. (former STC Technologies; Pennsylvania, USA) with its research partners SRI International (California, USA) and Leiden University Medical Center (the Netherlands) were the first to demonstrate the use of UCPs in lateral flow tests for various analytes. The first papers described immunoassays for the cardiac marker troponin T (sandwich-type assay for a protein), for a food pathogen (sandwich-type assay for a whole bacteria cell) and for several metabolites of drugs of abuse (competitive assay for small molecules) (Niedbala *et al.*, 2000; Niedbala *et al.*, 2001). Examples of the UCP-based LF immunoassays have been collected in Table 2. They are mainly targeted at pathogen identification (food pathogens and possible biological weapons) or infection diagnostics. The LOD of these immunoassays has not been directly compared with other label technologies in LF format, but the large number of LF tests for the pregnancy hormone human chorionic gonadotropin (hCG) provides data for comparisons. The preliminary studies with UCP labels enabled a 10–100-fold improvement in the detection limit (LOD <1 mIU/mL in a non-biological matrix) compared to gold and colored latex particles (Hampl *et al.*, 2001). However, modern hypersensitive hCG assays based on enzyme-catalyzed chemiluminescence of luminol may reach the LOD of even 1 nIU/mL (Kim and Pyun, 2009), which is 10^6 times better than the UCP-based result. On the other hand, the technology based on chemiluminescence requires the addition of luminol substrate and the activity of the enzyme needs to be assured, which may be problematic in low-resource situations. Comparisons of the UCP-based LF immunoassays with other methods than LF format have been carried out in many papers. Corstjens *et al.* (2008a; 2008b) and Li *et al.* (2009) have reported 10–20-fold better analytical sensitivities compared to ELISA tests (enzyme-linked immunosorbent assay).

A method for nucleic acid detection on the LF platform (Table 3) has mainly been studied by Corstjens's research group in Leiden University Medical Center. The kinetic characteristics of nucleic acid hybridization between complementary sequences are more complicated at the solid–liquid interface (e.g., immobilized probe) compared to the hybridization of strands in solution (Levicky and Horgan, 2005). In addition, the capillary flow on LF strip limits the contact time between the target sequence and the test line probes, therefore requiring a fast annealing rate. Consequently, Corstjens *et al.* did not use nucleic acid probes on LF test lines, but captured the pre-hybridized double-stranded

complexes on the test line through haptens (Corstjens *et al.*, 2001). Two specific haptenized probes conjugated with either biotin or digoxigenin were hybridized with the amplified and heat-denatured target sequence (human papillomavirus type 16) in the solution phase. The formed sandwich complex can be captured and detected with universally adaptable LF strips containing an avidin test line and UCP conjugates recognizing digoxigenin hapten. The LF platform allowed detection of low attomole quantities of target DNA molecules, which translates into a 10^2–10^4-fold improvement in LOD compared to gold nanoparticle labels in an LF test and up to 10^5-fold compared to ethidium bromide-stained agarose gel electrophoresis (Corstjens *et al.*, 2005). The nucleic acid amplification step may sometimes cause false results due to amplification artifacts or inhibition. In addition, the required thermal cycler and polymerase enzyme add the complexity and costs of the test. It was anticipated, that an ultrasensitive assay could possibly detect nucleic acid sequences without any amplification step. Based on a study, less than 1 ng of fragmented genomic *Streptococcus pneumoniae* DNA, corresponding to approximately 10^6 pathogenic bacterial cells, was required to detect the presence of one gene without any amplification step (Zuiderwijk *et al.*, 2003). This LOD may be acceptable for applications where the sample availability is not limited. However, by multiplying the number of targets (e.g., additional probe sets, multi-copy gene or abundant mRNA target), the amplification-free concept could be more widely applicable. Still, only single-stranded targets (e.g., RNA) can be quantified at ambient temperature because a thermal denaturation of the double-stranded genomic DNA at elevated temperature precedes the hybridization of haptenized probes (Corstjens *et al.*, 2003). In general, the amplification step is often included in nucleic acid detection.

Several variations of LF tests exist. The UCPs may be mounted on the LF strip in advance to allow a very simple assay procedure involving only addition of the sample (*single flow* format) (Yan *et al.*, 2006; Huang *et al.*, 2009). An alternative version is called the *consecutive flow* format, which involves a washing step to remove unbound sample material before addition of the UCP conjugate to the LF strip (Malamud *et al.*, 2005; Corstjens *et al.*, 2007). Various analytes may be detected simultaneously from one sample by discriminating between the analytes on the basis of test line position (Niedbala *et al.*, 2001; Hampl *et al.*, 2001; Corstjens *et al.*, 2007).

The ambitious aim of combining immunoassays and nucleic acid detection into a one integrated microfluidic system provides, when successfully completed, extensive data for simultaneous identification of pathogen (based on antigens, DNA and RNA) and evaluation of the host immunological responses (emerging antibodies) from a single non-invasive saliva sample (Malamud *et al.*, 2005; Corstjens *et al.*, 2007; Chen *et al.*, 2010a). The system is constructed on a disposable, self-contained microfluidic cassette comprising all reagents for upstream sample pre-treatment and an LF strip for multiplexed analysis of the processed sample. All operations are carried out automatically by the analyzer (Wang *et al.*, 2006; Chen *et al.*, 2005; Chen *et al.*, 2007), and the result is obtained in less than one hour, which sets strict time limits on each step (Qiu *et al.*, 2011). Different versions of portable analyzers with manual, mechanical or thermal actuations have been described, but no integrated LF strip scanner for reading the UCP emission has yet been included (Qiu *et al.*, 2011; Qiu *et al.*, 2009; Liu *et al.*, 2009).

Table 2. Examples of lateral flow immunoassays based on the UCP labels. The LF strips were constructed from a nitrocellulose membrane, and the single flow format was used if not stated otherwise.

Analyte	Special	Limit of detection	Sample volume	UCP material (coating, diameter)	Reference
Sandwich immunoassays					
Escherichia coli O157:H7 (food pathogen)	-	10^3 org./mL	100 µL (diluted culture)	Y_2O_2S:Yb,Er/Tm (silica, ∅ 400 nm)	Niedbala *et al.* (2000, 2001)
Human chorionic gonadotropin (hCG) (pregnancy hormone)	-	0.4 fmol (~0.9 mIU/mL)	150 µL (spiked buffer)	Y_2O_2S:Yb,Er (silica, ∅ 400 nm)	Hampl *et al.* (2001)
Anti-hepatitis C virus & anti-HIV or anti-tuberculosis antibodies (response to infection)	Multiplexed [a] strip, consecutive flow	Qualitative (not reported)	2 or 10 µL (diluted plasma)	Y_2O_2S:Yb,Er (silica, ∅ 400 nm)	Corstjens *et al.* (2007)
Respiratory syncytial virus (RSV) antigen (respiratory infection)	-	Semi-quantitative (not reported)	200 µL (naso-pharyngeal wash)	Y_2O_2S:Yb,Er (silica, ∅ 400 nm)	Mokkapati *et al.* (2007)
Schistosoma sp. antigen (parasite)	-	~0.1×10^{-3} fmol	10 µL (diluted serum)	Y_2O_2S:Yb,Er (silica, ∅ 400 nm)	Corstjens *et al.* (2008a)
Interferon gamma (cytokine)	-	<5×10^{-3} fmol	40 µL (stimula-ted cell culture)	Y_2O_2S:Yb,Er (silica, ∅ 400 nm)	Corstjens *et al.* (2008b)
	Cyclo-olefin polymer strip, 2D scanning	0.3 fmol	100 µL (spiked buffer)	Y_2O_2S:Yb,Er (silica, ∅ 400 nm)	Li J. *et al.* (2008)
Yersinia pestis (pathogen, possible biological weapon)	-	10^4 CFU/mL	100 µL (diluted culture)	$NaYF_4$:Yb,Er (silica, ∅ 400 nm)	Yan *et al.* (2006)
Yersinia pestis F1 antigen (pathogen, possible biological weapon)	-	3 fmol	10 µL (spiked buffer)	$NaYF_4$:Yb,Er (silica, ∅ 400 nm)	Huang *et al.* (2009)
Anti-*Yersinia pestis* antibodies (response to infection)	Multiplexed [a] LF disk	From tens to thousands of fmol	10 µL/strip (serum)	$NaYF_4$:Yb,Er (silica, ∅ 250 nm)	Hong *et al.* (2010)
Anti-hepatitis B antibody (response to infection)	-	20 mIU/mL	70 µL (serum)	$NaYF_4$:Yb,Er (silica, ∅ 250 nm)	Li L. *et al.* (2009)
Brucella (pathogen, possible biological weapon)	-	5×10^6 CFU/mL	70 µL (pure culture)	$NaYF_4$:Yb,Er (silica, ∅ 400 nm)	Qu *et al.* (2009)
Anti-HIV antibody (response to infection)	Automated [b] microfluidic system, conse-cutive flow	Qualitative (not reported)	10 µL (spiked plasma / spiked saliva)	Y_2O_2S:Yb,Er/Tm (silica, ∅ 400 nm)	Liu *et al.* (2009) / Qiu *et al.* (2009)
Competitive immunoassays					
Drugs of abuse (for 4 drugs)	Multiplexed [a] strip	Hundreds of fmol (<5 ng/mL)	100 µL (spiked saliva)	Y_2O_2S:Yb,Er/Tm (silica, ∅ 400 nm)	Niedbala *et al.* (2000, 2001)

Abbreviations: HIV, human immunodeficiency virus; CFU, colony-forming unit (viable bacteria).
[a] Several test lines on the same strip one after the other or separate strips positioned in a multi-channel LF disk.
[b] Self-contained microfluidic cassette comprising a pumping system, reagents, mixer and lateral flow strip.

Table 3. Examples of nucleic acid detection on the lateral flow platform based on the UCP labels. The LF strips were constructed from a nitrocellulose membrane, and the single flow format was used.

Analyte	Special	Limit of detection	Sample volume	UCP material (coating, diameter)	Reference
Nucleic acid detection					
Human papilloma-virus type 16 (HPV16; cause of cancer)	Separate PCR amplification	~30×10^{-3} fmol (10 pg)	2 µl (PCR solution)	Y_2O_2S:Yb,Er (silica, ∅ 400 nm)	Corstjens *et al.* (2001)
Streptococcus pneumoniae (pathogen)	No PCR amplification	<1000 pg genomic DNA (10^6 bacteria)	10 µL (digestion solution)	Y_2O_2S:Yb,Er (silica, ∅ 400 nm)	Zuiderwijk *et al.* (2003)
Emiliania huxleyi cDNA (phytoplancton)	No PCR amplification, no denaturation	0.1 fmol (3 pg ssDNA)	<10 µL	Y_2O_2S:Yb,Er (silica, ∅ 400 nm)	Corstjens *et al.* (2003)
Vibrio cholerae (pathogen)	Separate PCR amplification	0.3×10^{-3} fmol (0.1 pg)	5 µL (PCR dilution)	Y_2O_2S:Yb,Er (silica, ∅ 400 nm)	Corstjens *et al.* (2005)
Bacillus cereus (food pathogen)	Microfluidic system [a)]	5 fmol (1000 pg)	8 µL (PCR solution)	Y_2O_2S:Yb,Er (silica, ∅ 400 nm)	Wang J. *et al.* (2006)
	Microfluidic system [a)]	0.5 fmol (100 pg)	10 µL (PCR solution)	Y_2O_2S:Yb,Er (silica, ∅ 400 nm)	Liu *et al.* (2009)
	Microfluidic system [a)]	10^3–10^4 cells/mL	100 µL (spiked saliva)	Y_2O_2S:Yb,Tm (silica, ∅ 400 nm)	Chen D. *et al.* (2010a)

Abbreviations: cDNA, complementary DNA; ssDNA, single-stranded DNA.
[a)] Integrated DNA amplification (PCR), lateral flow and UCP detection (optical scanning) combined with microfluidistics.

Most of the commercial LF tests presently are based on colloidal gold as a label. The UCP labels provide improvements in the assay performance without any apparent disadvantages. However, if low detection limits are not required, the visual read-out of the colloidal gold is of course a simple and cost-effective option. In more demanding situations, the UCP label can be quantified with relatively simple instrumentation, which suits well the on-site testing usually associated with the LF platform.

2.4.4 Proximity-based homogeneous assays

Simple automation can be achieved with homogeneous assay concepts, also termed "mix-and-read" protocols or separation-free assays. Energy transfer between closely situated fluorophore and absorbing species can be employed in bioanalytical assays to indicate specific binding events. Two different energy transfer mechanisms combined with the UCP donors have been reported: resonance energy transfer and evanescent wave coupling.

Upconversion resonance energy transfer

The traditional resonance energy transfer (RET) discovered by Theodor Förster (1948) was described between the singlet states of two fluorophores. The lanthanides producing long-

lived luminescence from the triplet state mainly obey the same rules, but certain differences also exist and the term lanthanide (or luminescence) resonance energy transfer (LRET) is typically used. The energy is transferred over a short distance between the two resonant energy states through dipole–dipole interactions. The efficiency of RET strongly depends on the distance between the two molecules and it is typically quite inefficient over distances greater than 10 nm. As the dimensions of biomolecules in general are at the same range, RET can be utilized in the detection of biomolecules: if two biomolecules labeled with either a suitable donor or an acceptor are specifically bound to each other, the distance between the labels is short enough to facilitate the RET. Either the increase of sensitized acceptor emission intensity or decreasing donor emission intensity may be monitored. As RET is a close-proximity process, the acceptors further away remain "invisible".

The upconversion RET (UC-RET) from a UCP donor shares the valuable characteristics of LRET (Selvin, 1996) but also has some extra advantages mainly covered already in chapter 2.2.4. First, the Förster radius R_0 (the distance at which 50% of the energy is transferred) between the donor and the acceptor is longer for the lanthanides (even >7.5 nm) compared to conventional fluorophores and thus allows efficient energy transfer over extended distances. Second, the signal-to-background ratio of luminescence intensity measurement is improved due to the elimination of autofluorescence (with spectral separation or temporal resolution), which enables detection of lower signal levels corresponding to relatively large distances (potentially 4 times the R_0). As a consequence, the distance between the donor and the bound acceptor may be a bit longer than is generally the case with non-lanthanide donors. Third, the NIR excitation source for the UCP donor is incapable of directly exciting the acceptor fluorophores, and the observed acceptor emission originates entirely from those acceptors excited through the UCPs.

Several studies exploiting the UCPs as RET donors have been published since 2005 (Table 4). Two research groups independently submitted their first reports of the UC-RET within a few weeks, both using the strong binding affinity of biotin and (strept)avidin (Wilchek *et al.*, 2006; Diamandis and Christopoulos, 1991) to bring the donor and the acceptor into close proximity. Wang L. *et al.* (2005) utilized the absorption properties of gold nanoparticles to quench the green emission of nano-sized β-$NaYF_4$:Yb^{3+},Er^{3+} crystals, and they were able to detect 0.5–370 nM avidin concentrations with a sandwich-type bioaffinity assay (Figure 6a). However, even though the UCP emission was quenched as much as 70% (corresponding to 3.3-fold change) in tandem with the increasing avidin concentration, no control data providing information about the quantity of the photon reabsorption processes or other non-specific effects was reported. Kuningas *et al.* (2005c) measured, in contrary, the amount of biotin by following the sensitized emission intensity of a fluorescent B-phycoerythrin acceptor in a competitive bioaffinity assay (Figure 6b). The submicrometer-sized UCP crystals were physically bead-milled from a bulk La_2O_2S:Yb^{3+},Er^{3+} or Y_2O_2S:Yb^{3+},Er^{3+} material. Regardless of the less optimal UCPs, a similar detection limit (below 0.5 nM) to the above-mentioned avidin assay was achieved. Kuningas *et al.* also studied the proportion of background emission mainly originating from the unbound acceptors reabsorbing the UCP emission through a photon-mediated way, which is especially prominent in the case of UCP particles having a relatively large volume compared to the surface area. The activator ions locating in the core parts of the particle are too far away to participate in RET, and they can only take part in producing background luminescence. As the quantity of the photon reabsorption is concentration-dependent, it is possible to maximize the signal-to-background ratio of the homogeneous

RET-based assay by carefully optimizing the donor and acceptor concentrations. Kuningas *et al.* achieved a 10-fold and even greater signal modulation in association with increasing analyte concentration.

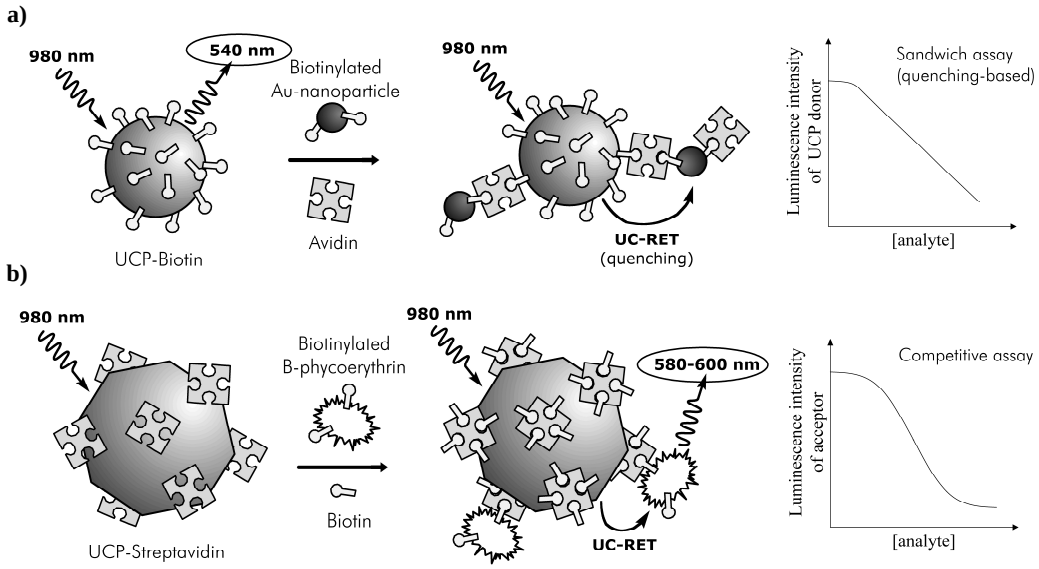

Figure 6. Principles of the first published upconversion RET-based assays. (**a**) Sandwich-type assay for detection of avidin (Wang L. *et al.*, 2005). Presence of avidin results in linearly decreasing UCP emission intensity due to quenching of close-proximity gold nanoparticles. (**b**) Competitive assay for biotin (Kuningas *et al.*, 2005c). Biotin blocks the binding of the biotinylated acceptor fluorophore, resulting in a sigmoidal inhibition curve with decreasing sensitized emission intensity along with increasing biotin concentration.

Later, Kuningas *et al.* developed the previous proof-of-principle into a competitive immunoassay for estradiol hormone (17β-estradiol, E2) (Kuningas *et al.*, 2006). The assay was modified to be totally compatible with whole blood by introducing a far-red acceptor matching with the red emission band (~660 nm) of the UCP (Kuningas *et al.*, 2007). No reduction of overall emission intensity was observed in strongly red-colored blood when compared to the colorless buffer solution, because wavelengths only above the absorption range of blood were utilized. The simple homogeneous assay principle and minimal sample pre-treatment appears to be a smart combination for low-resource or fast-operating applications.

Wang M. *et al.* (2009a) developed a sandwich-type assay for an antibody. β-$NaYF_4$:Yb^{3+},Er^{3+} nanocrystals and gold nanoparticles were bridged by a sandwich complex formed from 3 antibodies, which is likely to have dimensions greater than typical LRET distance. However, gold is capable of surface energy transfer (SET) from dipole to a metallic surface, which enables efficient energy transfer up to 25-nm distance (Ling and Huang, 2010). The maximal quenching efficiency (80%) and the dynamic range (6–225 nM) were consistent with the similar avidin assay (Wang *et al.*, 2005). A UC-RET-based system has also been utilized to investigate the interactions of a lectin (carbohydrate binding protein) and a sugar molecule (Bogdan *et al.*, 2010). The authors anticipated that this kind of assay could be utilized, for example, in detection of pathogens expressing mannose residues on the cell surface.

Many of the bioanalytical applications exploiting UC-RET are based on nucleic acid hybridization. An oligonucleotide sensor detecting a point mutation associated with sickle cell disease (Kumar *et al.*, 2009) was developed based on an earlier proof-of-principle sandwich hybridization assay (Zhang *et al.*, 2006). In the further advanced version, the rhodamine (TAMRA) acceptor was replaced by a DNA-intercalating dye (SYBR Green I cyanine dye) (Kumar and Zhang, 2009). The fluorescence quantum yield of the intercalating dye increases significantly when bound to a double-stranded DNA compared to a single-stranded one, and an increase in sensitized acceptor emission intensity was observed. The LOD (0.1 nM) of this simple sensor was about 6 times better than that of the first version with the TAMRA acceptor. The SYBR Green I absorbs at blue wavelengths and, therefore, Yb^{3+}–Tm^{3+}-doped UCPs were used as donors. If the UCPs were omitted from the sensor system and the NIR excitation was replaced with visible light, the LOD was impaired by a factor of 3500, highlighting the advantages of the UCP labels. Another application based on UC-RET to SYBR Green I was constructed to detect the presence of Hg^{2+} ions (Kumar and Zhang, 2010). A thymine-rich oligonucleotide conjugated with the UCP remains single-stranded in the absence of mercury at 50°C, but the thymine–Hg^{2+}–thymine coordination chemistry induces formation of a double-stranded hairpin structure, giving rise to the sensitized acceptor emission intensity. A detection limit for mercury was reported to be 0.06 nM.

To summarize, subnanomolar (<1 nM) detection limits are typical for the assay concepts based on the UC-RET. The analyte types vary from proteins and hormones to carbohydrates, oligonucleotides and even metal ions. Green, red and blue emitting Er^{3+} and Tm^{3+} activators have been utilized as energy donors and the selection of used acceptors is extensive: organic fluorophores, fluorescent proteins, intercalating dye and colloidal gold. The UC-RET to quantum dots has also been shown in heterostructures containing UCPs, but these specific examples did not involve a direct bioanalytical scope (Li *et al.*, 2008; Yan *et al.*, 2010).

Table 4. Examples of homogeneous bioaffinity assays based on UCP labels.

Analyte	Type of assay	Acceptor	Limit of detection	UCP material (coating, diameter)	Reference
Ligand binding assays					
Avidin (model assay)	Sandwich-type	Colloidal gold (quencher)	0.5 nM	$NaYF_4$:Yb,Er (LbL, ∅ 50 nm)	Wang L. *et al.* (2005)
Biotin (model assay)	Competitive	B-phycoerythrin	<0.5 nM	La_2O_2S:Yb,Er [a)] (PAA, ∅ 300 nm)	Kuningas *et al.* (2005c)
Immunoassays					
17β-estradiol (hormone)	Competitive	Oyster 556	<0.5 nM	La_2O_2S:Yb,Er [a)] (PAA, ∅ 280 nm)	Kuningas *et al.* (2006)
		AlexaFluor 680	<0.5 nM	La_2O_2S:Yb,Er [a)] (PAA, ∅ 390 nm)	Kuningas *et al.* (2007)
IgG (immune response)	Sandwich-type	Colloidal gold (quencher)	5.9 nM	$NaYF_4$:Yb,Er (silica, ∅ 47 nm)	Wang M. *et al.* (2009a)
Nucleic acid detection					
Target DNA (26 nt)	Sandwich hybridization	TAMRA	1.3 nM	$NaYF_4$:Er (silica)	Zhang P. *et al.* (2006)
Target DNA (30 nt)	Sandwich hybridization	TAMRA	10 nM	$NaYF_4$:Yb,Er (oleic acid, ∅ 13 nm)	Chen Z. *et al.* (2008)
Mutant hemoglobin β chain (HBB) gene	Sandwich hybridization	TAMRA	0.6 nM (120 fmol)	$NaYF_4$:Yb,Er (silica, ∅ 72 nm)	Kumar *et al.* (2009)
	Direct hybridization	SYBR Green I (intercalating dye)	0.1 nM (20 fmol)	$NaYF_4$:Yb,Tm (DTPA, ∅ 45 nm)	Kumar & Zhang (2009)
Other assays					
Mannose (carbohydrate)	Competitive lectin recognition	Rhodamine	-	$NaGdF_4$:Yb,Er (dendrimer, ∅ 25 nm)	Bogdan *et al.* (2010)
Hg^{2+} (metal ion)	Metal-assisted nucleic acid pairing	SYBR Green I (intercalating dye)	0.06 nM	$NaYF_4$:Yb,Tm (DTPA, ∅ 45 nm)	Kumar & Zhang (2010)
		Graphene oxide (quencher)	0.5 nM	$NaYF_4$:Yb,Er (PAA, ∅ 29 nm)	Liu *et al.* (2011)
ATP (coenzyme)	Conformation change of aptamer	Graphene oxide (quencher)	80 nM	$NaYF_4$:Yb,Er (PAA, ∅ 29 nm)	Liu *et al.* (2011)

Abbreviations: ATP, adenosine triphosphate; LbL, layer-by-layer coating; PAA, poly(acrylic acid) coating; DTPA, diethylenetriaminepentaacetic acid.
[a)] Ground UCP bulk material

Evanescent wave coupling

When light is totally internally reflected at the interface between the materials of high and low refractive index (e.g., glass and liquid), an electromagnetic field called an evanescent wave is formed at the interface. The wavelength of the evanescent wave is identical with the original light source, and its intensity decays exponentially when the distance to the interface increases. This phenomenon has been utilized in the total internal reflection fluorescence microscopy (for review see Fish (2009)) from the 1980s. The evanescent wave can transfer energy to fluorescent species that are typically within ~100 nm from the surface (Figure 7) (Axelrod *et al.*, 2002). Morgan and Mitchell have modified the technique by introducing an upconverting glass-ceramic called Yaglass (Morgan and Mitchell, 2006). The Yb^{3+}–Er^{3+} doped optically transparent material is primarily based on a lead fluoride and enables the use of NIR radiation. The custom-made planar Yaglass waveguides are 200 µm thick and covered with a thin protective titanium dioxide layer (50 nm).

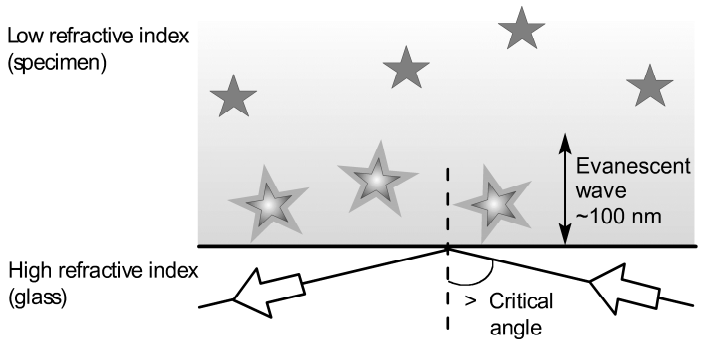

Figure 7. Evanescent wave excitation. Only those fluorophores near the interface of the two materials are excited. The white arrows indicate incident and reflected light.

Evanescent wave excitation-mediated energy transfer from the upconverting glass to surface-bound fluorophores was first demonstrated with an amine-modified Yaglass and carboxylated fluorescent beads (Morgan and Mitchell, 2006). A straightforward bioaffinity assay can be carried out on the surface of the Yaglass, in principle, without any washing steps. The presence of avidin was detected on the Yaglass by monitoring the fluorescence of the formed sandwich complex comprising a biotinylated fluorescent protein, R-phycoerythrin (Morgan and Mitchell, 2007). However, there is no evidence regarding whether different analyte concentrations can be reliably differentiated, and no estimations about the detection limit have been reported.

The evanescent wave coupling allows longer distances (~100 nm) compared to the short-range interactions of RET (~10 nm), hence it is anticipated that this technique could be utilized even in detection of large analytes (such as viruses) by sandwich-type assays. Based on Morgan and Mitchell, the final application could be a microplate format with an upconverting waveguide formed on the base of each well. Another option would be a non-planar assay-format involving microsphere resonators or ring resonators. The main challenge for this technique is to find an easy route to produce low-cost upconverting surfaces.

2.4.5 Optical sensors

Sensors reversibly respond to presence of the analyte and convert the quantity into a measurable signal. Wolfbeis with his research group has developed several sensor systems based on UCPs combined with compounds sensitive to either pH or oxygen. The UCP material ($NaYF_4$:Yb^{3+},Er^{3+}/Tm^{3+}) and the probe are both incorporated in a layer of suitable matrix to form a thin sensor film (typical thickness a few µm) (Figure 8). The UCPs are acting as energy donors, but in this case it is irrelevant whether the energy transfer is resonant (distance-dependent) or photon-mediated.

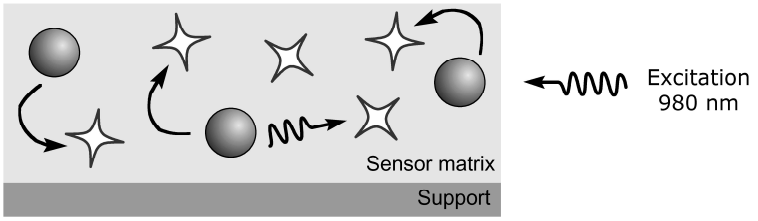

Figure 8. Principle of optical sensors based on UCPs. The thin, reversible sensor matrix consisting of UCPs (*gray balls*) and probes (*white stars*) is formed on the support material. The characteristics of the probe (e.g., absorption spectrum or fluorescence intensity) are affected by the surrounding environment (e.g., pH, O_2). The UCPs are excited with external NIR radiation, and the following emission is somehow modulated (e.g., quenching of UCP emission or emergence of sensitized acceptor emission) by the probe molecules. The curly arrows indicate photon-mediated processes and the bent arrows resonant energy transfer.

Separate sensors for pH (Sun *et al.*, 2009b), ammonia (Mader and Wolfbeis, 2010) and carbon dioxide (Ali *et al.*, 2010) were based on various pH-sensitive probes, whose absorption band shifts in line with the pH changes (Table 5). As a result, the UCP emission was either quenched or recovered when the analyte concentration increased. A transparent polyester support was used in all sensors. The sensor matrix for measuring the pH was constructed from a polyurethane hydrogel, while a polystyrene matrix was an excellent choice for the ammonium and the CO_2 sensors as the analytes can penetrate the matrix, but it is impermeable to protons (not sensitive to the pH of the environment). The CO_2 sensor was especially targeted at monitoring a low concentration range suitable for clinical and respiratory applications. The ammonia sensor was designed for environmental and industrial monitoring.

The oxygen sensor (Achatz *et al.*, 2011) differs from the other described sensors. It involved a fluorescent oxygen sensitive iridium(III) complex, whose excitation spectrum overlaps with the blue emission band of the Yb^{3+}–Tm^{3+}-doped UCP. The emission of the Ir^{3+} complex was followed under NIR excitation, and the presence of oxygen was detected based on a decrease in the emission intensity. The luminescent species were mounted in a thin oxygen-permeable ethyl cellulose matrix (2 µm). However, the sensor seemed to perform better under a blue excitation compared to the NIR excitation. The limited accessibility of oxygen and local heating caused by the UCPs were considered as possible causes for the lower quality of the response. In more complex systems involving highly autofluorescent biological sample materials (such as serum), the advantages of the NIR excitation would be more emphasized compared to these test runs with pure argon and oxygen gases.

A completely different UCP-based sensor responds to temperature changes in physiological temperature range (Vetrone *et al.*, 2010b; Fischer *et al.*, 2011). No probes are involved, but the upconversion efficiency of the UCPs themselves is temperature dependent. The rate of nonradiative relaxations increases with the raising temperature and results in decreased luminescence intensity. Different transitions have a different dependence, and therefore a ratiometric reading (e.g., I_{525nm}/I_{545nm} or I_{539nm}/I_{651nm}) can be used to rule out other variables affecting the emission intensity. Vetrone *et al.* (2010b) demonstrated the use of upconverting nanothermometers in measuring the temperature of living cancer cells.

Table 5. Examples of UCP-based sensors. Continuous monitoring of the analyte concentration is possible with these reversible sensors.

Analyte	**Probe**	**Way of action**	**Functional range**	**UCP material** (diameter)	**Reference**
pH	Bromothymol blue (dark quencher)	pH-induced red-shift of absorption quenches UCP emission (pH ↑)	pH 6–10	$NaYF_4$:Yb,Er (50 nm × 950 nm)	Sun *et al.* (2009b)
NH_3	Phenol red (dark quencher)	pH-induced red-shift of absorption quenches green UCP emission (NH_3 ↑)	1–20 mM (40–800 ppm)	$NaYF_4$:Yb,Er (∅ 60–90 nm)	Mader & Wolfbeis (2010)
CO_2	Bromothymol blue (dark quencher)	pH-induced blue-shift of absorption recovers UCP emission (CO_2 ↑)	0.11– <3%	$NaYF_4$:Yb,Er (∅ 40–100 nm)	Ali *et al.* (2010)
O_2	Iridium(III) complex (fluorescent)	Oxygen quenches the emission of Ir^{3+} complex	-	Y_2O_2S:Yb,Tm (∅ 80–120 nm)	Achatz *et al.* (2011)
Temperature	UCP (luminescent)	Temperature affects the intensity ratios of the emission bands	25–45°C	$NaYF_4$:Yb,Er (∅ 18 nm)	Vetrone *et al.* (2010b)
			18–33°C	$NaYF_4$:Yb,Er (∅ ~100 nm)	Fischer *et al.* (2011)

2.5 Instrumentation for detecting the UCP emission

The readers for the bioanalytical applications based on UCPs can generally be divided into three categories: optical scanners, plate readers and imagers. The scanners are used for reading the UCP emission from array-type platforms or across the LF strip either in a one-dimensional (1D; progress longitudinally along the strip) or a two-dimensional (2D; raster scanning) manner. The plate readers typically collect the UCP emission from each microtiter well (e.g., standard 96- and 384-well plates) for a certain short period of time and enable fast data collection from a large number of individual samples. The imager is an optional reader for the array-type solutions. It captures the UCP emission from a larger area without the need for scanning. Commercial readers for UCPs are not available at the moment, but several prototypes have been introduced in the literature (Table 6). Actually, the portable UP*link*™ analyser from OraSure Technologies was commercially launched, but the company soon replaced the test platform designed for drugs of abuse with other products not related to the UCPs.

Table 6. List of some instruments used for reading the UCP emission in bioanalytical applications.

Instrument	Max LD power output	Detector	Measurement time	Resolution	CV	Reference
Optical scanners for LF strips						
Modified Packard FluoroCount™	1.2 W	PMT	-	91 µm	<7%	Niedbala *et al.* (2000),. (2001)
Portable UP*link*™	1 W	PMT	-	-	-	Mokkapati *et al.* (2007), OraSure Technologies, Inc. (USA)
Portable scanner	0.05 W	PMT	1 min per strip	20 µm	<5%	Yan Z. *et al.* (2006), Huang *et al.*(2009)
2D scanner	1.2 W	PMT	8 min per strip	20 µm 500 µm	<2%	Li J. *et al.* (2008)
Plate readers						
Modified PlateChameleon™	0.2 W	PMT	2 s per well	n/a (500 µm)	-	Soukka *et al.* (2005)
Imagers						
Modified PlateChameleon™	8 W	CCD camera	1–30 s per well	-	-	Ylihärsilä *et al.* (2011)

Abbreviations: LD, laser diode; CV, coefficient of variation; LF, lateral flow; 2D, 2-dimensional; PMT, photomultiplier tube; CCD, charge-coupled device; n/a, not applicable; -, not reported.

The listing in Table 6 is not all-embracing, as, for example, spectrofluorometers equipped with sample cuvettes as well as fluorescence microscopes are omitted. The fluorescence measurement from a cuvette is only applicable in homogeneous assays or in assays performed on magnetic beads. Microtiter plates combined with plate readers provide much better solutions in terms of higher throughput and smaller sample volume. Few of the earliest papers exploited existing microscopes with Xenon lamps for visualizing the emission of the UCPs (van de Rijke *et al.*, 2001; Zijlmans *et al.*, 1999), but the white light source as such is not optimal for this purpose. Some of the instruments described in Table 6 exploit the base of existing fluorometers (FluoroCount™, Plate Chameleon™) but are modified to meet the requirements of the UCP detection by changing certain components.

The nonlinear relationship between the excitation power density and UCP emission intensity is worth consideration when choosing an excitation source. Laser diodes (LDs) provide a narrow, coherent excitation beam that is more easily focused on a small area compared to broad-area excitation sources such as Xenon lamps, and thus LDs provide a significantly higher power density. The emission bandwidth of an LD is typically only a few nanometers, which could be a limiting factor, but as suitable LDs emitting at ~980 nm are available, it may be regarded solely as an advantage in this case. The compact light emitting diodes (LEDs) also provide fairly narrow emission bandwidths (around tens of nanometers), and they operate with low power consumption, but the beam quality is not competitive with the LDs due to low spatial coherence (Demchenko, 2009). Therefore, the LDs predominate in the instrumentation constructed for the UCPs. Affordable continuous

wave LDs are commonly available from various commercial suppliers. They are offered with different output powers, and one may also choose a fiber-coupled diode or a diode equipped with a cooler (e.g., peltier element). A respectable LD for the UCP-based bioanalytical applications can be purchased with only a few hundred euros, and portable laser pointers for the on-site applications are in the same price category. The costs of an instrument become a focal issue in context of commercialization, and economical solutions naturally attract the end-users. The decentralized analyzers intended for POCT are a special market segment particularly calling for reasonable pricing.

The detector for the UCP emission is more commonly a photomultiplier tube (PMT) than a silicon-based detector (e.g., a charge-coupled device (CCD) or photodiode), due to its superior sensitivity, marginal noise level and lower response towards NIR radiation (Demchenko, 2009; Li *et al.*, 2008). The continuous NIR excitation is much more intense compared to the visible emission of the UCPs, and although optical filters are used for blocking the NIR radiation from the detector, it is an advantageous feature that the detector itself naturally filters out unwanted wavelengths originating from the excitation source. The silicon-based detectors are approximately 100 times more responsive to NIR photons than the PMTs. However, the most significant feature of the PMT is the signal amplification, which allows detection of minute amounts of photons. A 2D image may be produced either by scanning the desired area point by point or by utilizing a 2-dimensional matrix of detectors (e.g., CCD cameras), of which the latter usually operates quicker.

The PlateChameleon™-based imager differs from the other instruments in two ways. First, it is the only instrument discussed here that uses a CCD-camera as a detector. That is a logical choice as a 2D image is required. Second, the imager has a significantly more powerful LD compared to the other instruments in Table 6. However, the laser beam is spread over a relatively large area (a square of several millimeters), while in other instruments the beam is, on the contrary, focused on a small area. A more valid value in Table 6 would be the power density instead of the laser output power, but unfortunately that information is not available.

The measurement time per single sample varies according to the number of data points collected. Scanning the LF strips takes some time, rendering the LF assays therefore more suitable for individual testing, while the microtiter plate-based assays fit well with the high-throughput applications providing results rapidly. The substantially long time required for 2D raster scanning of the LF strips provides a large number of data points and allows therefore more sophisticated data analysis for the subtraction of the background signal and for the reduction of the random errors resulting from an inhomogeneous UCP distribution on each strip (Li *et al.*, 2008). However, the 8-minute data acquisition time for one LF strip is acceptable only for occasional testing; it is inconvenient for other applications.

The technological solutions for the anti-Stokes photoluminescence readers have been existing for a long time. It provides a lead over the other merging labels producing conventional fluorescence upon NIR excitation (e.g., molecular Yb^{3+} complexes and inorganic Yb^{3+}-doped nanocrystals (Zhang and Petoud, 2008; Zucchi *et al.*, 2009; Zhang *et al.*, 2007)), because good detectors for such high wavelengths are still in the development stage. Solid-state NIR-detectors are available, but the sensitivity of, for example, PMTs is not adequate at NIR wavelengths.

3 AIMS OF THE STUDY

The overall aim of this thesis was to evaluate the performance of upconverting phosphors in different bioanalytical assay concepts as an NIR-excitable energy donor. The separation-free UCP technology based on energy transfer was previously demonstrated to enable sensitive determination of an estradiol hormone even in the presence of whole blood. The purpose of the present study was to show the potential of the UCP technology also in homogeneous applications other than immunoassays, and to further develop the methods required for functionalization and bioconjugation of the UCPs. Finally, the energy transfer mechanisms between the UCP donor and an acceptor fluorophore were investigated to define the presence of the distance-dependent resonance energy transfer process, which is the basis for the homogeneous assays presented in this thesis.

More specifically the aims were:

I To enhance the performance of the bioaffinity assay based on upconversion resonance energy transfer by utilizing **a tandem dye acceptor** having a large pseudo-Stokes shift.

II To demonstrate a fluorescence quenching-based high-throughput screening concept for measuring **the activity of hydrolyzing enzymes**.

To compare the NIR-excitable photon upconversion-based technology with a conventional fluorescence method both in colorless buffer solution and in deeply red-colored whole blood dilution.

III To study the feasibility of a UCP donor in a homogeneous upconversion resonance energy transfer-based **multiparametric hybridization assay** utilizing only a single excitation wavelength.

To show that silica-encapsulation instead of poly(acrylic acid) adsorption as a **functionalization method** for UCPs is applicable to UC-RET-based homogeneous assays.

IV To characterize **the nature of the energy transfer** from UCPs to conventional fluorophores and fluorescent proteins.

4 SUMMARY OF MATERIALS AND METHODS

More detailed descriptions of the materials and methods employed in this study can be found in the original publications (**I**–**IV**). A brief summary with some additional information is presented here.

4.1 Upconverting materials

The UCP material in all original publications (**I**–**IV**) was composed of $NaYF_4$:Yb^{3+},Er^{3+}. The first three studies were carried out with a ground bulk material having a hexagonal β-phase crystallographic structure, while the last publication **(IV)** exploited a co-precipitated UCP material with mixed α- and β-phase. The phase-pure structure is preferred, but the size of the bulk material as such is far from the ideal nanomaterial. The particle size and surface modifications varied in different publications (Table 7).

Table 7. The specifications of the UCPs used in this study.

Publication and use		Origin of UCP	Particle diameter	Surface modification and resulting functional group		Conjugated with
I	Donor in biotin assay	Ground commercial PTIR550/F [a)]	~340 nm	Adsorption of PAA	-COOH	Streptavidin
II	Donor in enzyme activity assay	Ground commercial PTIR550/F [a)]	~340 nm	Adsorption of PAA	-COOH	Streptavidin
III	Donor in sandwich hybridization assay	Ground commercial PTIR550/F [a)]	~300 nm	Silica-encapsulation; TEOS + APTS	$-NH_2$ converted to -COOH	Capture oligonucleotide
IV	Study of energy transfer mechanisms	Co-precipitated UCP material [b)]	~110 nm [c)]	Adsorption of PAA	-COOH	Fluorescent protein, acceptor fluorophore or BSA

Abbreviations: PAA, poly(acrylic acid); TEOS, tetraethyl orthosilicate; APTS, 3-aminopropyl triethoxysilane; BSA, bovine serum albumin.
[a)] From Phosphor Technology Ltd. (UK)
[b)] Synthesized at the University of Turku (Finland)
[c)] Based on a TEM image; the other diameters were measured with a Coulter N4 plus submicron particle size analyzer

4.1.1 Origin of the UCPs

The commercial UCP bulk material PTIR550/F from Phosphor Technology Ltd. (Stevenage, UK) is originally intended for anti-counterfeiting and tagging applications to be read under NIR radiation. The UCPs can be added to printing inks or dispersed in plastics. The photophysical characterization and elemental analysis of this UCP material is described elsewhere (Soukka *et al.*, 2005). According to the manufacturer, the particle size of the bulk material was 2.3–6.0 µm, which is far too large to form the colloidal suspension required for bioaffinity applications. Prior to use, the UCPs were ground with a planetary ball mill (Planetary Mono Mill pulverisette 6; Fritsch GmbH, Idar-Oberstein, Germany) in aqueous solution (10 mM borate buffer, pH 9, containing 1 g/L Additol XW330 poly(acrylic acid)) and fractioned by sedimentation. The final particle size was measured

with a Coulter N4 plus submicron particle size analyzer (Beckman Coulter, Fullerton, CA). The milling procedure was shortened from days to 90 minutes when the planetary ball mill (**I**) was substituted for the previously used primitive method relying on vigorous shaking.

In the latest study (**IV**), the ground bulk UCP material was replaced with smaller UCPs synthesized by our collaboration group led by Professor Jorma Hölsä in the Laboratory of Materials Chemistry and Chemical Analysis, University of Turku (Finland). The co-precipitation method for preparation of $NaYF_4$:Yb^{3+},Er^{3+} material was originally published by Yi *et al.* (2004), and the synthesis protocol as well as the luminescence characterization of the UCPs utilized in the publication **IV** are described in detail by Hyppänen *et al.* (2009). The average particle size was manually measured from transmission electron microscopy (TEM) images. Samples for TEM were prepared by drying a small droplet (5 µL) of UCP suspension (0.25 mg/mL in deionised water) on the formvar/carbon-coated copper grid (300 mesh). Imaging was carried out with Tecnai 12 Bio Twin TEM (FEI, Hillsboro, OR) at Aalto University School of Science and Technology (Espoo, Finland) using an acceleration voltage of 120 kV.

4.1.2 Surface functionalization of the UCPs

The UCPs were modified to improve the dispersivity of hydrophobic UCPs into an aqueous solution and to provide functional groups suitable for bioconjugation purposes. In the publications **I**, **II** and **IV**, carboxylic acid groups were introduced by passively adsorbing a sodium salt of poly(acrylic acid) (Additol XW330; Surface Specialties Austria GmbH, Werndorf, Austria) on the surface of the UCPs (Figure 9). The adsorption was carried out in an aqueous solution overnight, followed by washing steps to remove the excess polymer.

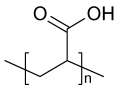

Figure 9. Chemical structure of poly(acrylic acid).

Another approach for surface modification was developed to avoid any possible leakage of the coating. A procedure for silica-encapsulation was optimized to produce a thin silica-layer around individual UCP particles (**III**). To control the thickness of the forming polymer layer, the reaction was carried out in a water-in-oil emulsion as described in the papers by Santra *et al.* (2001) and Tan *et al.* (2004). TEOS was copolymerized with APTS, providing useful amino groups (Figure 10). The volumetric ratio of TEOS and APTS was 1:2. The amino groups on the silica-encapsulated UCP surface were further converted into carboxylic acid groups by treating them with a glutaric anhydride, which also provides an additional 5-carbon spacer arm. The reaction was carried out in dry pyridine, which should be handled with caution due to its unpleasant odor and harmful nature.

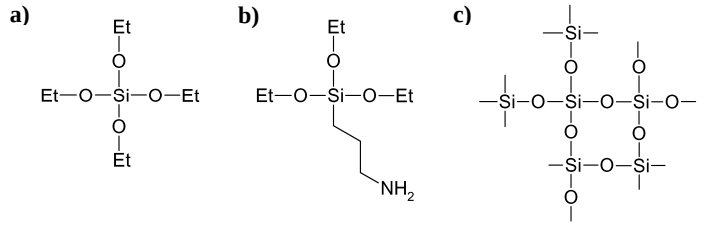

Figure 10. Chemical structures of the reagents used for the silica-encapsulation of the UCPs. (**a**) Tetraethyl orthosilicate (TEOS) is the basic building block of the polymer and (**b**) 3-aminopropyl triethoxysilane (APTS) introduces amino groups to the structure. (**c**) Silica polymer is formed as a result of hydrolysis reaction.

4.1.3 Conjugation of the UCPs

The carboxylic acid-functionalized UCPs were covalently coupled with primary amino groups of biomolecules or fluorophores by utilizing carbodiimide activation (**I**–**IV**). The protocol for bioconjugation originates from the publication of Kubitschko *et al*. (1997), but the procedure originally optimized for the carboxylated polystyrene nanoparticles was modified according to our own optimizations for the UCPs. The most notable change was the dramatic increase (18–27-fold) in the amount of the activation reagents, 1-ethyl-3-(3-dimethylaminopropyl) carbodiimide (EDC) and *N*-hydroxysulfo-succinimide (sulfo-NHS). EDC and sulfo-NHS must be removed from the UCP suspension before adding *proteins* to the solution, because otherwise the carboxylic acids of the biomolecules are activated as well, and protein cross-linking takes place. *Oligonucleotides* do not contain any carboxylic acid groups, and the above-mentioned washing step could be excluded from the protocol in those cases. Around 1.2–1.4 nmol of protein (streptavidin or bovine serum albumin (BSA)) or oligonucleotide (length 15 or 16 nucleotides) per 1 mg of the UCPs was added to the conjugation reaction when maximal conjugation density was the aim. Only a fraction of this amount was used in the case of *fluorescent molecules* (B-phycoerythrin, ATTO565 or DY556) so that the self-quenching of the fluorescence was reduced. All steps were carried out in 20 mM MES buffer (pH 6.1 or 6.5). Finally, the unconjugated biomolecules were removed, and the completed UCP conjugates were stored in a borate-based storage buffer (pH 8.5) containing 5 g/L of BSA, which serves as a blocking agent to cover the surface areas not covered by the conjugated (bio)molecules.

The UCP conjugates were characterized by determining both the UCP concentration and the concentration of the conjugated molecule. The fluorescent species (UCPs, fluorophores and fluorescent protein) were quantified based on the fluorescence intensity and the amount of biomolecules (streptavidin, oligonucleotides) was evaluated with a heterogeneous competitive assay for the biomolecule in question. The amount of conjugated BSA was irrelevant and was not determined at all.

4.2 Acceptor dyes

The fluorescent molecules used as acceptor dyes were chosen according to Förster's theory so that their excitation band overlaps with the emission band of the UCP donor (Figure 11). Note that green-to-red ratio of the UCP emission depends on the excitation power density, which differs between the instruments. The vertical lines in the fluorescence spectra emphasize the two emission maxima of the UCP donor, and in most of the cases the lines fall on the left side of the fluorophore's excitation maximum. Consequently, the emission maxima of B-phycoerythrin (BPE), AlexaFluor 680 (AF680), tandem dye (BPE–$AF680_5$),

AlexaFluor 546 (AF546), AlexaFluor 700 (AF700), ATTO565 and DY565 lie in a wavelength region where the UCP emission is minimal, almost non-existent. The physical properties of the fluorophores are collected in Table 8. In publication **II**, a BlackBerry Quencher 650 (BBQ650) with a wide absorption band was utilized to quench the emission of AF680.

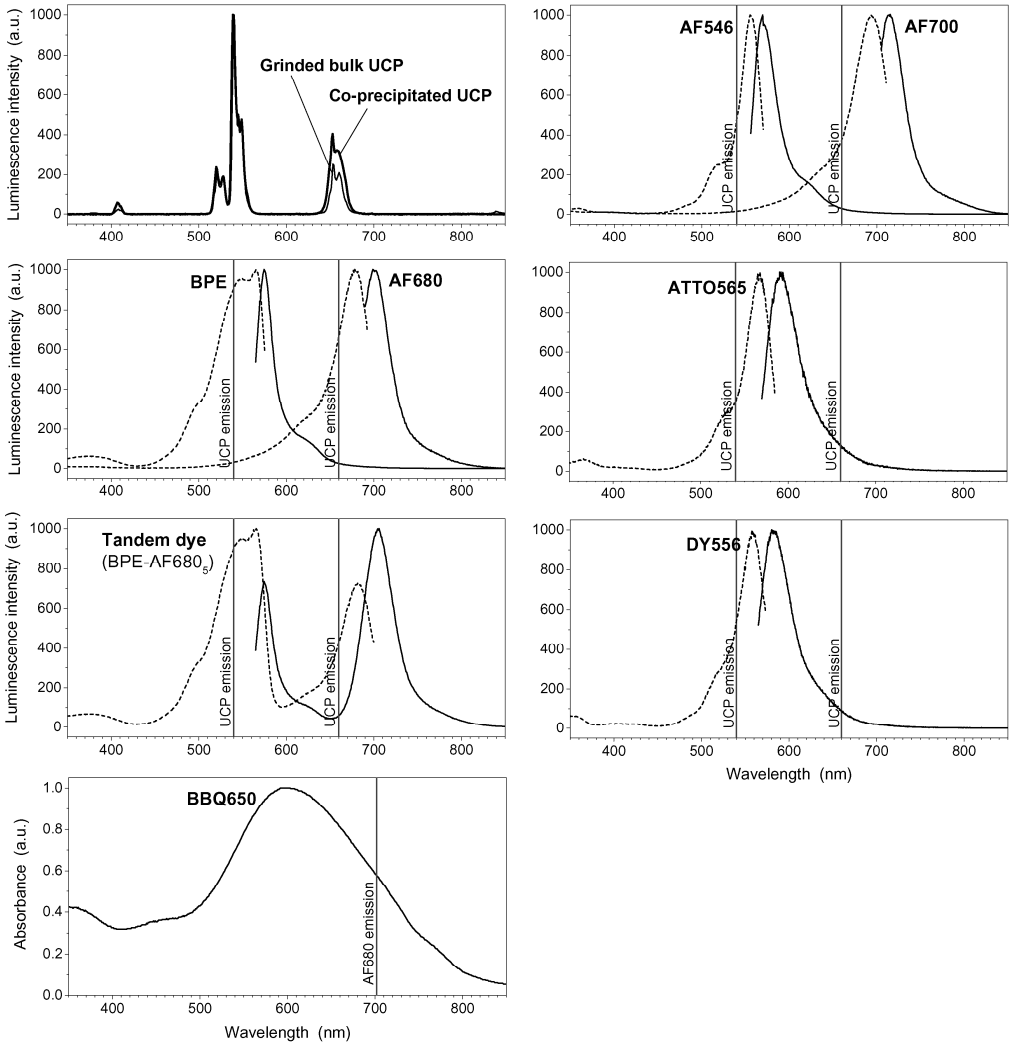

Figure 11. Normalized excitation (*dashed line*) and emission (*solid line*) spectra of all fluorescent species used in this study and an absorption spectrum of the BBQ650. There was no excitation spectrum available from the UCPs composed of $NaYF_4$ host material doped with Yb^{3+} and Er^{3+} ions, but both were exited with an NIR laser diode at ~980 nm. Vertical lines in the fluorescence spectra illustrate the emission maxima of the UCP donor. In the undermost absorption spectrum of the quencher molecule (BBQ650), the vertical line represents the emission maximum of the AF680. *a.u., arbitrary unit.*

The tandem dye is a conjugate composed of a large, fluorescent BPE protein and, on average, 5 AF680 fluorophores (**I**). Due to an internal energy transfer from BPE to AF680, the pseudo-Stokes' shift of the tandem dye is almost 140 nm, while the same value for the other dyes is only 9–29 nm. As the tandem dye has two excitation bands overlapping with both of the donor emission bands, it serves as an interesting acceptor dye candidate.

Table 8. Summary of the physical properties of the fluorophores used in the publications **I–IV**.

Fluorophore	Molecular weight	Excitation λ_{max}	Emission λ_{max}	Extinction coefficient ε	Publication
	g/mol	*nm*	*nm*	$cm^{-1}\ M^{-1}$	
B-phycoerythrin [a] (BPE)	~240 000	566	575	2 410 000	**I, IV**
AlexaFluor 680 [b] (AF680)	~1 150	679	702	184 000	**I**, **II**
Tandem dye (BPE–$AF680_5$)	~246 000	565 (681) [d]	704 (575) [d]	*N/A*	**I**
AlexaFluor 546 [b] (AF546)	1 079	556	573	104 000	**III**
AlexaFluor 700 [b] (AF700)	~1 400	702	723	192 000	**I**, **III**
ATTO565 [c]	666	563	592	120 000	**IV**
DY556 [c]	736	548	573	100 000	**IV**

Abbreviations: *N/A*, not available.
[a] From Cyanotech Corp. (Kailua-Kona, HI).
[b] The dye contains a carboxylic acid succinimidyl ester-modification for conjugation purposes. Purchased from Molecular Probes / Invitrogen (Carlsbad, CA).
[c] The dye is an amino-derivative. ATTO565 purchased from ATTO-TEC GmbH (Siegen, Germany) and DY556 from Dyomics GmbH (Jena, Germany).
[d] The second excitation or emission band in parenthesis.

4.3 Instrumentation for anti-Stokes photoluminescence measurements

Conventional fluorometers and related instruments were transformed to measure the anti-Stokes photoluminescence of UCPs or the emission of fluorophores sensitized by UCPs. The original excitation light source was replaced by an NIR laser diode, and appropriate optical components (e.g., filters) were added. To assure the quality of the NIR excitation beam, all instruments were equipped with long-pass filters blocking all wavelengths below 850 nm from entering the sample.

4.3.1 Plate reader

A modified microtiter plate reader based on an epi-fluorescence set-up (Plate Chameleon; Hidex Oy, Turku, Finland) was the key instrument in the bioaffinity assays of this study (**I–III**). The Xenon flash lamp was replaced with a continuous wave NIR laser diode module producing radiation at ~980 nm. The output power of the laser diode was about 200 mW, taking into account that individual laser diodes may have slight variation and aging and temperature changes also influence the performance of the diode. A different laser diode was used in publication **I**, but the specifications were equivalent to the one used in other publications. The excitation source was not accompanied by a cooling system in any of the plate reader versions. The excitation beam was focused on quite a small area (roughly estimated, the dimensions were 0.3 mm × 0.8 mm in **I** and somewhat smaller in **II**–**III**) in the microtiter well to maximize the power density and the emission intensity of the UCPs. In addition to the laser diode itself, the nature of the liquid in the reaction well also

certainly has some effects on the excitation power density (e.g., scattering of the excitation radiation due to blood cells). The emission light was collected for 2000 ms with a R4632 PMT (Hamamatsu Photonics, Hamamatsu City, Japan), which is also sensitive to red light produced by certain acceptor fluorophores used in this study. The first version of the modified plate reader has been described in a paper by Soukka *et al*. (2005). Some technological evolution related to component positioning, optics and PMT has taken place subsequently, but the platform has remained the same.

Optical filters play an especially important role in RET-based assays as well as in multiparametric assays, in which emissions from different fluorescent species must be separated from each other. A band-pass filter of 600/40 nm (center wavelength 600 nm, band half-width 40 nm) was used for measuring the sensitized emission of BPE and AF546, and the 740/40-nm band-pass filter was used for the tandem dye (BPE–$AF680_5$), AF680 and AF700. The emission intensity of the UCPs was also monitored either to confirm the equal amount of the donor in all reaction wells (**II**–**III**) or to normalize the intensity of sensitized emission of the acceptor in an early version of the modified Plate Chameleon (**I**), where signals were fluctuating for some reason (e.g., due to variation in excitation intensity) more than in the later versions. The green UCP emission was selected with an emission band-pass filter of 535/50 nm and the red UCP emission with a filter of 660/25 nm or 665/10 nm. Due to the highly intense anti-Stokes photoluminescence of the UCPs, absorptive neutral density filters with optical densities of 1.0 or 2.0 (i.e., average transmittance 10% or 1%) were used to limit the number of photons entering the PMT. All the selective emission band-pass filters were combined with a filter set preventing the excitation radiation from entering the PMT.

4.3.2 Fluorescence spectrophotometer

The emission spectra of the UCPs could be measured by modifying a Varian Cary Eclipse fluorescence spectrophotometer (Varian Scientific Instruments, Mulgrave, Australia). An external continuous wave laser diode module, which provides about 200 mW output power at ~980 nm, was added in the wide sample compartment of the instrument, while the unit comprising the original Xenon flash lamp was closed with an additional wall. The emission was recorded with a standard red-sensitive PMT (up to 900 nm). Measurements were carried out in a quartz fluorescence macro cell (inner dimensions 10 × 10 mm; Hellma, Müllheim, Germany).

Due to the lack of a good NIR excitation source with selectable wavelengths, the measurement of UCP excitation spectra was not possible, but from the literature it is known that the Yb^{3+} ion absorbs at around 980 nm (DeLoach *et al.*, 1993).

4.3.3 Frequency-domain luminometer

The luminescence lifetimes of UCPs were measured with an in-laboratory-made modular frequency-domain (FD) luminometer. The FD technique is a more efficient option for deconvolution of overlapping decay processes than the time-domain measurements, and it is especially suitable for lanthanide labels (Hyppänen *et al.*, 2010). The instrument is introduced in greater detail in publication **IV**. An NIR laser diode providing maximally 1200 mW power at 976 nm served as an excitation source. The modulation degree of the laser diode current was 10%. The sensitized emission of the fluorophores or the anti-Stokes emission of the UCP was collected by using a 600/40-nm or 544/10-nm band-pass filter,

respectively. Both emission filters were combined with a short-pass filter (good transmission at visible wavelengths) to block the NIR radiation. Aqueous samples were placed in short-cut quartz NMR tubes for measurements. A computer program written in Visual Fortran 90 equipped with the DISLIN graphics package was used to fit the collected data for analyzing the luminescence lifetimes.

4.4 Homogeneous assays based on upconversion resonance energy transfer

Specifications of all the three different homogeneous assays (**I**–**III**) are summarized in Table 9. All reactions were carried out in black half-area microtiter wells (Corning Inc, Corning, NY) covered with a plastic plate closure tape, and all dilutions were prepared in the assay buffer (50 mM Tris-HCl, pH 7.8, 9 g/L NaCl, 0.5 g/L NaN_3, 5 g/L BSA, 0.1 g/L Tween 40, 0.5 g/L bovine γ-globulin, and 20 μM diethylenetriamine pentaacetic acid; Innotrac Buffer or Kaivogen Buffer; Innotrac Diagnostics Oy or Kaivogen Oy, Turku, Finland). The plates were shaken during the incubations with a speed of 900 rpm, and the incubation temperature was +23°C if not otherwise stated.

Table 9. Summary of the assay specifications used in the homogeneous assays based on UC-RET (**I–III**).

Original publication	**I**	**II**	**III**
Analyte	D-biotin	Benzonase endonuclease activity	Single-stranded HLA-B27 and β-actin oligonucleotides
Type of the assay	Competitive bioaffinity assay	Fluorescence-quenching-based assay	Sandwich hybridization assay
Donor conjugate	UCP–streptavidin; *ground UCP coated with PAA*	UCP–streptavidin; *ground UCP coated with PAA*	UCP–oligonucleotide; *ground, silica-encapsulated UCP*
Acceptor	Tandem dye (BPE–$AF680_5$), AF680, BSA–$AF680_2$	AF680 *(internally quenched with BBQ650)*	AF546, AF700
Matrix	Assay buffer	Assay buffer (+ 20% v/v whole blood)	Assay buffer with increased NaCl concentration *(1 M)*
Reaction volume	80 µL	50 µL	80 µL
Incubation [a)]	15 min (donor + analyte) 15 min (+ acceptor)	20 min (labeled substrate + enzyme; +37°C) 15 min (+ donor) 1 min (+ blood)	30 min (donor + target; +60°C and +35°C) 20 min (+ acceptor; +35°C)
Emission filters [b)]	740/40 nm (665/10 nm for correction)	740/40 nm	600/40 nm 740/40 nm
Calibration curve	Sigmoidal inhibition curve	Linearly increasing signal until saturation	Linearly increasing signal until saturation

Abbreviations: PAA, poly(acrylic acid); BPE, B-phycoerythrin; AF, AlexaFluor; BSA, bovine serum albumin; BBQ650, BlackBerry Quencher 650.
[a)] Incubation time for each step. Added components and incubation temperatures differing from the room temperature in parenthesis.
[b)] Center wavelength / band half-width

4.4.1 Biotin assay utilizing a tandem dye acceptor (I)

The principle of the biotin assay is illustrated in Figure 12. D-biotin was chosen as a model analyte due to its extremely strong interaction with streptavidin. A calibration curve was determined by utilizing both a conventional acceptor fluorophore (AF680) and a tandem dye acceptor (BPE-AF680$_5$).

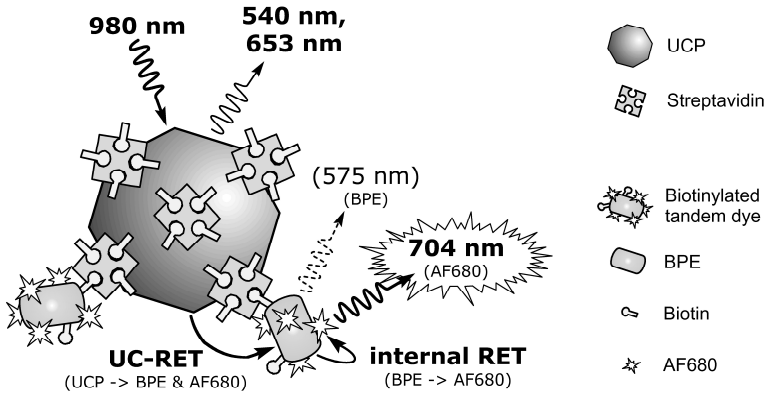

Figure 12. Principle of the competitive biotin assay utilizing the tandem dye acceptor. The UCP donor conjugated with streptavidin generates emission at 540 and 653 nm under NIR excitation (980 nm). The biotinylated tandem dye acceptors (BPE-AF680$_5$) bound to streptavidin are excited through UC-RET and the sensitized emission is measured at wavelengths >700 nm. *RET, resonance energy transfer; UC-RET, upconversion-RET.*

The PAA-coated UCPs (1.2 µg) conjugated with streptavidin were mixed with different amounts of D-biotin (0–8 and 800 pmol). The biotinylated acceptor fluorophore (0.128 pmol tandem dye or 0.352 pmol AF680) was added, and the sensitized emission at red wavelengths was measured with the modified Plate Chameleon. The read-out was corrected for variation in laser intensity by utilizing the measured emission intensity of the donor UCP at 665 nm (Equation 1).

$$\text{Corrected sensitized emission of acceptor} = [I_{740\ \text{nm}}\ (I^*_{665\ \text{nm}} / I_{665\ \text{nm}})] - I^*_{740\ \text{nm}}, \qquad (\mathbf{1})$$

where I_x is the emission intensity at wavelength x in the presence of both the donor and the acceptor and I^*_x is the emission intensity at wavelength x in the presence of only the UCP without acceptor. Before any corrections, the instrument background originating from the PMT dark current was subtracted from all values. In other words, non-corrected sensitized emission intensity of the acceptor ($I_{740\ \text{nm}}$) was multiplied by the correction factor ($I^*_{665\ \text{nm}}$ / $I_{665\ \text{nm}}$), and finally the background resulting from UCP cross-talk ($I^*_{740\ \text{nm}}$) was subtracted. The correction factor was calculated by proportioning the intensity of UCP emission ($I_{665\ \text{nm}}$) in each reaction well to the control signal from UCP only ($I^*_{665\ \text{nm}}$). Increased excitation laser intensity resulted in correction factors below 1 and a decrease in the laser intensity led to corrections factor greater than 1. Due to the nonlinear relationship between the excitation power density and the emission intensity of UCPs, the small fluctuations in the laser power causes a second power change in the UCP emission intensity. Donor emission can be utilized for correction because the emission intensity of this large particles is unaffected by the UC-RET. Only the near-surface emitting ions of the

UCP can participate in UC-RET, while the major part of the emission is originating from the core part of the UCP. It is important to notice that Equation 1 is not valid with nano-sized donor crystals.

The amount of acceptor fluorophores with substantially differing molecular weights (tandem dye ~246 000 g/mol; AF680 ~1150 g/mol) were optimized independently. To explain the different outcomes depending on the acceptor choice (the tandem dye or AF680), a "carrier protein dye" comprising non-fluorescent BSA protein (molecular weight ~66 000 g/mol) conjugated, on average, with two AF680 dye molecules was also tested.

4.4.2 Enzyme-activity assay (II)

Benzonase endonuclease (Merck KgaA, Darmstadt, Germany) efficiently degrades all forms of DNA and RNA into shorter fragments (2–5 bases) without strict sequence dependence, although it favors GC-rich regions. A synthetic single-stranded substrate oligonucleotide (5'-TGGGCGCGCGG-3'; Biomers.net GmbH, Ulm, Germany) had three modifications: biotin and AF680 fluorophore at the 5'end and BBQ650 quencher at the 3' end. This internally quenched substrate oligonucleotide was almost completely non-fluorescent in an intact form (quenching efficiency >96%), but release of the quencher as a consequence of enzymatic hydrolysis resulted in recovery of the AF680 fluorescence. Biotin and AF680 fluorophore were located in such a way that benzonase could not separate these two functions.

The activity of the hydrolyzing enzyme was measured with two assay principles: a conventional fluorescence method using visible light for excitation (Figure 13a) and an NIR-excitable UCP-based method (Figure 13b). The UCP technology was evaluated against the conventional form and also the interference of whole blood (20% v/v) on fluorescence measurement was tested in both cases. The substrate oligonucleotide (25, 50, or 100 fmol) was first degraded with benzonase endonuclease (0–4 U) in enzyme reaction buffer (50 mM Tris-HCl, pH 8, 1 mM $MgCl_2$, 1 g/L BSA) for 20 minutes at +37°C. The amount of biotinylated substrate oligonucleotide was optimized so that it did not exceed the binding sites provided by the streptavidin molecules conjugated to the UCPs. The biotinylated substrates (intact or cleaved) were collected by the UCP conjugates (25, 50, or 100 ng) in the NIR-excitable version of the assay. Finally, 10 µL of either whole blood or assay buffer was added to wells and shaken briefly to mix the components (total volume 50 µL). In the conventional method the emission intensity of AF680 was measured with Victor 1420 Multilabel Counter (PerkinElmer LAS, Wallac Oy, Turku, Finland) equipped with a red-sensitive photomultiplier tube. The correct excitation wavelength from a halogen lamp was selected with a 655/22-nm excitation band-pass filter, and the emission was collected for 2000 ms utilizing a 720/45-nm emission band-pass filter. In the case of the UCP-based method, the sensitized emission of AF680 fluorophore was measured with the modified Plate Chameleon under NIR excitation. Because a second-generation version of the Plate Chameleon with a more stable excitation was in use, no corrections of emission intensity were carried out.

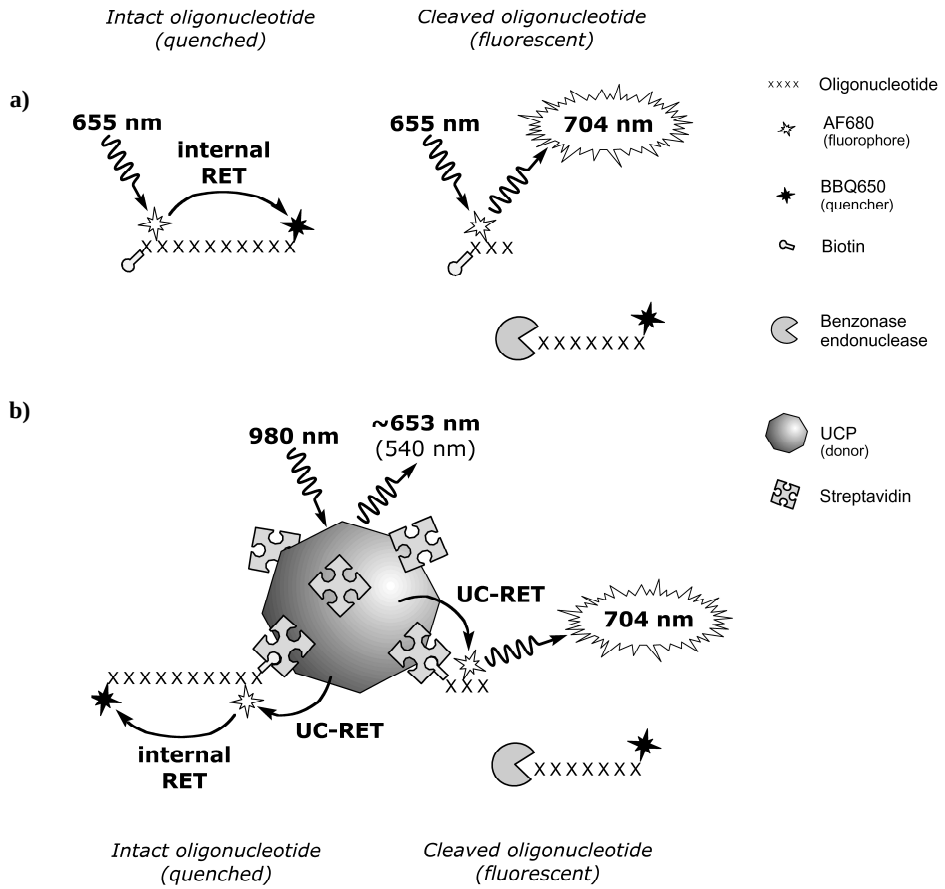

Figure 13. Principle of the enzyme activity assay for hydrolyzing enzymes utilizing either (**a**) the conventional fluorescent method or (**b**) UCP technology. In the case of hydrolytic enzyme reaction (right), the quencher of the synthetic substrate oligonucleotide is released, and the sensitized emission of the acceptor fluorophore can be detected around 700 nm. If the double-labeled substrate oligonucleotide remains intact (left), the sensitized emission of AF680 is quenched and no signal is observed. The AF680 fluorophore could be excited (**a**) directly with red light (655 nm) or (**b**) through the UCP donors excitable with NIR radiation (980 nm). The UCPs were conjugated with streptavidin in order to collect all biotinylated oligonucleotides (intact and cleaved) present in the reaction well. *RET, resonance energy transfer; UC-RET, upconversion-RET.*

4.4.3 Dual-parameter sandwich hybridization assay (III)

Two nucleotide sequences were detected simultaneously from the same reaction well by utilizing two different acceptor fluorophores matching with the green and red emission bands of the UCP donor (Figure 14). The target sequences from the HLA-B27 allele (human leukocyte antigen) (target 1, T1) and β-actin gene (target 2, T2) are identical to those in a previously published PCR-based assay for ankylosing spondylitis diagnostics (Välimaa *et al.*, 1998). Calibration curves were determined by measuring the two targets from the separate reaction wells as well as from the same well.

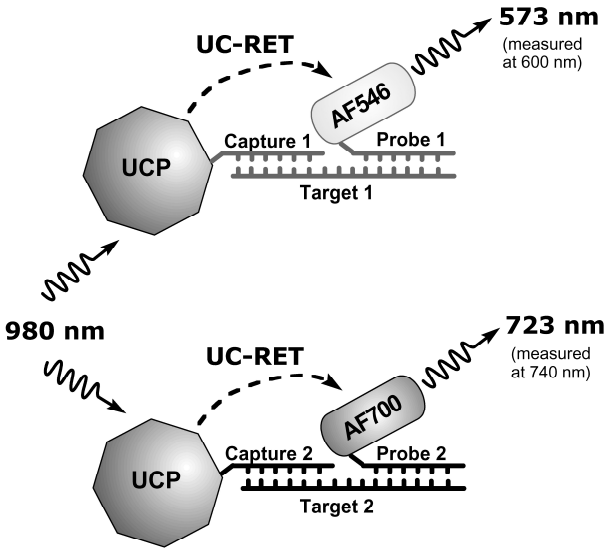

Figure 14. Principle of the dual-parameter sandwich hybridization assay. The target oligonucleotide hybridizes with a complementary oligonucleotide conjugated to the UCP and also with a fluorophore-labeled probe. The formation of the sandwich complex enables resonance energy transfer from the UCP to the acceptor fluorophore. Two different target sequences can be detected simultaneously from the same reaction well by utilizing the two emission bands of the UCP donor (540 nm and 653 nm) along with two spectrally distinguishable acceptor fluorophores (AF546 and AF700). For simplicity, only one capture oligonucleotide per UCP is depicted. *UC-RET, upconversion resonance energy transfer; Target 1, β-actin sequence; Target 2, HLA-B27 sequence.*

The NaCl concentration of the assay buffer was raised to 1 M (6.7 times higher than normally) to enhance the hybridization efficiency. The synthetic target oligonucleotides (0–0.4 pmol of β-actin target and/or HLA-B27 target; Biomers.net GmbH) were hybridized with AF546- and AF700-labeled probes (0.56 pmol of β-actin probe and 0.64 pmol of HLA-B27 probe) for 30 minutes, of which the first 10 minutes were at 60°C to unfold possible secondary structures of the oligonucleotides and the remaining 20 minutes were at 35°C to enable specific hybridization. The silica-encapsulated UCPs (0.6 µg and 1 µg) conjugated with capture oligonucleotides specific for either the β-actin or the HLA-B27 target sequence were added, and the amount of formed sandwich complexes was measured with the modified Plate Chameleon at room temperature because the instrument did not support temperature control. The sensitized emission of AF546 and AF700 were selected with different emission band-pass filters and the second-generation instrument allowed intensity correction to be ignored. The data analysis involved only subtraction of the background fluorescence (originating from e.g., the photon reabsorption by the acceptor) from the raw data.

Prior to constructing the sandwich assay, the feasibility of the oligonucleotide–UCP conjugate was tested in a more simple direct hybridization assay. In this study, a labeled test probe was complementary with the capture oligonucleotide conjugated with the UCP (no target oligonucleotide involved at all). The direct hybridization assay was utilized to evaluate the performance of two approaches to coupling the capture oligonucleotide with the UCP (**unpublished**): direct conjugation (oligonucleotide–UCP) or biotinylated capture oligonucleotides bound to a streptavidin–UCP conjugate. In addition, silica-encapsulated UCPs were compared with PAA-coated UCPs because the thickness of the coating layer is

crucial in the UC-RET-based assays, and in our laboratory this was the first application utilizing the silica polymerization.

4.5 Energy transfer from UCPs (IV)

The nature of the energy transfer from the UCP donor to the acceptor fluorophores was studied by measuring the luminescence lifetime of the UCP with the modular FD luminometer in different situations: the UCP alone without any fluorophores ('D only' sample), the UCP conjugated with fluorescent acceptor molecules ('D→A' sample), and the UCP in presence of fluorescent acceptor molecules, but not conjugated with them ('D+A' and 'D+(5×)A' samples). The aim was to find changes in the donor luminescence lifetime that would confirm the distance-dependent resonance energy transfer process in 'D→A' samples. Three different acceptors (BPE, ATTO565 or DY556) were tested to add to the reliability of the results, and accordingly three sample sets were prepared. The UCP concentration in all samples was fixed (0.2 mg/mL), and the acceptor amount was equal in the 'D→A' and the 'D+A' samples containing the same acceptor molecule. The 'D+(5×)A' sample contained a 5-fold acceptor concentration compared to the 'D+A' sample to increase the intensity of acceptor emission. The acceptor concentrations were determined based on fluorescence intensity measurements. A possible self-quenching phenomenon in those 'D→A' samples having high acceptor load may result in biased apparent acceptor concentration. Actually, the concentrations do not affect the luminescence lifetimes at all but only luminescence intensity and, consequently, there was no need to ensure the exact concentrations. A more precise method for determining the amount of the dye would have been based on the absorbance reading, but the strong scattering caused by the UCP particles confused the results.

The luminescence lifetime measurements were carried out in an aqueous environment (10 mM borate buffer (pH 8.5) containing 1 g/L Tween 20). The systematic deviations originating from the instrument were compensated by measuring the scattered excitation radiation from a control sample consisting of colloidal silica (LUDOX® HS-40, Sigma-Aldrich, St. Louis, MO) that does not induce phase shift in the signal within the used frequency range (10–100 000 Hz corresponding to 1.6–16 000 μs).

The principles of the data analysis have been described in previous publications (Hyppänen *et al.*, 2010; Kankare and Hyppänen, 2011), and the mathematical formulas are reported in original publication **IV**. The out-of-phase signals of the donor ('D only'; measured at 544 nm) and the acceptor ('D→A', 'D+A' or 'D+(5×)A'; measured at 600 nm) samples were fitted together.Thus, both samples attain the same set of lifetime values (τ) but different values of relative amplitudes (A_k) and relative sum of amplitude factors (ρ). As a result, the acceptor-induced changes in the luminescence lifetimes can be easily observed.

5 SUMMARY OF RESULTS AND DISCUSSION

5.1 Colloidal UCPs for biocompatible applications

5.1.1 UCP material

The $NaYF_4$ host material is about four times denser than water (Pyatenko and Voronkov, 1962). To form a stabile colloid, where the UCPs are evenly dispersed in aqueous solution, submicrometer-sized (below 400 nm) or more preferably nano-sized (below 100 nm) particles were pursued. The final size of the ground UCP bulk material was around 340 nm (**I**–**II**) or 300 nm (**III**) on average, based on measurements with the Coulter N4 plus analyzer. However, the size distribution was inevitably wide and the particle shape irregular due to an uneven grinding outcome (Figure 15a). These features may slightly bias the result of the Coulter analyzer, which relies on the different Brownian movement and light scattering properties of particles with differing size, and is not able to discriminate between size populations with only small differences. TEM images, which were predominantly used for characterization in the latest studies (**IV**), show particles equally despite the size, but sample preparation may affect the outcome, and sometimes it is difficult to find a representative spot on the TEM grid. The nanocrystals synthesized with the co-precipitation method (**IV**) were quite uniform in size (~110 nm), and the shape was spherical-like according to the TEM images (Figure 15b).

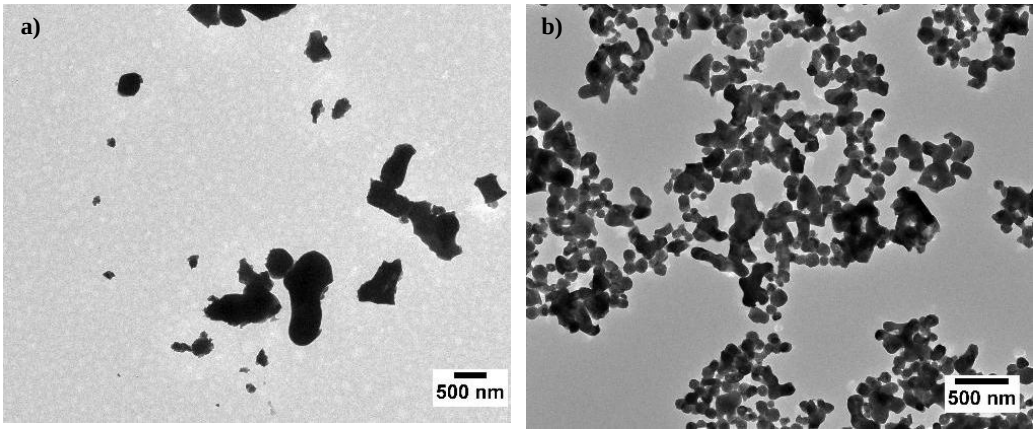

Figure 15. TEM images (**a**) from the ground UCP bulk material and (**b**) from the UCPs synthesized with the co-precipitation method. The UCP bulk material in the image was silica-encapsulated and conjugated with streptavidin (not visible), while the co-precipitated UCPs bore no modifications. Note that the scale bar is not identical in the figures. (**unpublished)**

The decrease in the UCP particle size increases the surface area-to-mass ratio enabling higher bioconjugation capacity per certain mass of UCPs. As a result, a larger amount of acceptor molecules can be bound to the UCP conjugates, and thus the dynamic range of the homogeneous bioaffinity assays is expanded. In addition, the volume of the UCP core, which promotes the background fluorescence rather than participates in the UC-RET, is decreased and greater signal-to-background ratios are expected. A narrow size distribution of the UCPs is of course pursued, but this feature is more important in heterogeneous assays, where the luminescence of the UCPs is monitored and each binding event should result in an equal change in the luminescence intensity. In the UC-RET-based homogeneous assays, the intensity of the sensitized emission of the acceptor changes with the analyte concentration. In this case, the equality of the donor particles is not of that high

importance as only a small fraction of emitting ions participate in transferring energy to one individual acceptor. The shape of the UCP particle may affect the non-specific binding properties as a spherical object can only have a pointed contact surface with a flat article, while all other shapes offer a wider contact surface and possibly more interactions leading to stronger binding. To conclude, nanocrystalline UCP materials meet the expectations better than the ground bulk material although it is very suitable for the UC-RET applications as demonstrated in this study.

The commercial PTIR550/F bulk material was criticized in the literature by Morgan *et al.* (2008) when they discovered that this UCP material was heterogeneous in spectral properties. Because no detailed data was provided to support the claim that some UCP crystals emit primarily red light while others show more intense green emission, we asked a collaboration group from the Leiden University Medical Centre (Leiden, the Netherlands) to confirm the findings. Dr. Paul Cortsjens and his research group examined the PTIR550/F material with a confocal fluorescence microscope equipped with a two-photon NIR laser and concluded that it indeed contains UCP crystals with varying red-to-green ratios (from 0.77 to >2.26; **unpublished**). The differences between individual crystals were independent of the crystal size and the focal plane (i.e., laser focus). Morgan *et al.* advised avoiding the use of the PTIR550/F in UC-RET-based applications, but no alarming behavior related to this matter was observed during this study. Because all crystals were producing both green and red emission, it is likely that each crystal was able to transfer energy from both energy states to acceptor fluorophores in close proximity, and the assay performance was not greatly compromised due to the heterogeneity. Other materials than bulk UCP were constantly under development, but the reasons behind substitution of the PTIR550/F mainly arose from the size and morphological considerations.

The nearly nanocrystalline $NaYF_4$:Yb^{3+},Er^{3+} material used in original publication **IV** was prepared with the co-precipitation method (Hyppänen *et al.*, 2009; Yi *et al.*, 2004), requiring a solid-state annealing step at rather high temperature (typically 400°C for 5 h) to generate brightly luminescent hexagonal β-phase UCPs. The TEM images suggested that the UCP particles tend to partly sinter together during the annealing step at high temperatures forming large aggregates of β-phase UCPs (Figure 16a). In contrast, the lower annealing temperatures yielding separate, individual crystals (Figure 16b) produced predominantly cubic α-phase structure with significantly lower emission intensity.

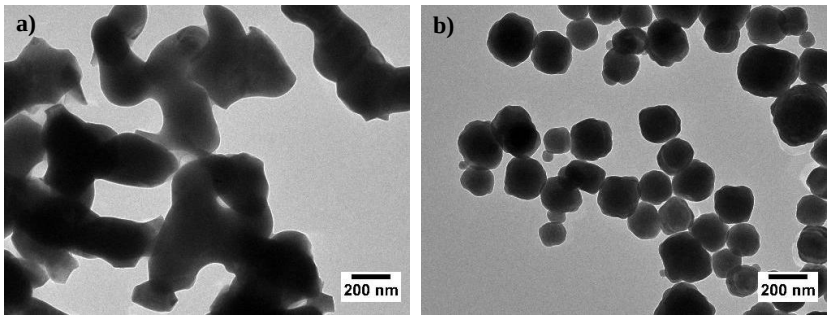

Figure 16. Effect of the annealing temperature upon the size and shape of the UCPs in the co-precipitation synthesis. TEM images from $NaYF_4$:Yb^{3+},Er^{3+} annealed for 5 h (**a**) at 450°C and (**b**) at 300°C. (**unpublished)**

In the future, the UCP synthesis protocol will be developed so that the crystal sintering is avoided. Promising options are those solution-phase methods that do not require a solid-state annealing step at all (see chapter 2.2.2). Some test syntheses in oleic acid solvent have already been carried out according to a recent publication (Wang *et al.*, 2010). The TEM images confirm that extremely small UCP nanocrystals are formed (diameter c. 10–20 nm) (Figure 17). The emission intensity of these nanocrystals has already been shown to be sufficient for the UC-RET applications (Arppe *et al.*, 2011), although a dramatic decrease was anticipated due to the surface defects and quenching (Suyver *et al.*, 2005a; Boyer and van Veggel, 2010). However, as most of the emitting ions in the UCP nanocrystal this small can participate in the RET process, significantly more efficient energy transfer compared to the larger UCP particles is likely achieved. The preliminary results suggest that by substituting the relatively large UCP material used in this study with the nanocrystalline material, the extra background luminescence originating from the core parts of the UCP particles is avoided and the detection limits are improved even from those reported here.

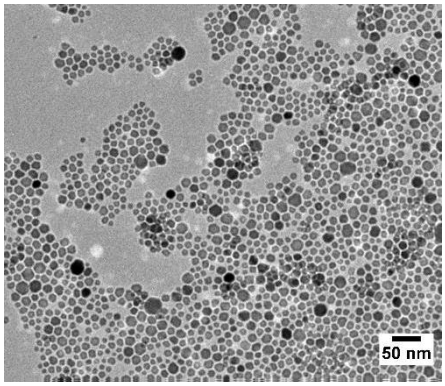

Figure 17. Size and shape of the UCPs synthesized in high-boiling point solvent (in oleic acid). TEM image of $NaYF_4$:Yb^{3+},Er^{3+} nanocrystals with diameter below 30 nm. (**unpublished)**

5.1.2 Surface functionalization of the UCPs

A simple coating was formed by adsorbing a functionalized polymer on the surface of the UCPs. Many kinds of PAAs with varying length (molecular weight on average 8 000–4 000 000 g/mol) were tested, but still no better PAA than Additol XW330 (average molecular weight 30 000–50 000 g/mol) was discovered. When further conjugated with streptavidin after the adsorption step, the Additol XW330 resulted in the highest biotin binding capacities for some reason (**unpublished**). The carboxylate ligands of the PAA polymer probably coordinate with the surface rare earth ions of the UCP, and the coating seems to be relatively stable. However, the nature of the coordination is presumably not totally irreversible, and detachment of the coating may occur during a longer storage period. We have no data about the thickness of the PAA layer, but the applicability to the UC-RET-based assays suggests a layer thinner than 10 nm. If the coating is formed from more than one layer of the polymer, only the monolayer closest to the UCP surface can be in contact with the rare earth ions, and the potential outer layers are more prone to detach. The free PAA molecules themselves cause no harm in the UC-RET applications, but the biomolecules conjugated to the detached PAA are able to bind the analyte without any modulation of the sensitized emission, resulting in impaired LOD of the assay. Other surface modification methods were constantly under investigation, but it was a challenge to

find a replacing method providing a thin coating with as high density of functional groups as the Additol-modified UCPs.

Growing a SiO_2 layer by hydrolyzing TEOS monomers has been commonly used for covering the nanoparticles and other surfaces (Graf *et al.*, 2003; Yi *et al.*, 2005; Selvan *et al.*, 2005; Darbandi *et al.*, 2005; Darbandi and Nann, 2006). The well-known Stöber method (Stöber *et al.*, 1968) carried out in ethanol solvent provided a too-efficient polymerization reaction which was impossible to control sufficiently to achieve a reproducible thin coating (**unpublished**). Satisfactory control of the thickness was finally attained in a water-in-oil microemulsion environment. The silylation procedure has recently been further developed (not used in this study) by adding another organosilane, a methylphosphonate, to inhibit the back bonding of the amino groups with the silanols on the particle surface and to increase the electrostatic repulsion between the UCP particles (Bagwe *et al.*, 2006).

The performance of the coatings could not be analyzed directly because an appropriate TEM for checking the thickness was not available at that time and the density of the functional groups on the modified UCP surface was not easily determined. Consequently, the conclusions were made based on post-bioconjugation tests (see next chapter). Later, when the silica-encapsulation was already established as a routine surface modification method in our research group, we observed from the TEM images that the silica layer was typically 5–15 nm thick (Figure 18). Although the coating is thin enough, this figure reveals the disadvantage of the silica-encapsulation method. The coating surrounds a UCP aggregate rather than encapsulates uniformly single nanocrystals. It is unknown whether the UCPs were already sintered together during the UCP synthesis or whether the silylation step was responsible for the aggregate formation. The PAA-coating is invisible in TEM images and no evidence on the thickness of the adsorbed layer is available.

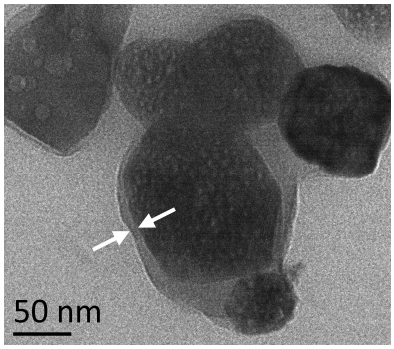

Figure 18. Thickness of the silica layer encapsulating the co-precipitated UCPs. The arrows in the TEM image indicate the less dense material covering the dark UCP material ($NaYF_4$:Yb^{3+},Er^{3+}). The UCPs were encapsulated in a silica shell, conjugated with streptavidin (not visible) and filtered to exclude large particles. (**unpublished)**

None of the surface functionalization methods is perfect, and the negative value of the various disadvantages had to be rated. Considering that the application was intended to be a UC-RET-based assay, the possible aggregation of the UCPs due to a silica-encapsulation limits the dynamic range of the assay (reduced surface area), while the detached PAA deteriorates the LOD of the assay (no signal modulation induced by a binding event).

Therefore, the silica-encapsulation has established its status as the dominant coating method in our research group after many years of optimization.

5.1.3 Conjugation of the UCPs

The aim was to attach as many streptavidin molecules or oligonucleotides as possible to each UCP crystal. A high analyte binding capacity translates to a wide dynamic range in the UC-RET-based bioaffinity assays. In the case of low binding capacity, more UCP conjugates are required in the assay and the background luminescence originating from the donor cross-talk and reabsorption increases. Several parameters have an influence on the conjugation outcome. First, the size of the UCP particles determines the surface area to be covered. Small particles surpass the larger ones by having greater area-to-mass ratio. Second, successful UCP functionalization is a key factor as low density and poor availability of the functional groups on the UCP surface may limit the conjugation yield. However, above a certain limit, the size of the biomolecule becomes more restrictive than the density of functional groups as one large biomolecule may obscure several adjacent functional groups. Finally, by using an excess of biomolecules and a large amount of the relatively cheap activating reagents (EDC and sulfo-NHS), the yield in the conjugation reaction can be maximized. Nonetheless, owing to cost-effective production, the use of expensive biomolecules is usually limited. Table 10 summarizes the UCP conjugates prepared for this study.

The yield in HLA-B27 oligonucleotide conjugation was repeatedly almost twice as high as that of the β-actin oligonucleotide conjugation. Because the amount of oligonucleotide in the UCP conjugate was quantified based on hybridization capacity, hybridization efficiency plays an important role as well. However, the length and the GC content determining the stability of double-stranded DNA was similar for both oligonucleotide sequences having melting temperatures over 50°C, and no reason for different conjugation behavior was found.

Even though the oligonucleotides (14 or 15 nt) had a molecular weight over an order of magnitude smaller than the massive streptavidin protein, based on the binding capacity the oligonucleotide density in the conjugate was still lower than the streptavidin density. Up to 4 binding sites may be reachable in one streptavidin molecule, which compensates for some of the size difference, but explains the high binding capacity only partly. It has been anticipated that proteins could spontaneously absorb on the UCP surface, intensifying the conjugation reaction. The number of weak interactions between the UCP and the molecule to be conjugated depends among other things on the size of the molecule, which favors large protein molecules.

The fluorescent molecules can be divided into organic fluorophores (ATTO565 and DY556) and fluorescent proteins (BPE). Again, the protein conjugation was significantly more successful than the conjugation of the small molecules with only one functional group per molecule. No reason was found for the poor conjugation yields that were achieved with the organic fluorophores. Also, many other fluorophore conjugates were prepared, but the yields were comparable (data not shown).

The PAA-coating and the silica-encapsulation methods cannot be compared based on these results, because different biomolecules were used with the different UCP functionalization approaches. From other experiments we have discovered that approximately the same

binding capacities may be achieved with both methods, and sometimes the silica-layer provides even better bioconjugation yields (data not shown).

Table 10. Summary of the UCP conjugates used in this study.

Biomolecule or acceptor dye	**Conjugation reaction**			**Relative surface/volume ratio of the UCP** [c]	**Publication**
	In [a] *nmol / (mg UCP)*	**Out** [b] *nmol / (mg UCP)*	**Yield** %		
Streptavidin *(biotin binder)*	1.4	0.34	24	1.0	**I, II**
Oligonucleotide *(complementary hybridization)*	1.2 *(HLA-B27)* 1.2 *(β-actin)*	0.12 [d] 0.063 [d]	10 [d] 5.3 [d]	1.1 1.1	**III** **III**
BSA *(no specific interactions)*	1.2	*N/A*	*N/A*	3.1	**IV**
BPE [e]	0.025	0.013	52	3.1	**IV**
ATTO565 [e]	12	0.141	1.2	3.1	**IV**
DY556 [e]	67	0.241	0.36	3.1	**IV**

Abbreviations: BSA, bovine serum albumin; BPE, B-phycoerythrin; *N/A*, not available
[a] Amount of biomolecule or acceptor dye in the conjugation reaction per 1 mg of UCP
[b] Amount of biomolecule or acceptor dye in the UCP conjugate per 1 mg of UCP based on binding capacity determination or fluorescence intensity, respectively
[c] Surface-to-volume ratio of each UCP particle is proportioned to the largest UCPs used in publications **I**–**II**
[d] Silica-encapsulated UCPs, while the other conjugates were constructed from PAA-coated UCPs
[e] To avoid self-quenching, the density of fluorescent molecules was kept low

5.2 Homogeneous assays based on upconversion resonance energy transfer

One issue that differentiates the UC-RET-based applications constructed in the University of Turku from the others is that quite low concentrations of the UCP donor and acceptors are used. Another difference has been the utilization of the ground UCP bulk material instead of nanocrystalline UCPs. A commonly-shared feature in the UC-RET-based bioanalytical assays has been the detection limits at sub-nanomolar range.

5.2.1 Energy transfer acceptors

There is a very large selection of commercial organic fluorophores and fluorescent proteins spanning the entire visible wavelength range. In addition, particulate fluorescent labels are available, but they are less suitable for UC-RET acceptors because of steric issues and the formation of particle aggregates due to multiple binding sites. An ideal acceptor fluorophore would have an optimally overlapping excitation band with the donor emission band, allowing efficient energy transfer. The emission band of the acceptor, in turn, should match the emission minimum of the donor. Finally, acceptors with bright emission and high stability against photobleaching facilitate the reading of the assay result.

Another choice for an energy transfer acceptor is a dark quencher that gives the energy off via molecular vibrations (i.e., heat) without any fluorescence. In this case, the decreasing donor emission is monitored instead of the increasing sensitized emission of the acceptor, but an ultimate detection limit is difficult to achieve with this concept as distinguishing a small reduction in intense emission caused by a tiny amount of analyte is not straightforward. Two different variations of energy transfer acceptors aiming to better performance in bioaffinity assays were studied in this thesis.

*Spectral tuning: Tandem dye (**I**)*

The conventional fluorophores have characteristically broad excitation and emission bands with a small Stokes shift around 20 nm (the difference between the excitation and emission maxima) and possibly a red tail in the emission band extending to the longer wavelengths. A larger Stokes shift would facilitate the spectral separation by allowing the measurement of the sensitized emission intensity of the acceptor fluorophore without any cross-talk from the donor. A fluorescent molecule with tunable excitation and emission maxima far apart from each other would alleviate the limitations generally confronted when using conventional fluorophores. Usually, either the excitation wavelength or the reading wavelength is a compromise from the ideal situation. *Quantum dots* have an eminently broad excitation band at UV region, and the position of the narrower emission band depends on the size of the dot (Xing and Rao, 2008; Medintz and Mattoussi, 2009). Polystyrene microspheres loaded with two or more fluorescent dyes capable of transferring energy to the fluorophore with the longest emission wavelength (*TransFluoSpheres*®; Molecular Probes Inc., Eugene, OR) are another option to widen the Stokes shift (Roberts *et al.*, 1998; Bhalgat *et al.*, 1998). A similar relay approach is exploited in *tandem dyes*, where the compatible fluorophores are covalently conjugated to each other. Tandem dyes are not particles like the two other versions of tunable acceptors, and they are already in general use, for example in flow cytometry applications (Hulspas *et al.*, 2009).

A biotinylated tandem dye composed of a large phycobiliprotein BPE (absorber) and several AF680 fluorophores (emitters) was constructed. The tandem dye, BPE–$AF680_5$, had a pseudo-Stokes shift of 139 nm, which is significantly greater than the Stokes shifts of individual BPE (9 nm) and AF680 (23 nm). The molar ratio between the absorber dye and the emitter dye was optimized by preparing various trial versions of the tandem dye. The overlap of the fluorescence spectra was limited (Figure 19a), but still adequate for the RET between the closely conjugated fluorophores. No energy transfer was observed in solution containing the same components unattached to each other. The quantity of the emitter molecule in the tandem dye was extremely critical: two AF680 fluorophores per BPE was too few and nine too much. The former trial version was spectrally emphasizing the absorber rather than showing an efficient internal energy transfer to the emitter (Figure 19b), and the latter version with effective energy transfer showed reduced emission intensity at 704 nm due to a self-quenching phenomenon (not evident from the figure due to the normalization of the fluorescence intensity) (Figure 19c). Instead, around five AF680 dyes conjugated with BPE produced a tandem dye with an excitation maximum at green wavelengths (characteristic to the absorber) and an emission maximum at red (characteristic to the emitter) (Figure 19d). However, a remarkable part of the BPE emission (at 575 nm) was unattenuated, revealing non-complete internal energy transfer. The BPE molecule has several chromophores (38 phycoerythrobilins and at least 2 phycourobilins), and the outer dimensions of this disc-shaped phycobiliprotein are 12 nm

and 6 nm (Glazer and Hixson, 1977). It is possible that more energy is donated by the BPE than five AF680 molecules randomly distributed all over the BPE are capable of accepting (i.e., no AF680 molecules at the ground state). The extra energy in this case is emitted at a wavelength characteristic to BPE. Increase in the AF680 amount resulted in more attenuated BPE emission intensity, supporting this hypothesis. However, as discussed above, self-quenching limited the use of high emitter amounts.

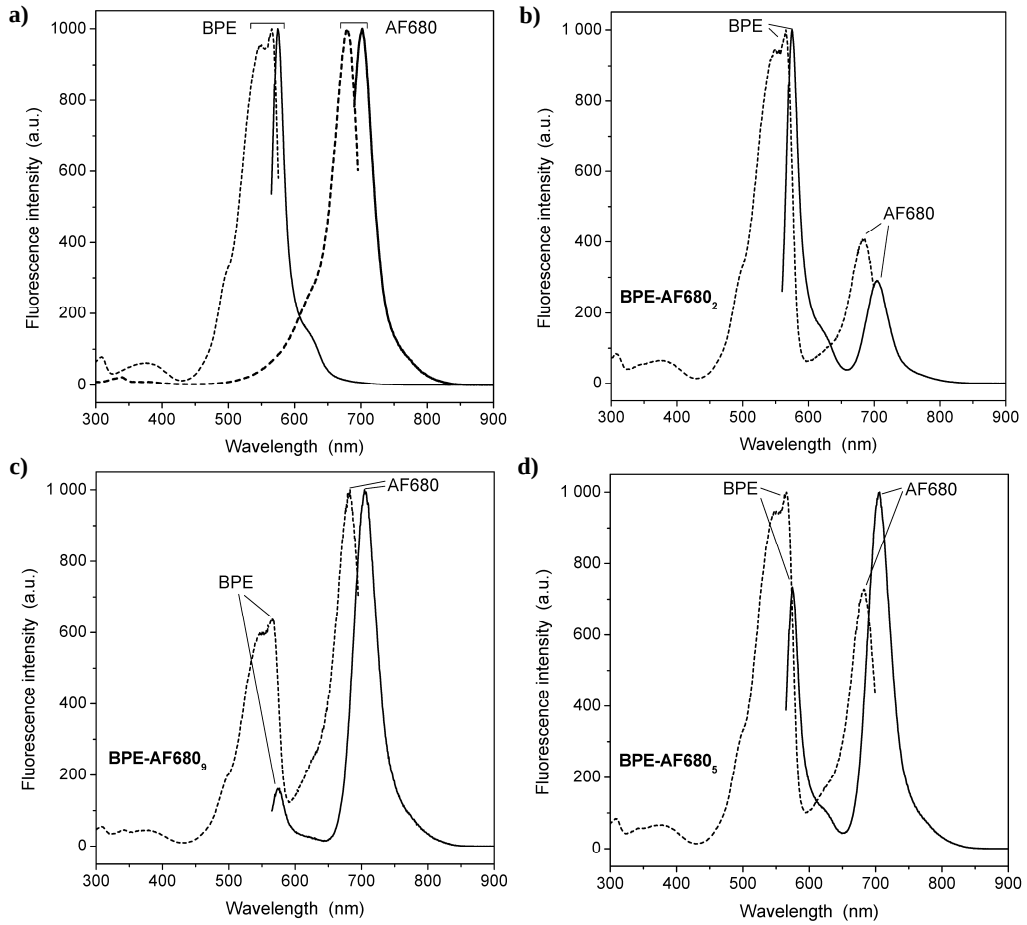

Figure 19. Fluorescence spectra of (**a**) BPE and AF680 separately, and tandem dyes composed of BPE conjugated with approximately (**b**) 2, (**c**) 9 or (**d**) 5 AF680 fluorophores. Excitation (*dashed line*) and emission (*solid line*) bands characteristic to BPE and AF680 are distinguishable. *a.u., arbitrary unit.* (**I**)

The performance of the tandem dye (BPE–AF680$_5$) as an energy transfer acceptor was tested by mixing various amounts of the biotinylated fluorophore with the streptavidin-conjugated UCPs emitting at 540nm and at 655 nm (Figure 20). The non-specific background signal (i.e., instrument noise, non-specific binding and photon reabsorption) was excluded from the specific signals presented in the figure. For comparison, the same test was carried out with the individual AF680 fluorophore and BPE. In addition, a carrier protein dye (BSA–AF680$_2$), in which the fluorescent BPE was replaced with a non-fluorescent BSA protein, was tested as a control to show the environmental effects resulting from the protein conjugation of the AF680. The BPE alone did not generate a distinctive emission at 740 nm, which was expected based on the emission spectrum. In the

case of other acceptors, the intensity of the sensitized emission was increased until the density of acceptors was too high, favoring the self-quenching phenomenon. The optimal acceptor conjugate concentrations were lower for the two protein-containing acceptor conjugates (~1.6 nM) compared to the AF680 (~4.4 nM), which is explained by the size difference (60–200-fold) and differing AF680 load. The most important observation was that the highest specific signal from one binding event was obtained with the tandem dye. This usually translates to a lower detection limit, because less binding events are required for a distinguishable signal.

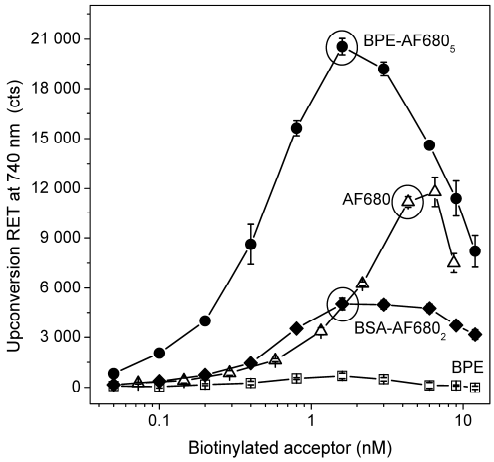

Figure 20. Comparison of different biotinylated acceptor dyes as energy acceptors in combination with the UCP donor. The sensitized emission of the tandem dye BPE–AF680$_5$ (*filled circles*), AF680 (*open triangles*), carrier protein dye BSA–AF680$_2$ (*filled diamond*; control) and BPE (*open square*; control) was measured at 740 nm under NIR excitation. Circled data points represent optimal concentrations of the biotinylated acceptors for the UCP–streptavidin conjugate in question (note the significantly differing molecular weights of the acceptors). Data points are means from four independent replicas, and error bars show standard deviation. *RET, resonance energy transfer; cts, counts.* (**I**)

The main benefit from the tandem dye in this study can be explained with a total spectral overlap: both of the excitation bands (characteristic to BPE and AF680) match perfectly with the two emission bands of the Yb^{3+}–Er^{3+}-doped UCP. The internal energy transfer in the tandem dye results in an increased emission intensity at red wavelengths, which was monitored in the assay. To further refine the concept of tandem dye, replacement of the phycobiliprotein absorber with an organic fluorophore would eliminate some of the drawbacks. In the protein-based tandem dye and carrier protein dye, the emission intensity per single AF680 fluorophore at 704 nm was about one third of that without protein conjugation. Decreasing the dye content in the conjugate did not restore the fluorescence intensity of the AF680, which suggests that the decline was not merely due to the self-quenching of AF680 but also other reasons, such as environmental change in the protein conjugate, influenced the fluorescence properties of the AF680. Another challenge with a protein-based tandem dye is the variation in conjugation degree between the individual conjugates and between the conjugation batches. Conjugation of the absorber and the emitter in a more controllable manner (e.g., only one reactive group per molecule) would result in a reproducible tandem dye. A smaller size of acceptor molecule could also be beneficial in terms of steric hindrance and distance limitations related to the RET.

*Fluorescence quenching: Internally quenched fluorogenic substrate molecule (**II**)*

Although stated otherwise at the beginning of this chapter, in some special energy transfer applications the quenchers are actually more advantageous than the fluorophores. Classical examples are the activity assays for hydrolyzing enzymes exploiting double-labeled fluorogenic substrates. An energy donor and an acceptor in the substrate molecule are separated by a specific recognition site for the enzyme and the enzyme activity will result in the release of the acceptor. By choosing a dark quencher over a fluorophore to be combined with the donor, the monitored signal will increase along with the enzyme activity (Figure 21a). The relative change in the signal at low enzyme activities is rather large, and thus easier to detect, if the calibration curve is growing from a minimal signal towards a maximal level. In the opposite case, with a downward calibration line (Figure 21b), a small decrease in a maximal signal is impossible to distinguish from the standard deviation of the signal. To achieve an even better LOD in the enzyme activity assay, the fluorescence quenching was brought together with the UCP technology. However, it was not possible to directly quench the emission of the submicrometer-sized UCPs with an organic quencher molecule, BBQ650, because the RET-based quenching is efficient only at a short range (<10 nm). In large particles having a diameter of 340 nm, approximately 80% of the emitting ions are situated in the core, too far away to be quenched. This calculation does not take into account the thickness of the surface modification, which will still increase the proportion of the unreachable emitter ions. We measured the emission of a UCP–streptavidin conjugate in both the absence and presence of the biotinylated BBQ650 quencher. No change in the UCP emission intensity was observed even though practically all binding sites on the UCP conjugate were occupied by the quencher molecules (**unpublished**). Wang *et al.* (2005) has reported an avidin assay where 70% of the UCP emission was quenched with gold nanoparticles. This was possible because the diameter of the UCPs was only 50 nm and, in addition, gold colloid allows surface energy transfer over longer distances (Ling and Huang, 2010) than RET.

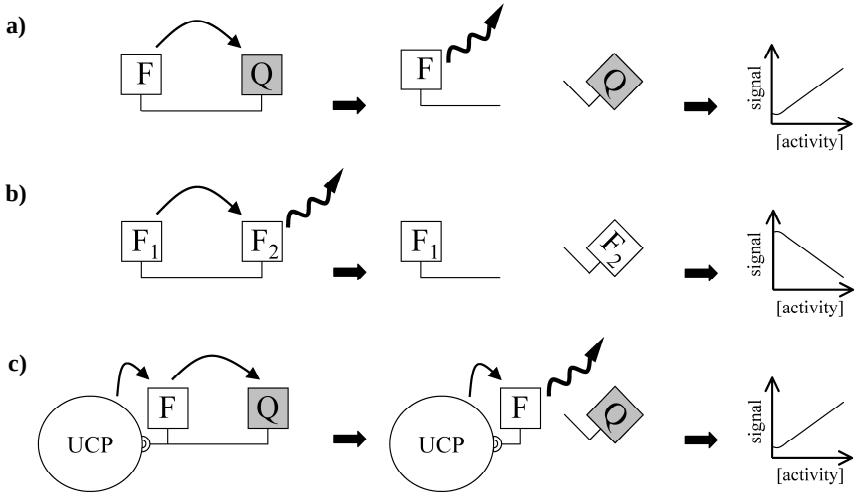

Figure 21. Labeling options for a cleavable double-labeled fluorogenic substrate. A fluorescent donor is combined with (**a**) a dark quencher, (**b**) an acceptor fluorophore or (**c**) an internally quenched fluorophore acceptor. *F, fluorophore; Q, dark quencher; curved arrow, resonance energy transfer; waved arrow, monitored emission.*

For larger, unquenchable donor particles, the problem can be solved with a sequential RET-based concept, where the particle serves as an energy donor to a quenchable fluorophore instead of acting as a monitored fluorophore itself (Figure 21c). In publication **II**, the sensitized emission intensity of the AF680 fluorophore bound to a UCP donor was dependent on the vicinity of the quencher, which translated directly to the activity of the hydrolyzing enzyme. The AF680 and BBQ650 quencher were conjugated to opposite ends of a short synthetic oligonucleotide consisting of 10 nucleotides. The quenching efficiency in an intact substrate molecule was almost complete (96%). It is difficult to achieve an absolute quenching, because even minor remains of unconjugated fluorophores or quencher-missing substrates produce some undesirable fluorescence. The use of an internally quenched substrate is an extremely intelligent solution in terms of avoiding the background fluorescence. Large amounts of labeled substrate can be used without any concern for the background fluorescence produced through photon reabsorption and, therefore, a wide dynamic range in the enzyme activity assay is achieved.

5.2.2 Model assay designs based on upconversion RET

*Competitive assay for small molecules (**I**)*

Haptens and other small molecules can only be captured by one binder at a time. As two-sided sandwich assays are not applicable for determining the amount of small molecules (such as toxins, drug molecules and hormones), less-sensitive competitive assays fill this gap. D-Biotin is a small vitamin molecule expressing extremely strong interaction with the streptavidin. A homogeneous biotin assay was constructed based on a streptavidin-conjugated UCP donor and a biotinylated acceptor. In each case, either optimized concentration of AF680 (4.4 nM) or tandem dye (BPE–$AF680_5$; 1.6 nM) acceptor was exploited. Low-nanomolar concentrations could be detected regardless of the acceptor choice (Figure 22). The IC_{50} values (analyte concentrations that inhibited 50% of the maximum signal) were around 10 nM D-biotin. The specific signal in absence of the analyte (i.e., maximal signal) was 1.7 times greater with the tandem dye acceptor compared to the AF680. However, the signal-to-background ratio of the tandem dye (~8) was lower due to elevated background, but still absolutely sufficient for precise analysis.

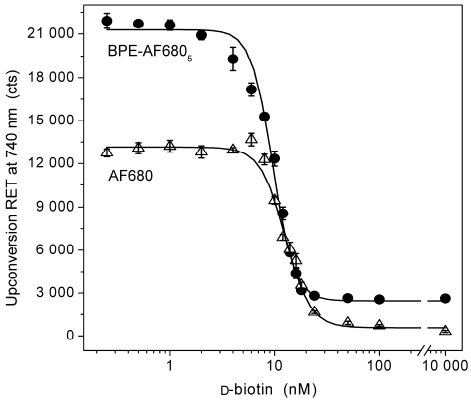

Figure 22. Calibration curves for D-biotin. Either the biotinylated tandem dye BPE–$AF680_5$ (*filled circles*) or AF680 (*open triangles*) was utilized as an energy transfer acceptor in UC-RET-based biotin assay. Data points are means from four independent replicas, and error bars show standard deviation. *RET, resonance energy transfer; cts, counts.* (**I**)

*Enzyme activity assay (**II**)*

A homogeneous assay principle based on a double-labeled fluorogenic substrate with a cleavage site is commonly employed for screening the activity of hydrolyzing enzymes (e.g., proteases (Carmona *et al.*, 2009)), for example in drug discovery applications. A model assay for determining the activity of a benzonase enzyme was constructed by utilizing sequential energy transfer from a UCP donor to a fluorophore (AF680) and further to a quencher (BBQ650) in the case of an intact substrate. Benzonase activities at around 0.01 U (Figure 23) were detected by monitoring the recovery of AF680 fluorescence as a consequence of the enzyme reaction. Increases in the substrate concentration (and, therefore, UCP concentration) yielded greater specific signals and thereby better discrimination of the signal from the background. The cross-talk from the UCP donor resulted in increasing background luminescence in line with the UCP concentration. Due to high specific signal levels this was not a problem, but LOD could be improved by totally blocking the UCP cross-talk with high-quality filter choices.

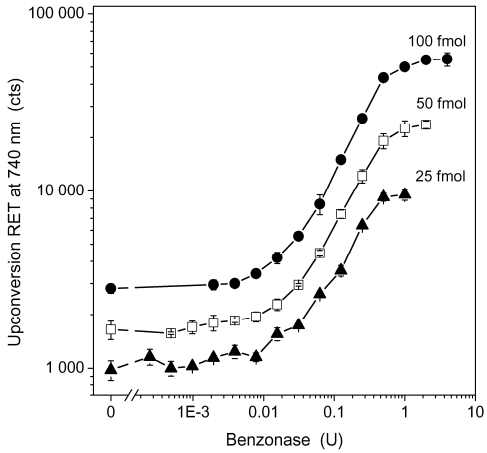

Figure 23. Calibration curves for the hydrolyzing activity of a benzonase enzyme. Three substrate amounts were utilized together with accordingly optimized UCP concentrations: 25 fmol substrate (*filled triangles*), 50 fmol substrate (*open squares*) and 100 fmol substrate (*filled circles*). Data points are means from three independent replicas, and error bars show standard deviation. *RET, resonance energy transfer; cts, counts; U, units.* (**II**)

The assay concept described in publication **II** demonstrated the feasibility of the UCP technology in fluorescence-quenching based assays suitable for drug screening purposes. The results even suggested that the infrared-excitable assay concept provides better performance compared to the conventional method tested in parallel (see chapter 5.2.3).

*Dual-parameter sandwich hybridization assay (**III**)*

Sandwich-type assays can be utilized to quantify analytes capable of binding simultaneously with two specific biomolecules. Immunoassays based on RET between the components of the sandwich complex are almost non-existent because the massive size of the antibodies (around 10 nm long (Harris *et al.*, 1998)) prevents close proximity of the donor and the acceptor. Wang M. *et al.* (2009a) managed to demonstrate the quantification of immunoglobulin G with a sandwich-type assay utilizing a silica-encapsulated UCP donor (diameter ~50 nm) and gold nanoparticle quenchers respectively conjugated to a pair of specific antibodies recognizing different epitopes of the analyte. Maximally ~80%

quenching efficiency was achieved, which was surprisingly successful with the antibody binders. Again, gold nanoparticles are exceptional quenchers compared to organic dyes, allowing efficient energy transfer over a distance double the length typical for RET (Ling and Huang, 2010). One way to reduce the dimensions of the binders is to use antibody fragments (e.g., $F(ab')_2$, Fab' or single-chain variable fragment (scFv)) instead of whole antibodies. However, some stability issues may limit the use of certain antibody fragments. A special open sandwich immunoassay utilizes antigen-dependent stabilization of heavy and light antibody variable regions (V_H and V_L) and allows RET without problems derived from the dimension (Ueda, 2002), but not all antibodies exhibit suitable interaction properties and use is therefore limited.

RET-based sandwich assays in nucleic acid detection are easier to realize, as one nucleotide unit is only approximately 0.33 nm long (Mandelkern, 1981). In publication **III**, sandwich assays for HLA-B27 and β-actin sequences were constructed by utilizing adjacent hybridization probes. The UCP donor conjugated with a capture oligonucleotide and a fluorescent acceptor coupled with a probe oligonucleotide were maximally ~6 nm apart from each other when a sandwich complex was formed in the presence of the target sequence. The surface modification of the UCP increased the distance between the labels to some extent, but the actual thickness of the surface layer was not known. A sandwich complex consisting of oligonucleotides is not rigid, and the orientation (bended vs. straight) of course also affects the distance between the donor and the acceptor.

The sandwich hybridization assay was carried out separately for the two targets (single-parameter assays) and, in addition, the two assays were combined into the same reaction well to multiplex the detection (a dual-parameter format). Specific probes labeled with green-absorbing AF546 or red-absorbing AF700 acceptors were utilized to detect the HLA-B27 and β-actin target sequences, respectively. The ground PTIR550/F UCP donor showed more intense overall green emission than red, and even though the high extinction coefficient of the AF700 acceptor compensated the divergence slightly, 1.7 times more UCP conjugate specific for the HLA-B27 was used compared to the β-actin-specific conjugate to equalize the intensity of the sensitized emissions. The calibration lines of the single- and dual-parameter assays were comparable without severe interference caused by multiplexing (Figure 24). The background fluorescence was elevated in the dual-parameter format, although it is not detectable in the figure presenting only the specific UC-RET signals. A major part of the additional background fluorescence can be explained with the higher UCP concentration (both UCP conjugates present), causing increased acceptor emission generated through the photon reabsorption of the donor emission. The “red tail” emission of the AF546 does not extend to the measurement window of the AF700, and no traces of cross-talk between the two acceptor molecules were observed. Mis-hybridizations of the oligonucleotides might lead to deceptive results; therefore, the sequences were carefully chosen to avoid all partial complementarities between non-specific oligonucleotides and intramolecular secondary structures. Formation of sandwich complexes based on mis-hybridizations was studied in the validity verification test, in which the results were recorded both at AF546- and AF700-specific wavelengths in the presence of only one of the targets. Maximally a 1.5-fold increase in the UC-RET signal for the absent target sequence was observed compared to the background signal (Figure 25). This increase was quite insignificant, but a higher temperature during the measurement step would probably decrease the amount of non-specific hybridization and, hence, improve the LOD of the assay. Unfortunately, the plate reader did not allow temperature

adjustment outside room temperature during the measurement. Reduction of the salt concentration in the assay buffer would also create more stringent conditions for specific hybridization.

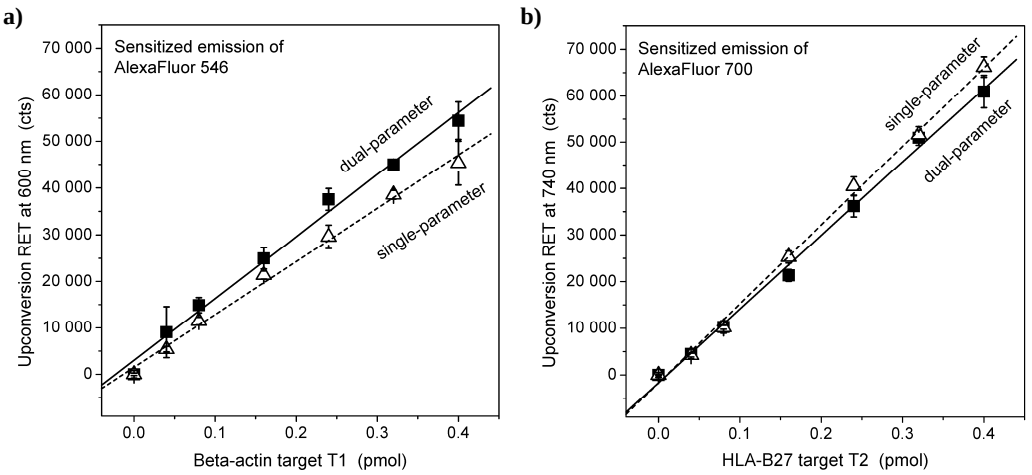

Figure 24. Calibration lines of the sandwich hybridization assay to quantify (**a**) β-actin target sequence (T1) and (**b**) HLA-B27 target sequence (T2). The probes were labeled with AlexaFluor 546 or AlexaFluor 700, respectively. The two targets were detected simultaneously using a dual-parameter assay format (*filled squares*) and separately by a single-parameter assay (*open triangles*). In the case of dual-parameter assay, the amounts of both target sequences coincided. Data points are means from three independent replicas, and error bars show standard deviation. *RET, resonance energy transfer; cts, counts.* (**III**)

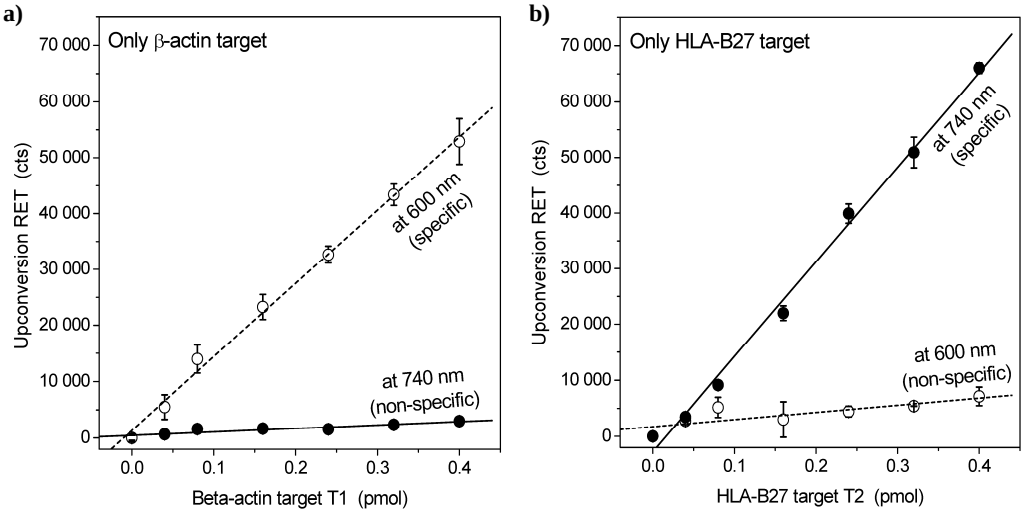

Figure 25. Validity verification of the dual-parameter sandwich hybridization assay (**a**) in the presence of different amounts of β-actin target sequence (T1) and absent HLA-B27 target sequence (T2) and (**b**) *vice versa*. The sensitized emissions of AlexaFluor 546 (*open circles*) and AlexaFluor 700 (*filled circles*) were measured at 600 nm and 740 nm, respectively. The former was conjugated with the β-actin specific probe and the latter with the HLA-B27 specific probe. Data points are means from three independent replicas, and error bars show standard deviation. *RET, resonance energy transfer; cts, counts.* (**III**)

The LOD for both target sequences was below 0.028 pmol (corresponding to 0.35 nM) in the dual-parameter assay, and the dynamic range extended up to 0.4 pmol (5.4 nM). The LODs were calculated using the definition of three times the standard deviation above the signal measured in the absence of the target. Zhang *et al.* (2006) has described a similar single-parameter assay with a detection limit of 1.3 nM. Thus, there is agreement that UCP-based sandwich hybridization assays are capable of detecting low-nanomolar target concentrations. That is not a physiological concentration, but nucleic acid detection methods generally exploit a preceding amplification step, such as PCR. The dual-parameter hybridization assay described in publication **III** is applicable to the screening of a disease-inducing gene together with an internal housekeeping control sequence used for reporting on the success of the PCR amplification. Multiplexing is also convenient in the case of two related diagnostic markers providing extra information together or when a heterozygous carrier of a genetic disorder needs to be identified.

In this dual-parameter assay, only one wavelength was used for excitation, which simplifies the requirements for instrumentation. Addition of a third parameter is theoretically possible by introducing a blue-emitting UCP doped with Yb^{3+} and Tm^{3+} ions. More complex multiplexing is not possible with homogeneous RET-based assays, because cross-talk between the labels becomes a limiting factor.

5.2.3 Near-infrared excitation

The strength of the UCP-based bioaffinity assays is the NIR excitation, but at the same time the variation in the spectral properties of the UCPs depending on the excitation power density can be considered as a weakness of the UCP labels. In this section, the observations and phenomena related to excitation are discussed.

*Autofluorescence and sample absorption (**II**)*

Autofluorescence at visible wavelengths is one of the major sources of background fluorescence. In original publication **II**, the UC-RET-based technology was compared with a method relying on a conventional fluorescent label. The emission intensity (at ~700 nm) of AF680 fluorophore was modulated by the activity of a hydrolyzing enzyme. The fluorophore was excited either directly with red light (at 644–666 nm) or through energy transfer from the UCP donor under NIR (980 nm) excitation. The LOD of the assay in buffer solution containing no biological matrix was about three times better in the latter case utilizing the UCP technology. A more remarkable difference between the two methods was discovered in the signal-to-background ratios. The UCP technology reached a ratio of 20:1, while the specific signals measured with the conventional method remained low and the signal-to-background ratio was maximally only 3:1. One must take into account, that the type of the excitation source was different for the two methods, and the signal levels as such are not directly comparable. The UCPs were excited with an NIR laser diode (0.20 W) providing a narrow excitation band, while the conventional method utilized a tungsten-halogen lamp (75 W) producing a continuous spectrum from near-UV to infrared of which only a small band (~20 nm) was selected with a band-pass filter. However, the excitation power density affects the intensity of the specific and the non-specific signal equally; therefore, the signal-to-background ratios are totally comparable measures. It is possible to conclude that the proportion of the background fluorescence was significantly lower in the case of the UCP technology because the autofluorescence was totally excluded due to the photon upconversion.

The advantage of NIR excitation is emphasized if the sample matrix contains biological material and is also colored (i.e., absorbs certain visible wavelengths). In homogeneous assay concepts, the sample matrix is present during the fluorescence measurement and lower signal levels are expected if excitation and/or emission wavelengths are absorbed by the sample. Whole blood, one of the most common sample matrixes in health care, cannot be used as such in these kinds of applications; instead, the red blood cells need to be removed prior to the analysis due to the intensive absorption at wavelengths below 600 nm (Figure 26). Usually, methods other than luminescence-based ones (such as electrochemical detection (Duan and Meyerhoff, 1994; Meyerhoff *et al.*, 1995)) must be used for separation-free assays carried out in whole blood. The UCP technology exceptionally enables fluorescence measurements in presence of whole blood because the NIR excitation and the red emission band are both above 600 nm. Kuningas *et al.* (2007) already demonstrated the compatibility with blood a few years ago, showing equal calibration curves for the 17β-estradiol in colorless plasma and in red-colored whole blood (both 20% v/v). As the key solution is not related to the photon upconversion, all far-red- and NIR-fluorescent dyes should be applicable as well. The assumption was shown to be correct with the AF680 fluorophore utilized in the enzyme activity assay (the conventional method in **II**). However, the background signal level was almost doubled when the measurement was carried out in presence of whole blood (20% v/v) and, accordingly, the calibration curve seemed to be up-shifted compared to that measured in buffer (Figure 27). When the same assay was carried out under NIR excitation (AF680 excited through energy transfer from the UCP), there was no change in the background signal, but blood cell-induced scattering of the excitation radiation caused a slightly lower signal level collectively. (Note that the two methods are not equally sensitive to the excitation power density changes.) As a conclusion, although the absorption of the blood could be avoided with both methods, the large amount of biological material increased the autofluorescence in the case of downconversion, rendering the photon upconversion-based technology a more promising next-generation method in ultrasensitive bioaffinity assays.

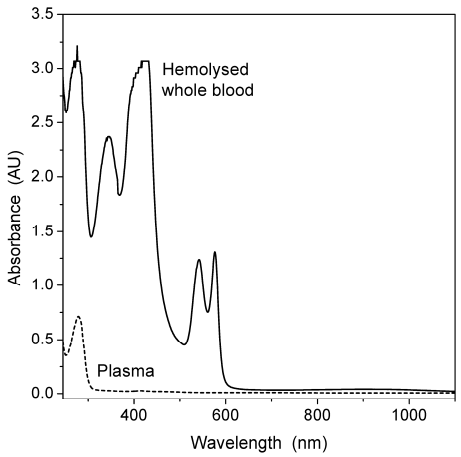

Figure 26. Absorption spectra of plasma (*dashed line*) and hemolysed whole blood (*solid line*). Plasma sample is a cell free fraction from the heparinized whole blood. The hypotonic dilution buffer was used to cause cell rupture in the whole blood sample, which minimized the light scattering. Both samples were heparinized and diluted 100-fold in 10 mM Tris-HCl (pH 8.0). *AU, absorbance unit.*

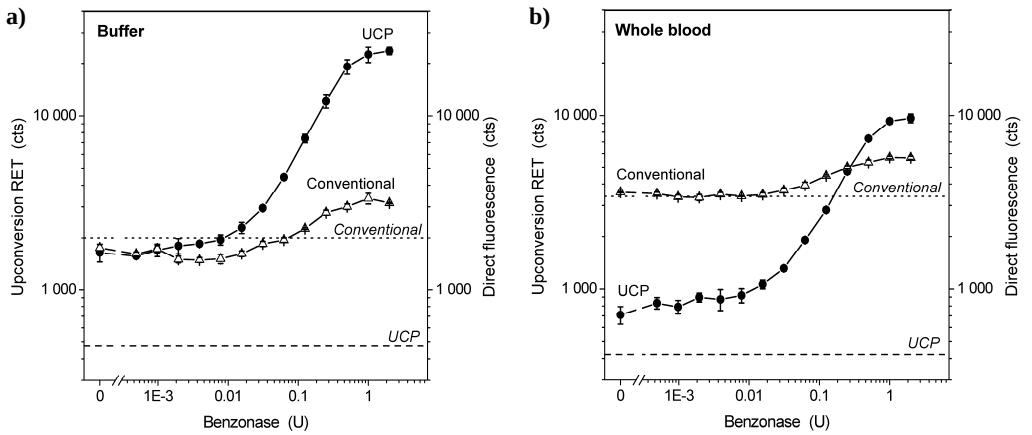

Figure 27. Calibration curves of the enzyme-activity assay measured from (**a**) buffer or (**b**) 20% (v/v) whole blood. The upconversion-based (*filled circles*; left y-axis) and the conventional downconverting-based (*open triangles*; right y-axis) methods were utilized. The horizontal lines represent the background-signal levels of upconversion-based (*lower dashed line*) and conventional (*upper dotted line*) methods measured without any fluorescent component present. The quantities of the substrate oligonucleotide for the benzonase enzyme and the UCP donor in the reaction were 50 fmol and 50 ng, respectively. Data points are means from three independent replicas, and error bars show standard deviation. *RET, resonance energy transfer; U, unit; cts, counts.* (**II**)

Excitation power density

Different excitation power densities can be obtained with the same NIR laser diode depending on the focus of the laser beam. The nonlinear relationship between the excitation and emission intensity of the UCP motivates the use of condensing lenses to maximize the excitation power in a small area. The emission intensity of the UCPs at green and red wavelengths were measured with the modified Plate Chameleon reader, utilizing less focused and highly focused excitation beams, while the current and the output power were kept constant (Figure 28). The focusing increased the intensity of the green emission (~540 nm) by a factor of 7, and the red emission (~655 nm) increased 14-fold (**unpublished**). This example exposes the fact that fair comparison of the scientific papers related to UCPs is practically impossible, because there is no proper way to exactly state the cross-section area of the beam and thus the excitation power density. An approximation may be calculated based on the output power of the laser diode and estimation of the illuminated area in the reaction vessel. The excitation power density has an enormous impact on the emission intensity and, in addition, the effect is not equal to the distinct emission bands (Suyver *et al.*, 2005b; Wang *et al.*, 2009b; Morgan and Mitchell, 2007).

All the homogeneous bioaffinity assays reported in this study were carried out in black, half-area, 96-well microtitration plates, because a small reaction volume decreases the background fluorescence. The RET can only take place on the surface of those UCP particles hit by the excitation beam (Figure 29). Other UCPs outside of the beam are left non-luminescent, and the analyte binding events are undetectable. In contrast, the acceptor fluorophores all over the reaction volume can reabsorb the photons emitted by the luminescent UCPs. This non-specific phenomenon, also called photon reabsorption or radiative energy transfer, generates background fluorescence. In the optimal situation, the excitation beam would cover the whole reaction volume, minimizing the useless volume only generating background fluorescence. However, as described above, it is not

encouraging to disperse the excitation beam. A more viable option is to reduce the reaction volume by selecting a compact reaction well. Even smaller wells (384- or 1536-well formats) than the half-area type would have been advantageous, but those are better suited for automatic pipetting robots than for manual liquid handling. The choice of the color of the plate material is also crucial. White material reflects both the excitation radiation and the UCP emission increasing the amount of excited UCPs, but also intensifies the photon reabsorption. On the contrary, black wells absorb all the light colliding with the walls and consequently the background fluorescence is significantly lower, but at the same time part of the specific signal is also absorbed by the walls. As the signal level was not a problem for the UCP technology, the black wells were a natural choice for use.

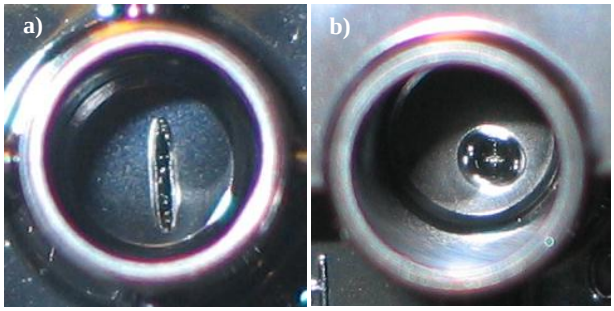

Figure 28. Shape of the laser beam (**a**) in less focused format and (**b**) in highly focused format. The images illustrate the melting pattern formed during a prolonged exposure on empty black wells made of polystyrene. (**unpublished**)

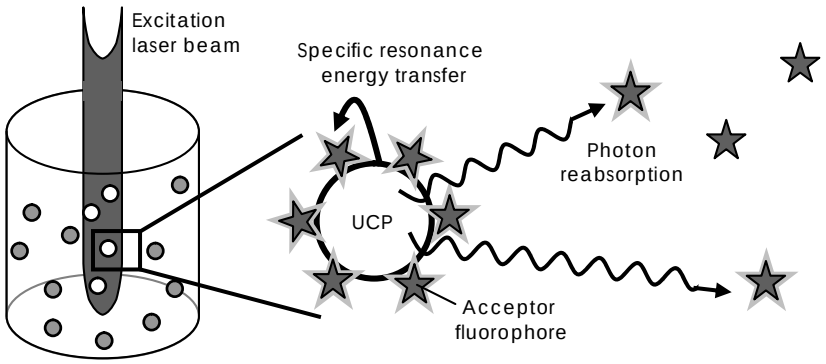

Figure 29. Relevance of the ratio between the volume of the excitation beam and the reaction vessel. Only those UCPs hit by the focused laser beam (*white dots*) are excited, while other UCPs remain non-luminescent (*gray dots*). Acceptor fluorophores (*stars*) further away may be excited non-specifically through photon reabsorption of the donor emission.

5.3 Energy transfer from UCPs

5.3.1 Distance consideration

The distance between the two labels involved in RET must be minimized to allow maximal energy transfer efficiency. The choices made during the UCP functionalization and conjugation are important, and common sense encourages the avoidance of any extra spacers. Preliminary tests (**unpublished**) were carried out with a simple hybridization assay. An acceptor-labeled probe was directly hybridized with a capture probe conjugated

to the UCP. First it was tested which UCP surface functionalization option (i.e., the PAA-adsorption or the silica-encapsulation) performed best in the hybridization assay. Second, the capture oligonucleotide was coupled with the UCP directly or through a streptavidin–biotin interaction. The differences between the outcomes were negligible (Figure 30) although more explicit results favoring the choice of the oligonucleotide–UCP conjugate were expected over the option involving additional streptavidin–biotin link. The dimensions of a streptavidin molecule are around 5×6 nm (Cooper *et al.*, 1994), which should have a clear impact on the efficiency of UC-RET. However, the present arrangement allowed considerable freedom related to the distances. First, streptavidin bears four binding sites for biotin, meaning that some of the binding sites are close to the UCP surface while the others are several nanometers farther. Second, the orientation of a non-rigid double-stranded DNA may vary according to micro-environment. Another test set-up for evaluation is required to answer the questions phrased, but these results were highly encouraging in the sense that all the tested conjugation options were functional.

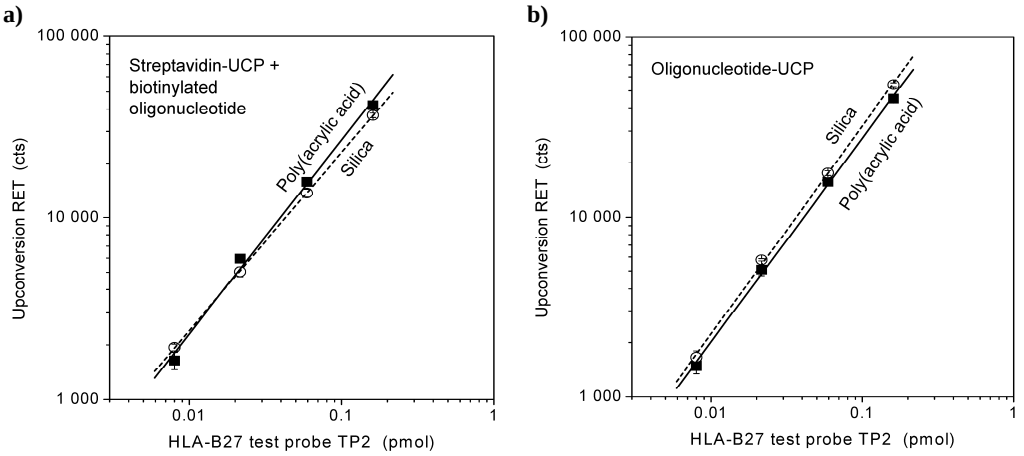

Figure 30. Comparison of different UCP conjugates in a hybridization assay. The capture oligonucleotide (HLA-B27 specific sequence) was coupled to the UCP (**a**) through a streptavidin–biotin interaction or (**b**) directly with a carbodiimide coupling reaction. The UCPs were coated with Additol poly(acrylic acid) (*filled square*) or encapsulated in a silica shell (*open circle*) prior to the bioconjugation. The energy transfer between the UCP donor and the AlexaFluor 700-labeled test probe after hybridization was measured under NIR excitation. Data points are means from three independent replicas, and error bars show standard deviation. *RET, resonance energy transfer; cts, counts.* (**unpublished**)

5.3.2 Energy transfer mechanisms (IV)

If an additional relaxation pathway for an excited molecule is introduced, it will affect the excited state lifetime. Nonradiative energy transfer to a close-proximity acceptor causes decreased luminescence lifetime for the energy donor. In contrast, if the acceptor molecule is excited through a photon-mediated reabsorption process, no interaction between the donor and the acceptor takes place and no changes in the donor lifetime are triggered.

Energy transfer from UCP donors to fluorescent molecules was previously studied only in solid-state and without any surface functionalization of the donor crystals (Sun *et al.*, 2009a; Bednarkiewicz *et al.*, 2010). As the bioanalytical applications are carried out in aqueous medium, we decided to investigate whether there was any observable evidence of the UC-RET in an aqueous environment. The situation was very challenging as the emitting ions of the UCP donor (∅ ~110 nm) were spread over a large volume. The

distance between the emitting ion and the acceptor molecule could vary from a close-proximity distance (at the surface of the UCP) to distances too far away to facilitate the RET (the core parts of the UCP), which naturally results in a continuum of energy transfer efficiencies. The luminescence lifetimes of the UCP in both the presence and absence of acceptor molecules was measured with the FD technique. However, because a dominating proportion of the emitting ions were located in the core parts of the UCP, no significant changes in the luminescence lifetimes were observed at 544 nm (specific wavelength for the UCP emission). An indirect way to study only those emitting ions participating in the energy transfer (radiative or nonradiative) was to collect the sensitized emission of the acceptors at 600 nm (the specific wavelength for the acceptor emission). Because the acceptors were not capable of producing anti-Stokes photoluminescence, the acceptor emission under the NIR excitation purely originated from the energy transfer and thus reflected the luminescence lifetime of the donor (Figure 31).

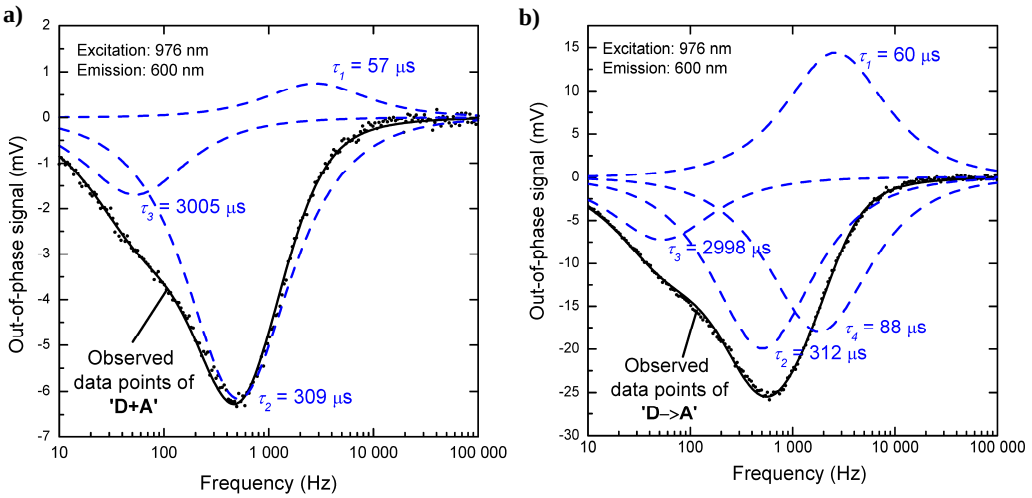

Figure 31. Lifetime components (*dashed lines*) of the sum curve (*solid line*) measured at the wavelength specific for the acceptor (600 nm). The observed data points of (**a**) the 'D+A' sample containing UCPs and ATTO565 fluorophore mixed freely in a solution or (**b**) the 'D→A' sample containing a UCP–ATTO565 conjugate were fitted together with the 'D only' sample (measured at the donor-specific wavelength 544 nm) to 3 or 4 lifetimes, respectively. (**IV**)

We found no changes in the luminescence lifetime if the UCP donor and the acceptor molecules were randomly distributed in the solution without any specific interaction ('D+A' and 'D+(5×)A' samples). Further, the relative amplitudes of these samples were nearly equal, with the 'D only' sample containing no acceptor at all. In contrast, the UCP–acceptor conjugates ('D→A' samples) did not behave similarly, but an additional lifetime with relatively strong amplitude was observed. The luminescence lifetime was 64–74% reduced (depending on the acceptor) compared to the dominating lifetime in the 'D only' sample, indicating that an alternative relaxation pathway existed and that the nonradiative energy transfer was strongly supported. A significant part but not all of the energy was transferred through a nonradiative process. The dominating amplitude in the 'D→A' samples was again the same as in the 'D only' sample, implying that photon reabsorption also plays an important role in systems involving relatively large UCPs as a donor. Although the distance between the UCP and the acceptor was fixed to be minimal in the 'D→A' samples, it is reasonable to assume that some of the energy transfer originates from

the emitting ions located in the UCP core, thus the reabsorption mechanism inevitably is always present to some extent.

The proportion of the reabsorption is likely minimized if nano-sized UCP donors (diameter below 20 nm) are exploited and the amount of the fluorescent species (the donor and the fluorescent acceptor) is limited to low concentrations. These actions will add the probability of UC-RET as the excess of emitters is removed. This hypothesis seems to be correct based on the preliminary evaluation of UC-RET applications with nanocrystalline UCP material producing less background luminescence, but confirmation for the deduction can be attained by repeating these luminescence lifetime experiments with the nanocrystals. The method is now straightforward as the instrumentation and the data analysis have been developed and tested.

6 CONCLUSIONS

Photoluminescent label techniques have established their position in analyte detection due to their low detection limits, relatively easy handling (no stability problems) and possibility for direct measurement (no addition of enhancers or substrates). The luminescence-based assays are ideal for testing the abundant analytes, but autofluorescence limits the detection of sparse molecules. Optically challenging sample matrixes (e.g., high absorptivity at certain wavelengths, strong scattering of radiation) complicate the photoluminescence measurement, and a pretreatment step prior the analysis or removal of the sample matrix before reading the emission intensity may be required. These extra steps are inconvenient in rapid and simplified on-site testing, which is one of the focal development trends in the bioanalytical field. The limitations can be avoided by exploiting photon upconversion and NIR excitation.

In this study, the performance of a novel label technology relying on photon upconversion was evaluated in various homogeneous assay concepts based on energy transfer from the UCPs to acceptor fluorophores. The bioanalytical model assays for detecting a hapten molecule, enzyme activity or oligonucleotide sequences utilized NIR radiation to excite the UCP donors, and the read-out of the sensitized emission of the acceptor was carried out at visible wavelengths. The distance-dependent signal modulation of the acceptor fluorophore was studied in detail by monitoring the luminescence lifetime changes.

The main conclusions based on the original publications are:

I The excitation and emission wavelengths of the acceptor may be fine tuned by utilizing a tandem dye composed of two fluorophores capable of internal energy transfer. In RET-based applications, the tandem dyes can improve the spectral overlap between the donor and the acceptor fluorophore and facilitate the separation of the sensitized acceptor emission. Fluorescent protein as a part of a tandem dye provides an exceptionally high extinction coefficient, ensuring high emission intensity. However, this kind of acceptor entity has large dimensions and is difficult to produce in a reproducible way.

II The bright anti-Stokes photoluminescence of a submicrometer-sized UCP is impossible to quench efficiently with an organic dark quencher, as the emitter ions located in the core parts of the UCP are too far away for distance-dependent processes such as RET. The problem can be solved by a sequential energy-transfer-based system where the UCP donor transfers energy to an acceptor fluorophore whose sensitized emission intensity is further modulated by a near-proximity quencher. This system may be utilized in bioanalytical assays in which a biological event (e.g., hydrolyzing enzyme reaction) releases the quencher and restores the sensitized emission.

III Lanthanide-based UCPs have typically at least two emission bands that can both be utilized simultaneously to report the concentration of two different analytes. A UC-RET-based dual-parameter assay utilizing a single excitation wavelength can be constructed by combining one type of UCP donor with two different acceptor fluorophores matching with the separate UCP emission bands. In the sandwich hybridization assay, there was no cross-talk between the two acceptor fluorophores,

and two oligonucleotide sequences could be quantitatively detected from the same reaction vessel with high confidence.

IV The energy transfer between a UCP donor and a close-proximity acceptor fluorophore occurs at least partly by means of a nonradiative mechanism (i.e., RET), although reabsorption of the donor emission always causes some of the sensitized acceptor emission. A decreased luminescence lifetime of the UCP donor in the presence of acceptor fluorophores within close proximity proved the presence of the RET process. The frequency-domain technique proved to be well suited to determine the luminescence lifetime changes of the relatively large UCPs (diameter 110 nm), which dominantly produced unaffected emission from the emitting ions located in the core parts of the particle.

The methods for handling and modifying the UCP material were developed alongside the assay development. The procedure for grinding the commercial UCP bulk material into submicrometer-sized colloidal particles was significantly accelerated by a planetary ball mill that completes the task within 90 minutes. The grinding step could be excluded when morphologically more favorable and highly luminescent UCP material (spherical particles with a diameter below 150 nm) was directly synthesized with a solid-state co-precipitation method. Similar modification procedures (i.e., functionalization and bioconjugation) could be successfully carried out with both ground and synthesized UCP material. An optional functionalization method was developed and optimized to substitute for the previous polymer adsorption-based procedure. The density of the functional groups in the optimized silica coating was sufficient, and the layer was thin enough to enable efficient RET from the UCP emitter ions to an acceptor fluorophore.

In conclusion, UCP technology with its special photoluminescent features theoretically provides an opportunity for ultrasensitive detection of analyte molecules with simple instrumentation. The potential of the UCPs has been shown in various proof-of-principle bioanalytical assays, and the natural extension would be to test the operation in real clinical situations and to evaluate the performance of this label technology against other labels. Today, the major problem related to UCP technology has been solved, as the recent development in the synthesis of the nanocrystalline UCPs has enabled the replacement of the ground bulk materials. Although the surface functionalization of the UCPs remains a challenge, as with other inorganic labels (e.g., quantum dots), several optional coating methods have been reported and a suitable version may be chosen depending on the application. Instrumentation for reading the UCP emission is not yet commonly available, but the elements and the technological solutions exist to enable the potential commercial exploitation of UCP technology.

ACKNOWLEDGEMENTS

This study was carried out at the Department of Biotechnology, University of Turku, during the years 2006–2011. Financial support from the Finnish Funding Agency for Technology and Innovation (Tekes), the Academy of Finland (Grant numbers 209417, 114903, 119497, 140758) and the industrial companies involved is gratefully acknowledged as well as the technological support from Hidex Oy in the anti-Stokes photoluminescence measurements.

I wish to thank Professor Emeritus Timo Lövgren, former head of the department, for giving me the opportunity to carry out my PhD studies at the Department of Biotechnology, providing high quality of teaching and wide selection of research instrumentation. Together with Professor Kim Pettersson and Professor Tero Soukka, he has created a unique cluster of knowledge and team spirit. The professors have offered me encouragement and support in research challenges, but also attractive opportunities in the form of teaching positions and other responsibilities. Soon after my recent knee operation, I realized that I actually enjoy my job quite a lot, and not even an expert orthopedist could make me stay at home for the full recovery time! Not all workplaces are as appealing, I was told…

One of the most essential pieces of the puzzle has been my supervisor Professor Tero Soukka. I want to express my deepest gratitude and respect to him for his brilliant and unique ideas, never-ending enthusiasm, unbelievable technical expertise, helpful advice and valuable guidance. I feel really fortunate for being a member of his research group that has an excellent reputation. Tero's fair actions and ability to listen (not only to hear) make him an exceptionally good boss. Additionally, despite his busy schedule, he saved my thesis several times from my evil computer that was not always cooperative.

The esteemed pre-examiners Professor Emeritus Ulf-Håkan Stenman (Helsinki University and Helsinki University Central Hospital) and Professor Sakari Kulmala (Aalto Univeristy) sacrificed their summer holidays to review my thesis, and I am very grateful for their valuable comments. I found this learning experience and future coaching extremely positive. I also want to thank Damon Tringham who checked the English language of the thesis and guided me through "the tricks and traps of grammar".

Then it is time to thank the ladies. A hard-working and skilful team of co-workers has supported my way to this point. It is Dr. Katri Kuningas who is to blame for this thesis. She was my role model, my mentor and my everything at the beginning of my researcher career. Soon our team was strengthened by extra girl-power from Jaana Rosenberg, Telle Ukonaho, Henna Päkkilä, Johanna Vuojola, Marja-Leena Järvenpää, Riikka Arppe, Minna Ylihärsilä and Marika Nummela. The estrogen domination was afterwards diluted by Sami Blom and Timo Valta, the pioneering males in "Tero's ompelukerho". The students Laura Jämsen, Maija Karp, Marika Ibrahim, Lumi Jaakkola, Satu Lahtinen, Kari Kopra, Essi Kulta, Leena Mattsson, Anna Ahomaa and Mikko Pyykkö have also contributed to the research with diligence. Special thanks I owe to Henna, who reviewed the thesis before it was handed to the pre-examiners, and who has lately shared the every-day ups and downs related both to work and personal life. I also owe thanks to Johanna who solved so many Word formatting problems that I hugged her spontaneously at least three times (always on stressful deadline days).

I want to express my warmest thanks to Professor Emeritus Jouko Kankare and Iko Hyppänen (Laboratory of Materials Chemistry and Chemical Analysis) for interesting cooperation, especially related to the publication IV. I learned a lot from these two gentlemen, who are experts with all kinds of formulas and fitting parameters. I am very grateful also to Professor Jorma Hölsä, Dr. Mika Lastusaari, Laura Pihlgren and Emilia Harju (Laboratory of Materials Chemistry and Chemical Analysis) for personal backup related to inorganic materials and photoluminescence properties. The UCP synthesis, a crucial component in my studies, would not have been possible without the valuable input of the chemists.

International collaboration has been one part of my studies and enriched my life in so many ways. I want to thank Professor Hans Tanke, Dr. Paul Corstjens, Claudia de Dood, Annelies van der Laan, Karien Wiesmeijer, Christian Bertholle and Jan Slats (Leiden University Medical Center) who provided a unique experience by welcoming me so warmly to the Netherlands, by sharing their expertise and by introducing new analytical methods to me. The 3-month stay in Leiden increased my self-confidence as a researcher, but also added extra value to my free time in terms of boxing, running and musicals. Afterwards, Paul and Jan also provided important data for my thesis that I was not able to measure at my home university. In Turku, the visits of international students, Juan Godoy-Navajas, Heike Mader, Daniela Achatz and Raphaela Liebherr, have also been educational and included many nice events for which I want to thank you.

I wish to express my warmest thanks to all the present and former colleagues who have worked at the Department of Biotechnology. The input of technical and administrative personnel Mirja Jaala, Martti Sointusalo, Marja Maula, Marja-Liisa Knuuti, Kaisa Linderborg, Görel Salomaa and Marika Silvennoinen, has been indispensable. I am also grateful to Pirjo Laaksonen for the numerous blood samples she has collected and also for the pleasant exercise moments along with Lambada and other “hits”. I have been fortunate to have a teaching position at the department and the other teachers, past and present, are acknowledged for their cooperation and support. Mari Peltola, Tiina Myyryläinen and the previous PhDs, especially Dr. Katri Kuningas, Dr. Saara Wittfooth, Dr. Eeva-Christine Brockmann and Dr. Gaurav Batra, are acknowledged for their practical advice and encouragement in the final phase of my studies. In the middle of the haste, extra energy is always welcome and I owe my thanks to the “lunch team” including Henna Päkkilä, Dr. Saara Wittfooth, Ulla Karhunen, Noora Ristiniemi, Susanne Nuorti and some occasionally visiting stars, who have turned the lunch time into a social event that recharges my batteries day after day.

I used to have more free time for friends before I started the writing process, and I apologize for the lost moments that we could have shared during the past year. I am extremely grateful to Antti, Elisa, Janne, Johanna, Juuso, Kaisa, Maarit, Pauliina, Teija, Tytti, Virpi and their spouses, for the journey that began 10 years ago at the university and for all the entertaining and relaxing get-togethers after that. Additionally, I want to thank Teija and Elisa for taking me to the first dancing lesson in Turku. All those countless workout hours and shows with the fantastic fellow “ballerinas” (e.g., Leena and Tiina!) and jazz dancers have balanced the scientific side of my life. Despite my present home in Turku, my roots are still in Pori as well as many dear friends who year after year share the joys of Midsummer, Pori Jazz festival and other events. The New Year has been removed

from the list for a special reason. I am glad that friendship ignores even the physical distances between people.

Valtavat kiitokset teille, äiti ja isä. Rakkaus, huolenpito, kasvatus, kannustus ja taloudellinen tuki ovat luoneet edellytykset kaikelle sille, mitä olen tänään ja tulevaisuudessa. In addition to my parents, I want to express my gratitude to the other members of the family and also to Tuula, Jouni and Paula who have warmly welcomed me as a part of their family. Your confidence in me has been a strong motivator.

Finally, there are no words to express how much I value the support of my beloved husband Riku. It was 12 years ago when you stole my heart and since then you have guaranteed my happiness. I appreciate how you saw the limitations set by the hours in a day and the energy packed into one girl. You took full responsibility at home letting me concentrate on finalizing the thesis. I can never forget the sandwiches on the kitchen table waiting for the hungry wife returning from work around midnight. Among other things, those sandwiches were spelling out your love and care – the love that means everything to me. Guess what, my best friend, lover and soul-mate, this is it: the thesis is ready and the wife is back at home. Take my hand and show me the way to the future.

This thesis is a huge milestone in my life – I will be "Doctor Riuttamäki" every single day for the rest of my life. You cannot imagine how grateful I am to all of you who made it possible!

Turku, October 2011

Terhi Riuttamäki

REFERENCES

www.clinchem.org/info_ar/info_authors.dtl#standards (2011) Description of analytical methods and results. Clinical Chemistry editorial office, (Accessed 08/302011).

Achatz DE, Meier RJ, Fischer LH & Wolfbeis OS (2011) Luminescent sensing of oxygen using a quenchable probe and upconverting nanoparticles. *Angew Chem Int Ed* **50:**260–263.

Aebischer A, Hostettler M, Hauser J, Krämer K, Weber T, Güdel HU & Bürgi HB (2006) Structural and spectroscopic characterization of active sites in a family of light-emitting sodium lanthanide tetrafluorides. *Angew Chem Int Ed* **45:**2802–2806.

Ali R, Saleh SM, Meier RJ, Azab HA, Abdelgawad II & Wolfbeis OS (2010) Upconverting nanoparticle based optical sensor for carbon dioxide. *Sensors Actuators B: Chem* **150:**126–131.

Armstrong J, Bloembergen N, Ducuing J & Pershan P (1962) Interactions between light waves in a nonlinear dielectric [Review]. *Physical Review* **127:**1918–1939.

Arppe R, Harju E, Valta T, Lahtinen S, Lastusaari M, Hölsä J & Soukka T (2011) Biofunctionalized nanosized upconverting phosphors for bioanalytical applications [Poster] #1082. *Clin Chem Lab Med* **49:**S747.

Auzel F (1966a) Compteur quantique par transfert d'energie entre deux ions de terres reres dans un tungstate mixte et dans un verre. *Compt Rend Acad Sci (Paris)* **262:**1016–1019.

Auzel F (1966b) Compteur quantique par transfert d'energie entre de Yb^{3+} a Tm^{3+} dans un tungstate mixte et dans verre germanate. *Compt Rend Acad Sci (Paris)* **163:**819–821.

Auzel F (2004) Upconversion and anti-Stokes processes with f and d ions in solids [Review]. *Chem Rev* **104:**139–173.

Axelrod D, Hellen EH & Fulbright RM (2002) Total internal reflection fluorescence in *Topics in fluorescence spectroscopy.* Plenum Press, New York. pp. 289–343.

Bagwe RP, Hilliard LR & Tan W (2006) Surface modification of silica nanoparticles to reduce aggregation and nonspecific binding. *Langmuir* **22:**4357–4362.

Bazin H, Trinquet E & Mathis G (2002) Time resolved amplification of cryptate emission: a versatile technology to trace biomolecular interactions. *J Biotechnol* **82:**233–250.

Bednarkiewicz A, Nyk M, Samoc M & Strek W (2010) Up-conversion FRET from Er^{3+}/Yb^{3+}:$NaYF_4$ nanophosphor to CdSe quantum dots. *J Phys Chem C* **114:**17535–17541.

Bhalgat MK, Haugland RP, Pollack JS, Swan S & Haugland RP (1998) Green- and red-fluorescent nanospheres for the detection of cell surface receptors by flow cytometry. *J Immunol Methods* **219:**57–68.

Bloembergen N (1959) Solid-state infrared quantum counters. *Phys Rev Lett* **2:**84–85.

Bogdan N, Vetrone F, Roy R & Capobianco JA (2010) Carbohydrate-coated lanthanide-doped upconverting nanoparticles for lectin recognition. *J Mater Chem* **20:**7543–7550.

Bogdan N, Vetrone F, Ozin GA & Capobianco JA (2011) Synthesis of ligand-free colloidally stable water dispersible brightly luminescent lanthanide-doped upconverting nanoparticles. *Nano Lett* **11:**835–840.

Boyer JC, Vetrone F, Cuccia LA & Capobianco JA (2006) Synthesis of colloidal upconverting $NaYF_4$ nanocrystals doped with Er^{3+}, Yb^{3+} and Tm^{3+}, Yb^{3+} via thermal decomposition of lanthanide trifluoroacetate precursors. *J Am Chem Soc* **128:**7444–7445.

Boyer JC, Cuccia LA & Capobianco JA (2007) Synthesis of colloidal upconverting $NaYF_4$: $Er^{3+}/Yb^{3+}$and Tm^{3+}/Yb^{3+} monodisperse nanocrystals. *Nano Lett* **7:**847–852.

Boyer JC, Manseau MP, Murray JI & van Veggel FC (2010) Surface modification of upconverting $NaYF_4$ nanoparticles with PEG-phosphate ligands for NIR (800 nm) biolabeling within the biological window. *Langmuir* **26:**1157–1164.

Boyer JC & van Veggel FC (2010) Absolute quantum yield measurements of colloidal $NaYF_4$: Er^3+, Yb^{3+} upconverting nanoparticles. *Nanoscale* **2:**1417–1419.

Bril A, Sommerdijk JL & de Jager AW (1975) On the efficiency of Yb^{3+}-Er^{3+} activated up-conversion phosphors. *J Electrochem Soc* **122:**660–663.

Bünzli JC & Piguet C (2005) Taking advantage of luminescent lanthanide ions [Review]. *Chem Soc Rev* **34:**1048–1077.

Carmona AK, Juliano MA & Juliano L (2009) The use of fluorescence resonance energy transfer (FRET) peptides for measurement of clinically important proteolytic enzymes. *An Acad Bras Cienc* **81:**381–392.

Caruso F, Lichtenfeld H, Donath E & Möhwald H (1999) Investigation of electrostatic interactions in polyelectrolyte multilayer films: Binding of anionic fluorescent probes to layers assembled onto colloids. *Macromolecules* **32:**2317–2328.

Chan EM, Xu C, Mao AW, Han G, Owen JS, Cohen BE & Milliron DJ (2010) Reproducible, high-throughput synthesis of colloidal nanocrystals for optimization in multidimensional parameter space. *Nano Lett* **10:**1874–1885.

Chen D, Mauk M, Qiu X, Liu C, Kim J, Ramprasad S, Ongagna S, Abrams WR, Malamud D, Corstjens PL & Bau HH (2010a) An integrated, self-contained microfluidic cassette for isolation, amplification, and detection of nucleic acids. *Biomed Microdevices* **12:**705–719.

Chen G, Ohulchanskyy TY, Kumar R, Ågren H & Prasad PN (2010b) Ultrasmall monodisperse $NaYF_4$:Yb^{3+}/Tm^{3+} nanocrystals with enhanced near-infrared to near-infrared upconversion photoluminescence. *ACS Nano* **4:**3163–3168.

Chen Z, Wang J, Qian S & Bau HH (2005) Thermally-actuated, phase change flow control for microfluidic systems. *Lab Chip* **5:**1277–1285.

Chen Z, Mauk MG, Wang J, Abrams WR, Corstjens PL, Niedbala RS, Malamud D & Bau HH (2007) A microfluidic system for saliva-based detection of infectious diseases. *Ann N Y Acad Sci* **1098:**429–436.

Chen Z, Chen H, Hu H, Yu M, Li F, Zhang Q, Zhou Z, Yi T & Huang C (2008) Versatile synthesis strategy for carboxylic acid-functionalized upconverting nanophosphors as biological labels. *J Am Chem Soc* **130:**3023–3029.

Cheng L, Yang K, Shao M, Lee ST & Liu Z (2011) Multicolor in vivo imaging of upconversion nanoparticles with emissions tuned by luminescence resonance energy transfer. *J Phys Chem C* **115:**2686–2692.

Chivian JS, Case WE & Eden DD (1979) The photon avalanche: a new phenomenon in Pr^{3+}-based infrared quantum counters. *Appl Phys Lett* **35:**124–125.

Cooper JM, Shen J, Young FM, Connolly P, Barker JR & Moores G (1994) The imaging of streptavidin and avidin using scanning tunnelling microscopy. *J Mater Sci: Mater Electron* **5:**106–110.

Corstjens PL, Zuiderwijk M, Brink A, Li S, Feindt H, Niedbala RS & Tanke H (2001) Use of up-converting phosphor reporters in lateral-flow assays to detect specific nucleic acid sequences: a rapid, sensitive DNA test to identify human papillomavirus type 16 infection. *Clin Chem* **47:**1885–1893.

Corstjens PL, Zuiderwijk M, Nilsson M, Feindt H, Niedbala RS & Tanke HJ (2003) Lateral-flow and up-converting phosphor reporters to detect single-stranded nucleic acids in a sandwich-hybridization assay. *Anal Biochem* **312:**191–200.

Corstjens PL, Li S, Zuiderwijk M, Kardos K, Abrams WR, Niedbala RS & Tanke HJ (2005) Infrared up-converting phosphors for bioassays [Review]. *IEE Proc Nanobiotechnol* **152:**64–72.

Corstjens PL, Chen Z, Zuiderwijk M, Bau HH, Abrams WR, Malamud D, Niedbala RS & Tanke HJ (2007) Rapid assay format for multiplex detection of humoral immune responses to infectious disease pathogens (HIV, HCV, and TB). *Ann N Y Acad Sci* **1098:**437–445.

Corstjens PL, van Lieshout L, Zuiderwijk M, Kornelis D, Tanke HJ, Deelder AM & van Dam GJ (2008a) Up-converting phosphor technology-based lateral flow assay for detection of *Schistosoma* circulating anodic antigen in serum. *J Clin Microbiol* **46:**171–176.

Corstjens PL, Zuiderwijk M, Tanke HJ, van der Ploeg-van Schip JJ, Ottenhoff TH & Geluk A (2008b) A user-friendly, highly sensitive assay to detect the IFN-gamma secretion by T cells. *Clin Biochem* **41:**440–444.

Cotton S (2006) Lanthanide and actinide chemistry. Wiley, West Sussex, UK. pp. 263.

Darbandi M, Thomann R & Nann T (2005) Single quantum dots in silica spheres by microemulsion synthesis. *Chem Mater* **17:**5720–5725.

Darbandi M & Nann T (2006) One-pot synthesis of YF_3@silica core/shell nanoparticles. *Chem Commun* 776–778.

Davies C (2005) Introduction to immunoassay principles in *The Immunoassay Handbook.* Elsevier Ltd., Oxford, UK. pp. 3–40.

Decher G (1997) Fuzzy nanoassemblies: Toward layered polymeric multicomposites. *Science* **277:**1232–1237.

DeLoach LD, Payne SA, Chase LL, Smith LK, Kway WL & Krupke WF (1993) Evaluation of absorption and emission properties of Yb^{3+} doped crystals for laser applications. *IEEE J Quant Electron* **29:**1179–1191.

Demchenko AP (2009) Introduction to Fluorescence Sensing. Springer, New York. pp. 590.

Denk W, Strickler JH & Webb WW (1990) Two-photon laser scanning fluorescence microscopy. *Science* **248:**73–76.

Diamandis EP & Christopoulos TK (1991) The biotin-(strept)avidin system: principles and applications in biotechnology [Review]. *Clin Chem* **37:**625–636.

Duan C & Meyerhoff ME (1994) Separation-free sandwich enzyme immunoassays using microporous gold electrodes and self-assembled monolayer/immobilized capture antibodies. *Anal Chem* **66:**1369–1377.

Eggeling C, Widengren J, Rigler R & Seidel CAM (1998) Photobleaching of fluorescent dyes under conditions used for single-molecule detection: Evidence of two-step photolysis. *Anal Chem* **70:**2651–2659.

Ekins R (1960) The estimation of thyroxine in human plasma by an electrophoretic technique. *Clin Chim Acta* **5:**453–459.

Ekins R (1998) Ligand assays: from electrophoresis to miniaturized microarrays [Review]. *Clin Chem* **44:**2015–2030.

Eliseeva SV & Bünzli JC (2010) Lanthanide luminescence for functional materials and bio-sciences [Review]. *Chem Soc Rev* **39:**189–227.

Fischer LH, Harms GS & Wolfbeis OS (2011) Upconverting nanoparticles for nanoscale thermometry [Review]. *Angew Chem Int Ed* **50:**4546–4551.

Fish KN (2009) Total internal reflection fluorescence (TIRF) microscopy. *Curr Protoc Cytom* **50:**12.18.1–12.18.13.

Förster T (1948) Zwischenmoleculare energiewanderung und fluoreszenz. *Ann Phys* **2:**55–75.

Franken P, Hill A, Peters C & Weinreich G (1961) Generation of optical harmonics. *Phys Rev Lett* **7:**118–119.

Gaigalas AK, Wang L & Vogt RF (2007) Frequency-domain measurement of the photodegradation process of fluorescein. *Photochem Photobiol* **76:**22–28.

Gamelin DR & Güdel HU (2001) Upconversion processes in transition metal and rare earth metal systems [Review]. *Top Curr Chem* **214:**1–56.

Glazer AN & Hixson CS (1977) Subunit structure and chromophore composition of rhodophytan phycoerythrins. Porphyridium cruentum B-phycoerythrin and b-phycoerythrin. *J Biol Chem* **252:**32–42.

Graf C, Vossen DLJ, Imhof A & van Blaaderen A (2003) A general method to coat colloidal particles with silica. *Langmuir* **19:**6693–6700.

Güdel HU (1998) New light-emitting inorganic materials. *Chimia* **52:**561–565.

Haase M, Haubold S, Ibarra F, Meysamy H, Riwotzky C & Weller H (2002) Synthesis of nanoparticles [Patent]. PCT/DE01/03433.

Haase M & Schäfer H (2011) Upconverting nanoparticles. *Angew Chem Int Ed* **50:**5808–5829.

Hampl J, Hall M, Mufti NA, Yao YM, MacQueen DB, Wright WH & Cooper DE (2001) Upconverting phosphor reporters in immunochromatographic assays. *Anal Biochem* **288:**176–187.

Hänninen P, Soukka J & Soini JT (2008) Two-photon excitation fluorescence bioassays. *Ann N Y Acad Sci* **1130:**320–326.

Harju E, Hyppänen I, Hölsä J, Kankare J, Lahtinen M, Lastusaari M, Pihlgren L & Soukka T (2011) Polymorphism of $NaYF_4$:Yb^{3+},Er^{3+} up-conversion luminescence materials. *Zeitschrift für Kristallographie*.

Harris LJ, Skaletsky E & McPherson A (1998) Crystallographic structure of an intact IgG1 monoclonal antibody. *J Mol Biol* **275:**861–872.

He GS, Tan LS, Zheng Q & Prasad PN (2008) Multiphoton absorbing materials: molecular designs, characterizations, and applications [Review]. *Chem Rev* **108:**1245–1330.

Heer S, Lehmann O, Haase M & Güdel HU (2003) Blue, green, and red upconversion emission from lanthanide-doped $LuPO_4$ and $YbPO_4$ nanocrystals in a transparent colloidal solution. *Angew Chem Int Ed* **42:**3179–3182.

Heer S, Kömpe K, Güdel HU & Haase M (2004) Highly efficient multicolour upconversion emission in transparent colloids of lanthanide-doped $NaYF_4$ nanocrystals. *Adv Mater* **16:**2102–2105.

Hemmilä I, Dakubu S, Mukkala V, Siitari H & Lövgren T (1984) Europium as a label in time-resolved immunofluorometric assays. *Anal Biochem* **137:**335–343.

Hermanson GT (2008) Bioconjugate Techniques. Academic Press, London, UK. pp. 1202.

Hong W, Huang L, Wang H, Qu J, Guo Z, Xie C, Zhu Z, Zhang Y, Du Z, Yan Y, Zheng Y, Huang H, Yang R & Zhou L (2010) Development of an up-converting phosphor technology-based 10-channel lateral flow assay for profiling antibodies against Yersinia pestis. *J Microbiol Methods* **83:**133–140.

Hu M, Yan J, He Y, Lu H, Weng L, Song S, Fan C & Wang L (2010) Ultrasensitive, multiplexed detection of cancer biomarkers directly in serum by using a quantum dot-based microfluidic protein chip. *ACS Nano* **4:**488–494.

Huang L, Zhou L, Zhang Y, Xie C, Qu J, Zeng A, Huang H, Yang R & Wang X (2009) A simple optical reader for upconverting phosphor particles captured on lateral flow strip. *IEEE Sens J* **9:**1185–1191.

Hulspas R, Dombkowski D, Preffer F, Douglas D, Kildew-Shah B & Gilbert J (2009) Flow cytometry and the stability of phycoerythrin-tandem dye conjugates. *Cytom Part A* **75A:**966–972.

Hyppänen I, Hölsä J, Kankare J, Lastusaari M, Pihlgren L & Soukka T (2009) Preparation and up-conversion luminescence properties of $NaYF_4$:Yb^{3+},Er^{3+} nanomaterials. *Terrae Rarae* **16:**1–6.

Hyppänen I, Soukka T & Kankare J (2010) Frequency-domain measurement of luminescent lanthanide chelates. *J Phys Chem A* **114:**7856–7867.

Jiang S & Zhang Y (2010) Upconversion nanoparticle-based FRET system for study of siRNA in live cells. *Langmuir* **26:**6689–6694.

Joubert M, Guy S & Jacquier B (1993) Model of the photon-avalanche effect. *Phys Rev B* **48:**10031–10037.

Junker R, Schlebusch H & Luppa PB (2010) Point-of-care testing in hospitals and primary care [Review]. *Dtsch Arztebl Int* **107:**561–567.

Kaiser W & Garrett C (1961) Two-Photon Excitation in CaF_2: Eu^{2+}. *Phys Rev Lett* **7:**229–231.

Kankare J & Hyppänen I (2011) Frequency-domain measurements in *Lanthanide Luminescence: Photophysical, Analytical and Biological Aspects.* Springer Verlag, Berlin. p.p. 279–312.

Kano T, Yamamoto H & Otomo Y (1972) $NaLnF_4$:Yb^{3+},Er^{3+} (Ln:Y,Gd,La): Efficient green-emitting infrared-excited phosphors. *J Electrochem Soc* **119:**1561.

Kim HS & Pyun JC (2009) Hyper sensitive strip test with chemi-luminescence signal band. *Procedia Chem* **1:**1043–1046.

Krämer KW, Biner D, Frei G, Güdel HU, Hehlen MP & Lüthi SR (2004) Hexagonal sodium yttrium fluoride based green and blue emitting upconversion phosphors. *Chem Mater* **16:**1244–1251.

Kubitschko S, Spinke J, Brückner T, Pohl S & Oranth N (1997) Sensitivity enhancement of optical immunosensors with nanoparticles. *Anal Biochem* **253:**112–122.

Kumar M, Guo Y & Zhang P (2009) Highly sensitive and selective oligonucleotide sensor for sickle cell disease gene using photon upconverting nanoparticles. *Biosens Bioelectron* **24:**1522–1526.

Kumar M & Zhang P (2009) Highly sensitive and selective label-free optical detection of DNA hybridization based on photon upconverting nanoparticles. *Langmuir* **25:**6024–6027.

Kumar M & Zhang P (2010) Highly sensitive and selective label-free optical detection of mercuric ions using photon upconverting nanoparticles. *Biosens Bioelectron* **25:**2431–2435.

Kuningas K, Rantanen T, Karhunen U, Lövgren T & Soukka T (2005a) Simultaneous use of time-resolved fluorescence and anti-stokes photoluminescence in a bioaffinity assay. *Anal Chem* **77:**2826–2834.

Kuningas K, Rantanen T, Lövgren T & Soukka T (2005b) Enhanced photoluminescence of up-converting phosphors in a solid phase bioaffinity assay. *Anal Chim Acta* **543:**130–136.

Kuningas K, Rantanen T, Ukonaho T, Lövgren T & Soukka T (2005c) Homogeneous assay technology based on upconverting phosphors. *Anal Chem* **77:**7348–7355.

Kuningas K, Ukonaho T, Päkkilä H, Rantanen T, Rosenberg J, Lövgren T & Soukka T (2006) Upconversion fluorescence resonance energy transfer in a homogeneous immunoassay for estradiol. *Anal Chem* **78:**4690–4696.

Kuningas K, Päkkilä H, Ukonaho T, Rantanen T, Lövgren T & Soukka T (2007) Upconversion fluorescence enables homogeneous immunoassay in whole blood. *Clin Chem* **53:**145–146.

LaMer VK & Dinegar RH (1950) Theory, production and mechanism of formation of monodispersed hydrosols. *J Am Chem Soc* **72:**4847–4854.

Lehmann O, Meyssamy H, Kömpe K, Schnablegger H & Haase M (2003) Synthesis, growth, and Er^{3+} luminescence of lanthanide phosphate nanoparticles. *J Phys Chem B* **107:**7449–7453.

Lemieux RU & von Rudloff E (1955) Periodate-permanganate oxidations: I. Oxidation of olefins. *Can J Chem* **33:**1701–1709.

Levicky R & Horgan A (2005) Physicochemical perspectives on DNA microarray and biosensor technologies. *Trends Biotechnol* **23:**143–149.

Li C & Lin J (2010) Rare earth fluoride nano-/microcrystals: synthesis, surface modification and application. *J Mater Chem* **20:**6831–6847.

Li JJ, Ouellette AL, Giovangrandi L, Cooper DE, Ricco AJ & Kovacs GTA (2008) Optical scanner for immunoassays with up-converting phosphorescent labels. *IEEE T Bio-Med Eng* **55:**1560–1571.

Li L, Zhou L, Yu Y, Zhu Z, Lin C, Lu C & Yang R (2009) Development of up-converting phosphor technology-based lateral-flow assay for rapidly quantitative detection of hepatitis B surface antibody. *Diagn Microbiol Infect Dis* **63:**165–172.

Li S, Feindt H, Giannaras G, Scarpino R, Salamone S & Niedbala RS (2002) Preparation, characterization, and fabrication of uniform coated $Y_2O_2S:RE^{3+}$ up-converting phosphor particles for biological detection applications. *Proc SPIE* **4809:**100–109.

Li Z & Zhang Y (2006) Monodisperse silica-coated polyvinylpyrrolidone/$NaYF_4$ nanocrystals with multicolor upconversion fluorescence emission. *Angew Chem Int Ed* **45:**7732–7735.

Li Z, Zhang Y & Jiang S (2008) Multicolor core/shell-structured upconversion fluorescent nanoparticles. *Adv Mater* **20:**4765–4769.

Liang L, Wu H, Hu H, Wu M & Su Q (2004) Enhanced blue and green upconversion in hydrothermally synthesized hexagonal $NaY_{1-x}Yb_xF_4:Ln^{3+}$ (Ln^{3+}: Er^{3+} or Tm^{3+}). *J Alloys Compd* **368:**94–100.

Liang S, Liu Y, Tang Y, Xie Y, Sun H, Zhang H & Yang B (2011) A user-friendly method for synthesizing high-quality $NaYF_4$:Yb,Er(Tm) nanocrystals in liquid paraffin. *J Nanomater* **2011:**Article ID 302364.

Ling J & Huang CZ (2010) Energy transfer with gold nanoparticles for analytical applications in the fields of biochemical and pharmaceutical sciences. *Anal Methods* **2:**1439–1447.

Liu C, Qiu X, Ongagna S, Chen D, Chen Z, Abrams WR, Malamud D, Corstjens PL & Bau HH (2009) A timer-actuated immunoassay cassette for detecting molecular markers in oral fluids. *Lab Chip* **9:**768–776.

Liu C, Wang Z, Jia H & Li Z (2011) Efficient fluorescence resonance energy transfer between upconversion nanophosphors and graphene oxide: a highly sensitive biosensing platform. *Chem Commun* **47:**4661–4663.

Lu H, Yi G, Zhao S, Chen D, Guo LH & Cheng J (2004) Synthesis and characterization of multi-functional nanoparticles possessing magnetic, up-conversion fluorescence and bio-affinity properties. *J Mater Chem* **14:**1336–1341.

Lu W, Cheng L, Zhong H, Sun J, Wan J, Tian Y & Chen B (2010) Dependence of upconversion emission intensity on Yb^{3+} concentration in Er^{3+}/Yb^{3+} co-doped flake shaped $Y_2(MoO_4)_3$ phosphors. *J Phys D* **43:**085404.

Ma DK, Huang SM, Yu YY, Xu YF & Dong YQ (2009) Rare-earth-ion-doped hexagonal-phase $NaYF_4$ nanowires: Controlled synthesis and luminescent properties. *J Phys Chem C* **113:**8136–8142.

Mader HS, Link M, Achatz DE, Uhlmann K, Li X & Wolfbeis OS (2010) Surface-modified upconverting microparticles and nanoparticles for use in click chemistries. *Chemistry* **16:**5416–5424.

Mader HS & Wolfbeis OS (2010) Optical ammonia sensor based on upconverting luminescent nanoparticles. *Anal Chem* **82:**5002–5004.

Mai HX, Zhang YW, Si R, Yan ZG, Sun LD, You LP & Yan CH (2006) High-quality sodium rare-earth fluoride nanocrystals: Controlled synthesis and optical properties. *J Am Chem Soc* **128:**6426–6436.

Mai HX, Zhang YW, Sun LD & Yan CH (2007) Highly efficient multicolor up-conversion emissions and their mechanisms of monodisperse $NaYF_4$:Yb,Er core and core/shell-structured nanocrystals. *J Phys Chem C* **111:**13721–13729.

Malamud D, Bau H, Niedbala SR & Corstjens PL (2005) Point detection of pathogens in oral samples. *Adv Dent Res* **18:**12–16.

Mandelkern M (1981) The dimensions of DNA in solution. *J Mol Biol* **152:**153–161.

Mathews M, Ambekar BR, Tyagi AK & Köhler J (2004) High temperature X-ray diffraction studies on sodium yttrium fluoride. *J Alloys Compounds* **377:**162–166.

Medintz IL & Mattoussi H (2009) Quantum dot-based resonance energy transfer and its growing application in biology. *Phys Chem Chem Phys* **11:**17–45.

Menyuk N, Dwight K & Pinaud F (1972) $NaYF_4$:Yb,Er – an efficient upconversion phosphor. *Appl Phys Lett* **21:**159–161.

Meyerhoff ME, Duan C & Meusel M (1995) Novel nonseparation sandwich-type electrochemical enzyme immunoassay system for detecting marker proteins in undiluted blood. *Clin Chem* **41:**1378–1384.

Mita Y (2007) Infrared up-converting phosphors in *Phosphor Handbook.* CRC Press, Boca Raton, FL. pp. 775–783.

Mokkapati VK, Niedbala SR, Kardos K, Perez RJ, Guo M, Tanke HJ & Corstjens PL (2007) Evaluation of UPlink-RSV: prototype rapid antigen test for detection of respiratory syncytial virus infection. *Ann N Y Acad Sci* **1098:**476–485.

Morgan CG & Mitchell AC (2006) Total internal reflection fluorescence imaging using an upconverting cover slip for multicolour evanescent excitation. *J Microsc* **222:**48–57.

Morgan CG & Mitchell AC (2007) Prospects for applications of lanthanide-based upconverting surfaces to bioassay and detection. *Biosens Bioelectron* **22:**1769–1775.

Morgan CG, Dad S & Mitchell AC (2008) Present status of, and future prospects for, upconverting phosphors in proximity-based bioassay [Review]. *J Alloys Compd* **451:**526–529.

Nakazawa E & Shionoya S (1970) Cooperative Luminescence in $YbPO_4$. *Phys Rev Lett* **25:**1710–1712.

Näreoja T, Vehniäinen M, Lamminmäki U, Hänninen PE & Härmä H (2009) Study on nonspecificity of an immuoassay using Eu-doped polystyrene nanoparticle labels. *J Immunol Methods* **345:**80–89.

Niedbala RS, Vail TL, Feindt H, Li S & Burton JL (2000) Multiphoton up-converting phosphors for use in rapid immunoassays. *Proc SPIE* **3913:**193–203.

Niedbala RS, Feindt H, Kardos K, Vail T, Burton J, Bielska B, Li S, Milunic D, Bourdelle P & Vallejo R (2001) Detection of analytes by immunoassay using up-converting phosphor technology. *Anal Biochem* **293:**22–30.

Nyk M, Kumar R, Ohulchanskyy TY, Bergey EJ & Prasad PN (2008) High contrast in vitro and in vivo photoluminescence bioimaging using near infrared to near infrared up-conversion in Tm^{3+} and Yb^{3+} doped fluoride nanophosphors. *Nano Lett* **8:**3834–3838.

Ohmori M & Matijevic E (1992) Preparation and properties of uniform coated colloidal particles. VII. Silica on hematite. *J Colloid Interface Sci* **150:**594–598.

Ong LC, Gnanasammandhan MK, Nagarajan S & Zhang Y (2010) Upconversion: road to El Dorado of the fluorescence world [Review]. *Luminescence* **25:**290–293.

Ovsyankin V & Feofilov PP (1966) Mechanism of summation of electronic excitations in activated crystals. *JETP Lett* **3:**322–323.

Page RH, Schaffers KI, Waide PA, Tassano JB, Payne SA, Krupke WF & Bischel WK (1998) Upconversion-pumped luminescence efficiency of rare-earth-doped hosts sensitized with trivalent ytterbium. *J Opt Soc Am B* **15:**996–1008.

Peng C, Li Z, Zhu Y, Chen W, Yuan Y, Liu L, Li Q, Xu D, Qiao R, Wang L, Zhu S, Jin Z & Xu C (2009) Simultaneous and sensitive determination of multiplex chemical residues based on multicolor quantum dot probes. *Biosens Bioelectron* **24:**3657–3662.

Pollnau M, Gamelin D, Lüthi S, Güdel H & Hehlen M (2000) Power dependence of upconversion luminescence in lanthanide and transition-metal-ion systems [Review]. *Phys Rev B* **61:**3337–3346.

Pyatenko YA & Voronkov AA (1962) The formula of gagarinite. *J Struct Chem* **3:**696–697.

Qiu X, Thompson JA, Chen Z, Liu C, Chen D, Ramprasad S, Mauk MG, Ongagna S, Barber C, Abrams WR, Malamud D, Corstjens PL & Bau HH (2009) Finger-actuated, self-contained immunoassay cassettes. *Biomed Microdevices* **11:**1175–1186.

Qiu X, Chen D, Liu C, Mauk MG, Kientz T & Bau HH (2011) A portable, integrated analyzer for microfluidic-based molecular analysis. *Biomed Microdevices* **13:**809–817.

Qu Q, Zhu Z, Wang Y, Zhong Z, Zhao J, Qiao F, Du X, Wang Z, Yang R, Huang L, Yu Y, Zhou L & Chen Z (2009) Rapid and quantitative detection of Brucella by up-converting phosphor technology-based lateral-flow assay. *J Microbiol Methods* **79:**121–123.

Reinhard C & Güdel HU (2002) High-resolution optical spectroscopy of $Na_3[Ln(dpa)_3]\cdot 13H_2O$ with Ln = Er^{3+}, Tm^{3+}, Yb^{3+}. *Inorg Chem* **41:**1048–1055.

Riedener T, Krämer K & Güdel HU (1995) Upconversion luminescence in Er^{3+}-doped $RbGd_2Cl_7$ and $RbGd_2Br_7$. *Inorg Chem* **34:**2745–2752.

Roberts D, Wittmershaus BP, Zhang YZ, Swan S & Klinosky MP (1998) Efficient excitation energy transfer among multiple dyes in polystyrene microspheres. *J Lumin* **79:**225–231.

Rostovtsev VV, Green LG, Fokin VV & Sharpless KB (2002) A stepwise huisgen cycloaddition process: Copper(I)-catalyzed regioselective ligation of azides and terminal alkynes. *Angew Chem Int Ed* **41:**2596–2599.

Rufaihah AJ & Zhang Y (2008) Biocompatibility of silica coated $NaYF_4$ upconversion fluorescent nanocrystals. *Biomaterials* **29:**4122–4128.

Sanjuro A, Lau KH, Lowe D, Canizales A, Jiang N, Schneider LV, Mufti N, Rewicj RT, Johansson M & Kardos K (2000) Production of subtantially monodisperse phosphor particles [Patent]. 08/986196.

Santra S, Zhang P, Wang K, Tapec R & Tan W (2001) Conjugation of biomolecules with luminophore-doped silica nanoparticles for photostable biomarkers. *Anal Chem* **73:**4988–4993.

Schäfer H, Ptacek P, Eickmeier H & Haase M (2009) Synthesis of hexagonal Yb^{3+},Er^{3+}-Doped $NaYF_4$ nanocrystals at low temperature. *Adv Funct Mater* **19:**3091–3097.

Selvan ST, Tan TT & Ying JY (2005) Robust, non-cytotoxic, silica-coated CdSe quantum dots with efficient photoluminescence. *Adv Mater* **17:**1620–1625.

Selvin PR (1996) Lanthanide-based resonance energy transfer [Review]. *IEEE J Sel Top Quant Electr* **2:**1077–1087.

Selvin PR (2002) Principles and biophysical applications of lanthanide-based probes [Review]. *Annu Rev Biophys Biomol Struct* **31:**275–302.

Siitari H, Hemmilä I, Soini E, Lövgren T & Koistinen V (1983) Detection of hepatitis B surface antigen using time-resolved fluoroimmunoassay. *Nature* **301:**258–260.

Simpson CR, Kohl M, Essenpreis M & Cope M (1998) Near-infrared optical properties of *ex vivo* human skin and subcutaneous tissues measured using the Monte Carlo inversion technique. *Phys Med Biol* **43:**2465–2478.

Sivakumar S, Diamente PR & van Veggel FC (2006) Silica-coated Ln^{3+}-doped LaF_3 nanoparticles as robust down- and upconverting biolabels. *Chem -Eur J* **12:**5878–5884.

Snitzer E & Woodcock R (1965) Yb^{3+}-Er^{3+} glass laser. *Appl Phys Lett* **6:**45–46.

Soini E & Hemmilä I (1979) Fluoroimmunoassay: Present status and key problems [Review]. *Clin Chem* **25:**353–361.

Soini E & Kojola H (1983) Time-resolved fluorometer for lanthanide chelates--a new generation of nonisotopic immunoassays. *Clin Chem* **29:**65–68.

Soini E, Lövgren T & Reimer C (1987) Time-resolved fluorescence of lanthanide probes and applications in biotechnology [Review]. *Crit Rev Anal Chem* **18:**105–154.

Sommerdijk J (1973) Influence of host lattice on the infrared-excited visible luminescence in Yb^{3+}, Er^{3+}-doped fluorides. *J Lumin* **6:**61–67.

Soukka T, Kuningas K, Rantanen T, Haaslahti V & Lövgren T (2005) Photochemical characterization of up-converting inorganic lanthanide phosphors as potential labels. *J Fluoresc* **15:**513–528.

Stöber W, Fink A & Bohn E (1968) Controlled growth of monodisperse silica spheres in the micron size range. *J Colloid Interface Sci* **26:**62–69.

Sun LD, Gu JQ, Zhang SZ, Zhang YW & Yan CH (2009a) Luminescence resonance energy transfer based on ß-$NaYF_4$:Yb,Er nanoparticles and TRITC dye. *Sci China Ser B* **52:**1590–1595.

Sun LN, Peng H, Stich MI, Achatz D & Wolfbeis OS (2009b) pH sensor based on upconverting luminescent lanthanide nanorods. *Chem Commun* 5000–5002.

Suyver JF, Aebischer A, Biner D, Gerner P, Grimm J, Heer S, Krämer K, Reinhard C & Güdel HU (2005a) Novel materials doped with trivalent lanthanides and transition metal ions showing near-infrared to visible photon upconversion. *Opt Mater* **27:**1111–1130.

Suyver JF, Aebischer A, García-Revilla S, Gerner P & Güdel HU (2005b) Anomalous power dependence of sensitized upconversion luminescence [Review]. *Phys Rev B* **71:**125123.

Suyver JF, Grimm J, Krämer KW & Güdel HU (2005c) Highly efficient near-infrared to visible up-conversion process in $NaYF_4$:Er^{3+},Yb^{3+}. *J Lumin* **114:**53–59.

Suyver JF, Grimm J, van Veen MK, Biner D, Krämer KW & Güdel HU (2006) Upconversion spectroscopy and properties of $NaYF_4$ doped with Er^{3+}, Tm^{3+} and/or Yb^{3+}. *J Lumin* **117:**1–12.

Tan M, Ye Z, Wang G & Yuan J (2004) Preparation and time-resolved fluorometric application of luminescent europium nanoparticles. *Chem Mater* **16:**2494–2498.

Tornoe CW, Christensen C & Meldal M (2002) Peptidotriazoles on solid phase: [1,2,3]-triazoles by regiospecific copper(I)-catalyzed 1,3-dipolar cycloadditions of terminal alkynes to azides. *J Org Chem* **67:**3057–3064.

Ueda H (2002) Open Sandwich Immunoassay: A novel immunoassay approach based on the interchain interaction of an antibody variable region [Review]. *J Biosci Bioeng* **94:**614–619.

Ukonaho T, Rantanen T, Jämsen L, Kuningas K, Päkkilä H, Lövgren T & Soukka T (2007) Comparison of infrared-excited up-converting phosphors and europium nanoparticles as labels in a two-site immunoassay. *Anal Chim Acta* **596:**106–115.

Välimaa L, Sjöroos M, Luhtala M, Toivanen P, Lövgren T & Ilonen J (1998) Detection of HLA-B27 alleles by group-specific amplification and time-resolved fluorometry. *J Immunol Methods* **219:**131–137.

van de Rijke F, Zijlmans H, Li S, Vail T, Raap AK, Niedbala RS & Tanke HJ (2001) Up-converting phosphor reporters for nucleic acid microarrays. *Nature Biotech* **19:**273–276.

Vetrone F, Boyer JC, Capobianco JA, Speghini A & Bettinelli M (2003) Effect of Yb^{3+} codoping on the upconversion emission in nanocrystalline Y_2O_3:Er^{3+}. *J Phys Chem B* **107:**1107–1112.

Vetrone F, Naccache R, Morgan CG & Capobianco JA (2010a) Luminescence resonance energy transfer from an upconverting nanoparticle to a fluorescent phycobiliprotein. *Nanoscale* **2:**1185.

Vetrone F, Naccache R, Zamarron A, de la Fuente AJ, Sanz-Rodriguez F, Martinez Maestro L, Martin Rodriguez E, Jaque D, Garcia Sole J & Capobianco JA (2010b) Temperature sensing using fluorescent nanothermometers. *ACS Nano* **4:**3254–3258.

Wang F & Liu X (2008) Upconversion multicolor fine-tuning: Visible to near-infrared emission from lanthanide-doped $NaYF_4$ nanoparticles. *J Am Chem Soc* **130:**5642–5643.

Wang F & Liu X (2009) Recent advances in the chemistry of lanthanide-doped upconversion nanocrystals [Review]. *Chem Soc Rev* **38:**976–989.

Wang F, Han Y, Lim CS, Lu Y, Wang J, Xu J, Chen H, Zhang C, Hong M & Liu X (2010) Simultaneous phase and size control of upconversion nanocrystals through lanthanide doping. *Nature* **463:**1061–1065.

Wang J, Chen Z, Corstjens PL, Mauk MG & Bau HH (2006) A disposable microfluidic cassette for DNA amplification and detection. *Lab Chip* **6:**46–53.

Wang L, Yan R, Huo Z, Wang L, Zeng J, Bao J, Wang X, Peng Q & Li Y (2005) Fluorescence resonant energy transfer biosensor based on upconversion-luminescent nanoparticles. *Angew Chem Int Ed* **44:**6054–6057.

Wang L & Li Y (2006) Green upconversion nanocrystals for DNA detection. *Chem Commun* **24:**2557–2559.

Wang M, Hou W, Mi CC, Wang WX, Xu ZR, Teng HH, Mao CB & Xu SK (2009a) Immunoassay of goat antihuman immunoglobulin G antibody based on luminescence resonance energy transfer between near-infrared responsive NaYF4:Yb, Er upconversion fluorescent nanoparticles and gold nanoparticles. *Anal Chem* **81:**8783–8789.

Wang Y, Tu L, Zhao J, Sun Y, Kong X & Zhang H (2009b) Upconversion luminescence of ß-$NaYF_4$: Yb^{3+}, Er^{3+}@ß-$NaYF_4$ core/shell nanoparticles: excitation power density and surface dependence. *J Phys Chem C* **113:**7164–7169.

Waynant RW, Ilev IK & Gannor I (2001) Mid-infrared laser applications in medicine and biology. *Phil Trans R Soc Lond A* **359:**635–644.

Wei Y, Lu F, Zhang X & Chen D (2007) Synthesis and characterization of efficient near-infrared upconversion Yb and Tm codoped $NaYF_4$ nanocrystal reporter. *J Alloys Compounds* **427:**333–340.

Wilchek M, Bayer EA & Livnah O (2006) Essentials of biorecognition: the (strept)avidin-biotin system as a model for protein-protein and protein-ligand interaction [Review]. *Immunol Lett* **103:**27–32.

Wollenberger LV, Yao YMM, Mufti NA & Schneider LV (1997) Detection of DNA using upconverting phosphor reporter probes. *Proc SPIE* **2985:**100–111.

Wright WH, Mufti NA, Tagg NT, Webb RR & Schneider LV (1997) High-sensitivity immunoassay using a novel upconverting phosphor reporter. *Proc SPIE* **2985:**248–255.

Wybourne BG (1965) Spectroscopic properties of rare earths. Interscience Publishers, New York. pp. 237.

Xiao X, Haushalter JP & Faris GW (2005) Upconversion from aqueous phase lanthanide chelates. *Opt Lett* **30:**1674–1676.

Xing Y & Rao J (2008) Quantum dot bioconjugates for in vitro diagnostics & in vivo imaging. *Cancer Biomark* **4:**307–319.

Xu CT, Axelsson J & Andersson-Engels S (2009) Fluorescence diffuse optical tomography using upconverting nanoparticles. *Appl Phys Lett* **94:**251107.

Yalow RS & Berson SA (1960) Immunoassay of endogenous plasma insulin in man. *J Clin Invest* **39:**1157–1175.

Yan C, Dadvand A, Rosei F & Perepichka DF (2010) Near-IR photoresponse in new up-converting CdSe/NaYF4:Yb,Er nanoheterostructures. *J Am Chem Soc* **132:**8868–8869.

Yan Z, Zhou L, Zhao Y, Wang J, Huang L, Hu K, Liu H, Wang H, Guo Z & Song Y (2006) Rapid quantitative detection of Yersinia pestis by lateral-flow immunoassay and up-converting phosphor technology-based biosensor. *Sensors Actuators B: Chem* **119:**656–663.

Ye X, Collins JE, Kang Y, Chen J, Chen DTN, Yodh AG & Murray CB (2010) Morphologically controlled synthesis of colloidal upconversion nanophosphors and their shape-directed self-assembly. *Proc Natl Acad Sci USA* **107:**22430–22435.

Yi DK, Selvan ST, Lee SS, Papaefthymiou GC, Kundaliya D & Ying JY (2005) Silica-coated nanocomposites of magnetic nanoparticles and quantum dots. *J Am Chem Soc* **127:**4990–4991.

Yi GS, Lu H, Zhao S, Ge Y, Yang W, Chen D & Guo LH (2004) Synthesis, characterization, and biological application of size-controlled nanocrystalline $NaYF_4$:Yb,Er infrared-to-visible up-conversion phosphors. *Nano Lett* **4:**2191–2196.

Yi GS & Chow GM (2006) Synthesis of hexagonal-phase $NaYF_4$:Yb,Er and $NaYF_4$:Yb,Tm nanocrystals with efficient up-conversion fluorescence. *Adv Funct Mater* **16:**2324–2329.

Yi GS & Chow GM (2007) Water-soluble $NaYF_4$:Yb,Er(Tm)/$NaYF_4$/polymer core/shell/shell nanoparticles with significant enhancement of upconversion fluorescence. *Chem Mater* **19:**341–343.

Ylihärsilä M, Valta T, Karp M, Hattara L, Harju E, Hölsä J, Saviranta P, Waris M & Soukka T (2011) Oligonucleotide array-in-well platform for detection and genotyping human adenoviruses by utilizing upconverting phosphor label technology. *Anal Chem* **83:**1456–1461.

Zarling DA, Rossi MJ, Peppers NA, Kane J, Faris GW & Dyer MJ (1994) Up-converting reporters for biological and other assays using laser excitation techniques [Patent]. PCT/US93/08712.

Zeng JH, Su J, Li ZH, Yan RX & Li YD (2005) Synthesis and upconversion luminescence of hexagonal-phase $NaYF_4$:Yb, Er^{3+} phosphors of controlled size and morphology. *Adv Mater* **17:**2119–2123.

Zeng SM, Yankowitz J, Widness JA & Strauss RG (2001) Etiology of differences in hematocrit between males and females: sequence-based polymorphisms in erythropoietin and its receptor. *J Gend Specif Med* **4:**35–40.

Zhang H & Meyerhoff ME (2006) Gold-coated magnetic particles for solid-phase immunoassays: enhancing immobilized antibody binding efficiency and analytical performance. *Anal Chem* **78:**609–616.

Zhang H, Li Y, Lin Y, Huang Y & Duan X (2011) Composition tuning the upconversion emission in $NaYF_4$:Yb/Tm hexaplate nanocrystals. *Nanoscale* **3:**963–966.

Zhang J, Shade CM, Chengelis DA & Petoud S (2007) A strategy to protect and sensitize near-infrared luminescent Nd^{3+} and Yb^{3+}: Organic tropolonate ligands for the sensitization of Ln^{3+}-doped $NaYF_4$ nanocrystals. *J Am Chem Soc* **129:**14834–14835.

Zhang J & Petoud S (2008) Azulene-moiety-based ligand for the efficient sensitization of four near-infrared luminescent lanthanide cations: Nd^3+, Er^{3+}, Tm^{3+}, and Yb^{3+}. *Chemistry* **14:**1264–1272.

Zhang L, Hu H, Qi C & Lin F (2001) Spectroscopic properties and energy transfer in Yb^{3+}/Er^{3+}-doped phosphate glasses. *Opt Mater* **17:**371–377.

Zhang P, Rogelj S, Nguyen K & Wheeler D (2006) Design of a highly sensitive and specific nucleotide sensor based on photon upconverting particles. *J Am Chem Soc* **128:**12410–12411.

Zhang Q, Song K, Zhao J, Kong X, Sun Y, Liu X, Zhang Y, Zeng Q & Zhang H (2009a) Hexanedioic acid mediated surface-ligand-exchange process for transferring $NaYF_4$:Yb/Er (or Yb/Tm) up-converting nanoparticles from hydrophobic to hydrophilic. *J Colloid Interface Sc* **336:**171–175.

Zhang SZ, Sun LD, Tian H, Liu Y, Wang JF & Yan CH (2009b) Reversible luminescence switching of $NaYF_4$:Yb,Er nanoparticles with controlled assembly of gold nanoparticles. *Chem Commun* 2547–2549.

Zijlmans HJ, Bonnet J, Burton J, Kardos K, Vail T, Niedbala RS & Tanke HJ (1999) Detection of cell and tissue surface antigens using up-converting phosphors: a new reporter technology. *Anal Biochem* **267:**30–36.

Zucchi G, Maury O, Thuéry P, Gumy F, Bünzli JC & Ephritikhine M (2009) 2,2'-Bipyrimidine as efficient sensitizer of the solid-state luminescence of lanthanide and uranyl ions from visible to near-infrared. *Chemistry* **15:**9686–9696.

Zuiderwijk M, Tanke HJ, Sam Niedbala R & Corstjens PL (2003) An amplification-free hybridization-based DNA assay to detect Streptococcus pneumoniae utilizing the up-converting phosphor technology. *Clin Biochem* **36:**401–403.